7-7-2020

Anisotropic Compressive Behavior of Rigid PVC and PES Foams at Elevated Strain Rates Up to 200 s-1

Yue Liu
University of Windsor

Anisotropic Compressive Behavior of Rigid PVC and PES Foams at Elevated Strain Rates Up to 200 s^{-1}

By

Yue Liu

A Thesis
Submitted to the Faculty of Graduate Studies
through the Department of **Mechanical, Automotive, and Materials Engineering**
in Partial Fulfillment of the Requirements for
the Degree of Master of Applied Science
at the University of Windsor

Windsor, Ontario, Canada

2020

Anisotropic Compressive Behavior of Rigid PVC and PES Foams at Elevated Strain Rates Up to 200 s^{-1}

by

Yue Liu

APPROVED BY:

_____

H. Hu
Department of Mechanical, Automotive, and Materials Engineering

_____

D. Green
Department of Mechanical, Automotive, and Materials Engineering

_____

W. Altenhof, Advisor
Department of Mechanical, Automotive, and Materials Engineering

April 23, 2020

DECLARATION OF CO-AUTHORSHIP / PREVIOUS PUBLICATION

I. Co-Authorship

I hereby certify that this thesis incorporates material that is a result of joint research, as follows: The thesis was developed by the author under the supervision of professor Dr. Altenhof, from the University of Windsor. In all cases, the key ideas, primary contributions, experimental design, data analysis, interpretation, and writing were performed by the author. The contribution of Mr. John Magliaro and Mr. Foad Rahimidehgolan were primarily through assisting in the experimental tests and editorial review of this thesis.

I am aware of the University of Windsor Senate Policy on Authorship and I certify that I have properly acknowledged the contribution of other researchers to my thesis, and have obtained written permission from each of the co-author(s) to include the above material(s) in my thesis.

I certify that, with the above qualification, this thesis, and the research to which it refers, is the product of my own work.

II. Previous Publication

This thesis contains one paper that has been previously published or submitted for publication within peer-reviewed journals as follows.

Thesis Chapters	Publication title/full citation	Publication status
4-8	Liu Y, Rahimidehgolan F, and Altenhof W. Anisotropic compression behavior of rigid PVC foam at strain rates up to 200 s^{-1}. Composites Part B. Submitted on February 10, 2020.	submitted

I certify that I have obtained written permission from the copyright owner(s) to include the above published material(s) in my thesis. I certify that the above material describes work completed during my registration as a graduate student at the University of Windsor.

III. General

I certify that, to the best of my knowledge, my thesis does not infringe upon anyone's copyright nor violate any proprietary rights and that any ideas, techniques, quotations, or any other material from the work of other people included in my thesis, published or otherwise, are fully acknowledged in accordance with the standard referencing practices. Furthermore, to the extent that I have included copyrighted material that surpasses the bounds of fair dealing within the meaning of the Canada Copyright Act, I certify that I have obtained written permission from the copyright owner(s) to include such material(s) in my thesis.

I declare that this is a true copy of my thesis, including any final revision, as approved by my thesis committee and the Graduate Studies office and that this thesis has not been submitted for a higher degree to any other University or Institution.

ABSTRACT

In this study, closed-cell polyvinyl chloride (PVC) foam with five different densities ranging from 45 to 200 kg/m^3, and polyethersulfone (PES) foam with three different densities ranging from 50 to 130 kg/m^3, were subjected to compressive loading under quasi-static and elevated strain rates for mechanical material assessment. Three orthogonal loading directions, (i.e., parallel and perpendicular to foam rise directions) were considered to investigate structural anisotropy. The elevated strain rate tests were performed using a customized drop tower device at three different strain rates of 50, 100, and 200 s^{-1}. Engineering stress/strain behavior, energy dissipation, and maximum stress capacity were obtained for each density and compared against each other. Experimental results indicated that elastic modulus, compressive strength, plateau stress, and energy-absorbing capacity of both PVC and PES foams were highly dependent on foam density. Except for the PVC foam with the lowest density of 45 kg/m^3, strain rate effects were clearly observed through increased compressive strength and plateau stress when loading in the foam rise direction for both PVC and PES foams. The strain rate effect was more evident at higher densities. When loading perpendicular to the foam rise direction, no significant strain rate effect was observed for PVC foam. However, a slight strain rate effect was observed for PES foam at the highest density of 130 kg/m^3 in one of the perpendicular to foam rise directions. Scanning electron microscopy (SEM) analysis showed that the cell wall thickness of both PVC and PES foams continuously increased with the increase of foam density. However, cell sizes were not simply dependent on foam density. For both quasi-static and elevated strain rate tests, plastic hinges were the primary deformation mechanism for both PVC and PES foam cells.

DEDICATION

To my parents Guilin Liu and Fengxia Yang, and my sister Longfei Liu: for their support and encouragement.

ACKNOWLEDGEMENTS

I would first like to express my deep gratitude and sincere appreciation to my advisor Dr. William Altenhof for his encouragement, guidance, and support. He was dedicated to guiding me in the best possible direction at each stage of this project. With his vast knowledge and experience in material characterization and finite element analysis, I have learned to understand the challenges better and devise several possible approaches towards problem solving. I must also thank him for his excellent teaching and advice on finite element analysis, which helped me successfully develop the dynamic testing apparatus. I would also like to thank my committee members, Dr. Green and Dr. Hu, for their help and support. I am also grateful to John Magliaro, Foad Rahimidehgolan, Matthew Bondy, and Anthony Gudisey for their help and friendship.

The technicians at the University of Windsor have also assisted in this project: I would like to thank Mr. Bruce Durfy for machining the components for the energy absorbing system. Mr. Matt St. Louis and Mr. Jerome Finnerty also deserve my thanks for guiding me to prepare the foam specimens.

Last but not least, the financial support of this research from the Natural Science and Engineering Research Council (NSERC) of Canada, and the Ontario Research Fund (ORF) are gratefully acknowledged.

TABLE OF CONTENTS

LIST OF TABLES

LIST OF FIGURES

LIST OF APPENDICES

LIST OF ABBREVIATIONS

ASTM	American Society for Testing and Materials
PVC	Polyvinyl Chloride
PES	Polyether Sulfone
FST	Fire, Smoke, and Toxicity
HSR	High Strain Rate
SHPB	Split Hopkinson Pressure Bar
FEA	Finite Element Analysis
FEM	Finite Element Method
FE	Finite Element
EDS	Energy Dispersive X-ray Spectroscope
SEM	Scanning Electron Microscope

NOMENCLATURE

ρ	Foam density
d	Compressive deformation
ε	Compressive strain
σ	Compressive stress
σ_{pr}	Proportional limit stress
E	Elastic modulus
σ_y	Yield stress
ε_y	Yield strain
ε_{cd}	Densification strain
$\eta(\varepsilon)$	Energy absorption efficiency
σ_{pl}	Plateau stress
E	Energy absorbed per unit volume
e	Average error
V	Validation metric
d_H	Cell horizontal diameter
d_V	Cell vertical diameter
t	Cell wall thickness
R	Shape anisotropy
S.D.	Standard deviation

1. INTRODUCTION

Foams are generally composed of solid and gas phases mixed together [1]. With modern technologies, foams now can be manufactured from almost any solids, including: polymers, metals, ceramics, glasses and even composites [2]. Polymeric foams are exploited ubiquitously in our daily lives and are extensively utilized as core materials in sandwich structures for aerospace, automotive, and marine applications due to their advantageous properties [3,4]. The density of these materials is low compared to traditional solid materials, and hence weight reduction is pronounced when foams are exploited as a novel substitute. This can directly increase fuel economy and reduce pollution in transportation systems. Additionally, the inherently high compressive energy absorbing capacity, particularly under impact loading, is favorable for reducing damage and occupant injuries in such applications [5,6].

According to the Road Safety Annual Report 2019 [7], approximately 1.3 million people were killed and 50 million people were severely injured by road crashes worldwide. Occupant safety is a critical concern for engineers when designing a vehicle, regardless of the mode of transportation. An ideal energy dissipation system should prevent death and significantly reduce, if not eliminate, potential injuries from an accident. Numerous energy dissipation modes for various polymeric foams were investigated [8,9] and found that compression is the primary energy-absorbing mechanism. For example, the energy absorbed of closed-cell PVC foams under compression could be greater by a factor of 5 in comparison to tensile loading [9].

Compressive stress/strain responses of polymeric foams are dependent upon the base material that the foams are comprised of and the cellular microstructure. Under compressive loading, the energy absorption occurs as the cell walls and edges bend, buckle, or fracture [2]. Different polymeric foams can have very different cell deformation mechanisms under

compression. According to the material properties of base polymers, polymeric foams can be classified into either thermosets and thermoplastics, which can be further divided into rigid or flexible foams [2]. Compared with flexible foams, rigid foams can always support higher loadings, but the compressive deformation of the rigid foams cannot be fully recovered after relieving the loadings. However, the compressive deformation of some flexible foams can be fully recovered. Thermoset polymeric foams cannot be re-heated to be reshaped or formed due to the chemical bonds created within their network structure. One of the most commonly utilized polymers for the thermoset foams is polyurethane (PU) which can exist as both rigid and flexible foams. Unlike the chemical crosslinks created in thermoset polymers, physical bonds are generated between chains in thermoplastic polymers. This allows thermoplastic polymer foams to be re-heated into a liquid phase and then shaped multiple times [2]. Polypropylene (PP), Polystyrene (PS), and polyethylene (PE) are commonly converted into thermoplastic foams [10].

Rigid closed-cell polyvinyl chloride (PVC) and thermoplastic polyethersulfone (PES) foams are lightweight, cellular materials that are widely utilized for aerospace and marine industries [11,12]. Additionally, PES foam is a relatively new material with excellent FST (Fire, Smoke, and Toxicity) properties, which can significantly decrease environmental impact [13]. The compressive responses of polymeric foams can be significantly different when loading in different material directions and at various strain rates [2]. Classification of different strain rate regions is shown in Table 1. Additionally, the anisotropy associated with foams increases the complexity associated with analysis and engineering design. The impetus of the work presented in this thesis was to characterize the compressive behaviors of rigid closed-cell PVC and thermoplastic PES foams with various densities, considering the simultaneous effects of structural anisotropy and

strain rate sensitivity in the intermediate strain rate range (up to 200 s^{-1}) to address the shortfall of mechanical material knowledge for both foams.

Table 1. Classification of different strain rate regions [14].

Regions	Strain Rate
Creep and stress-relaxation region	$< 10^{-5}$ s^{-1}
Quasi-static region	10^{-5} s^{-1} – 5 s^{-1}
Dynamic-low region (intermediate strain rate)	5 s^{-1} – 800 s^{-1}
Dynamic-high region	800 s^{-1} – 10^{5} s^{-1}

2. LITERATURE REVIEW

The mechanical responses of polymeric foams are dependent upon both the foam material properties and the exterior loading conditions. Considering the objectives of this study, a literature review was conducted on axial compression testing of polymeric foams considering the effect of foam density, strain rate, and material loading direction.

2.1. Typical compressive response of polymeric foams

Gibson and Ashby outlined the general compressive stress-strain response of foams in their pioneering work [2]. Three distinct phases were described as shown in Figure 1, namely, the linear elastic region, followed by a plateaued region and finally a densification region. The microscopic deformation associated with each region was also described. Linear elasticity is caused by cell edge elastic bending for open-cell foams and, in the case of closed cells, by stretching of the cell walls. Elastic modulus, E, which is the initial slope of the stress/strain response of the foam, can be obtained from the linear elastic region. Regarding the plateau region, the cell deformation mechanisms are different for elastomeric and elastic-plastic foams [2]. For elastomeric foams, the plateau region is dominated by elastic buckling of cell edges and there is no plastic deformation in a pure elastomeric foam. In contrast, cell edges of elastic-plastic foams collapse and form plastic hinges or rupture, which progresses at roughly constant load, defining the plateau region [2]. An elastic-plastic foam can experience significant plastic deformation. After most of the cells have elastically buckled or plastically collapsed, the cell walls start to pack and lock up, and further strain would compress the solid itself, defining the densification region. In this region the stress dramatically increases with the increase of strain.

According to ASTM standard D1621-16 [15], which was developed for characterizing compressive properties of rigid cellular plastics, the following terminologies are often used when

testing polymeric foams. Foam density, ρ, refers to how much a unit volume of the foam material weighs. Compressive deformation, *d*, is the decrease in length produced by a compressive load. Compressive strain, ε, is the dimensionless ratio of compressive deformation to the change in length per unit of original length along the longitudinal axis. Compressive stress, σ, is the compressive load per unit area of the minimum original cross section, carried by the test specimen at any given moment, expressed in force per unit area. Compressive stress/strain diagram is a diagram in which values of compressive stress are plotted as ordinates against corresponding values of compressive strain as abscissas. Proportional limit stress, σ_{pr}, is the greatest stress that a material is capable of sustaining without any deviation from proportionality of stress-to-strain expressed in force per unit area. Elastic modulus, *E*, is the ratio of stress to corresponding strain below the proportional limit of a material expressed in force per unit area. Compressive yield point is the first point on the stress/strain response or diagram at which an increase in strain occurs without an increase in stress. Compressive strength, which can be also referred to as yield stress or peak stress, σ_y, is the stress at the yield point if a yield point occurs before 10% deformation or, in the absence of such a yield point, the stress at 10% deformation. Densification strain, ε_{cd}, is the strain of the starting point of densification region, and it can be determined by the method based on the energy absorption efficiency curve [16]. The energy absorption efficiency, $\eta(\varepsilon)$, is defined as equation (1) based on the uniaxial stress/strain response of the foam material.

$$\eta(\varepsilon) = \frac{1}{\sigma(\varepsilon)} \int_0^{\varepsilon} \sigma(\varepsilon)\, d\varepsilon \tag{1}$$

The densification strain can be calculated by equation (2), where the energy absorption efficiency reaches a maximum value on the efficiency-strain curve.

$$\left.\frac{\mathrm{d}\eta(\varepsilon)}{\mathrm{d}\varepsilon}\right|_{\varepsilon=\varepsilon_{cd}} = 0 \tag{2}$$

Plateau stress, σ_{pl}, is the stress of the plateau region, and it can be calculated by equation (3),

$$\sigma_{pl} = \frac{\int_{\varepsilon_y}^{\varepsilon_{cd}} \sigma(\varepsilon)\,\mathrm{d}\varepsilon}{\varepsilon_{cd} - \varepsilon_y} \tag{3}$$

where, ε_y, is the strain at the compressive yield point corresponding to the beginning of the plateau region. Energy absorbed per unit volume, E, was defined as the area under the stress/strain curve. Calculation of the energy absorbed per unit volume is shown as the following equation [15]:

$$\mathrm{E} = \int_0^{\varepsilon} \sigma(\varepsilon)\, d\varepsilon \tag{4}$$

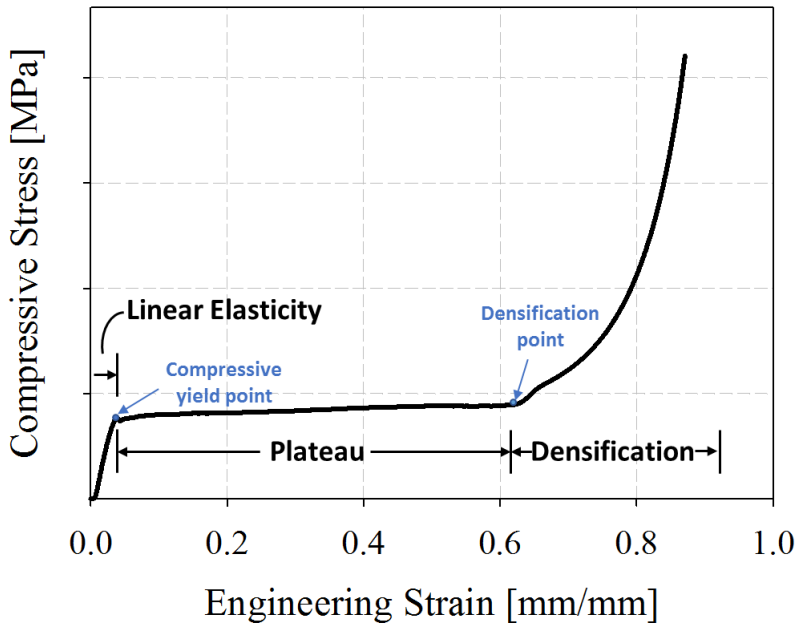

Figure 1. Typical compressive stress/strain response of elastic-plastic foams [2].

2.2. Effect of foam density

The density of a foam material without forming skins can simply be measured as the mass of a foam core specimen divided by its volume [17], it is an important variable that has influences on the mechanical properties of foams.

Numerous researchers have investigated the relationship between foam density and the mechanical response under compression testing. Thomas et al. [18] and Saha et al. [19] tested closed-cell PVC foams at densities of 75, 130 and 300 kg/m^3 utilizing a servo-hydraulic testing machine for quasi-static testing, and a modified split Hopkinson pressure bar to accommodate strain rates from 400 s^{-1} to 1900 s^{-1}. It was found that the compressive yield stress was directly related to the foam density. Additionally, the elastic modulus and plateau stress increased with increasing the foam density, whereas elongation of the plateaued region decreased. The peak stress and energy absorption of PVC foam under compression testing at various strain rates from the study [19] were plotted as a function of foam density, as shown in Figures 2(a) and (b), respectively. It was observed that both the peak stress and energy absorption increased with the increase of density, and this dependency was even more pronounced at higher strain rates.

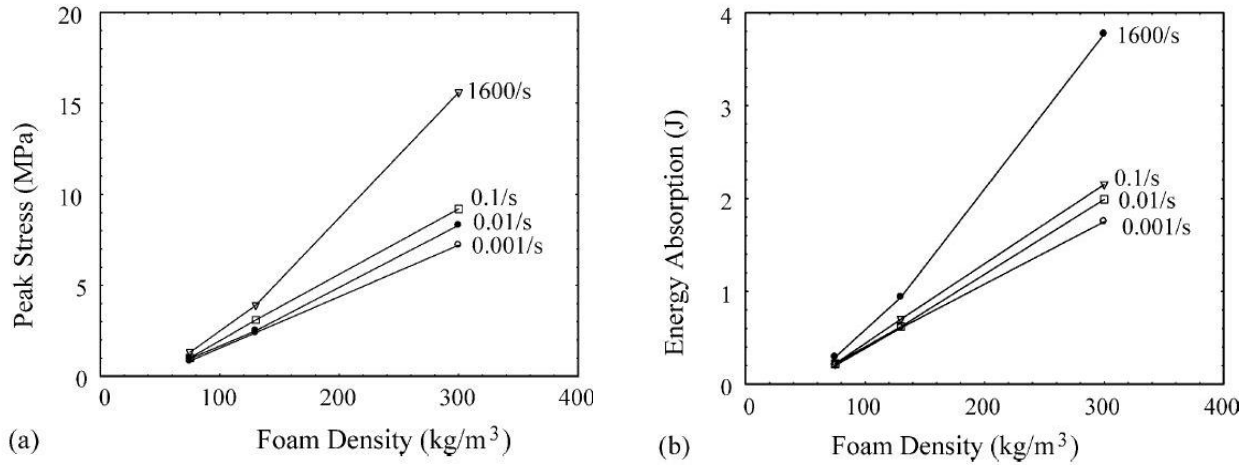

Figure 2. (a) Variation of peak stress and (b) energy absorption with foam density [19].

It seems that increasing the foam density would enhance material properties, but an opposite trend can be observed when the density exceeds its optimal value. For example, the influence of foam density on the mechanical properties of rigid PU foam was studied by Thirumal et al. [20]. As illustrated in Figure 3, the compressive stress at 10 % strain continuously increased from 0.196 MPa to 0.853 MPa as the density increased from 42 kg/m^3 to 116 kg/m^3. However, the compressive stress suddenly dropped from 0.853 MPa to 0.461 MPa as the density continued to increase from 116 kg/m^3 to 118 kg/m^3. A similar trend was observed for the change of the compressive modulus and energy absorption per unit volume of the PU foam, as illustrated in Table 2. This was because when the density reached its maximum value of 118 kg/m^3, there was "0 content" distilled water (chemical-blowing agent). In this case, a small amount of moisture from the surroundings remained as an inherent impurity in polyether polyol and acted as a blowing agent. Foam cells were much larger and broken because of the non-uniform distribution of the water or moisture, which significantly degraded the foam's mechanical performance. Similar results were obtained by the research of Deb and Shivakumar [21] who subjected three types of PU foams, namely, flexible high resilience viscoelastic and semi-rigid foams to compressive loading conditions. Load-bearing capacity and energy absorption were determined. Results showed that for each type of foam, an optimal foam density exists that maximizes load and energy-absorbing capabilities.

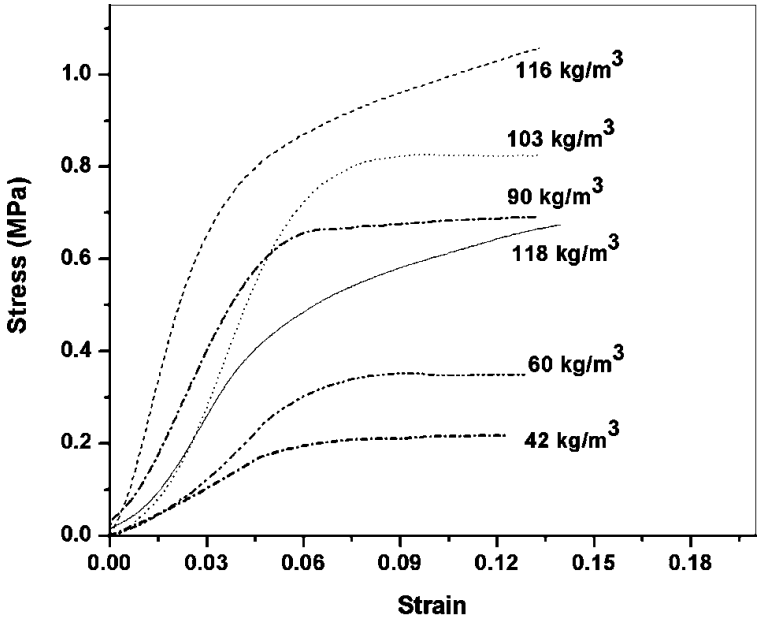

Figure 3. Stress/strain behaviors of the PU foam at different densities [20].

Table 2. Effect of density on the compressive properties of the PU foam [20].

Sr. No.	Sample	Water content (phr)	Density (kg/m^3)	Compressive stress at 10% strain (MPa)	Compressive modulus (MPa)	Energy Absorption per unit volume (J/cm^3)
1	WOBA	0.00	118.00	0.461	9.40	0.056
2	PUF-1	0.10	116.00	0.853	21.60	0.100
3	PUF-2	0.30	103.00	0.794	15.20	0.086
4	PUF-3	1.00	90.00	0.598	11.70	0.060
5	PUF-4	1.50	60.00	0.343	6.50	0.028
6	PUF-5	3.00	42.00	0.196	3.20	0.014

2.3. Effect of strain rate

Due to the viscoelastic nature of some solid polymers, polymeric foams often exhibit strain rate sensitivity under compressive loading. The strain rate effect can be further complicated by the presence of gas within the closed cells [19]. Thus, a thorough understanding of the mechanical response of the polymeric foams at higher strain rate compression loading is essential to engineers.

Many authors investigated polymeric foams at elevated strain rates [22-32]. For example, Ouellet et al. [32] studied the compressive response of expanded polystyrene (ESP), high-density

polyethylene (HDPE), and rigid polyurethane (PU) foams under quasi-static, medium and high strain rate conditions. Significant rate sensitivity was observed for all the foams investigated through increased compressive strength, plateau stress, and a decreased densification strain. The compressive stress/strain responses of EPS foam at 61 kg/m^3 under different strain rates tests are shown in Figure 4 as an example. Similar findings were observed in the research of Mane et al. [22] and Chen et al. [25] on rigid PU foam. Rigid PU foam exhibited a longer plateau region, although lower plateau stress under quasi-static test in comparison with the dynamic test.

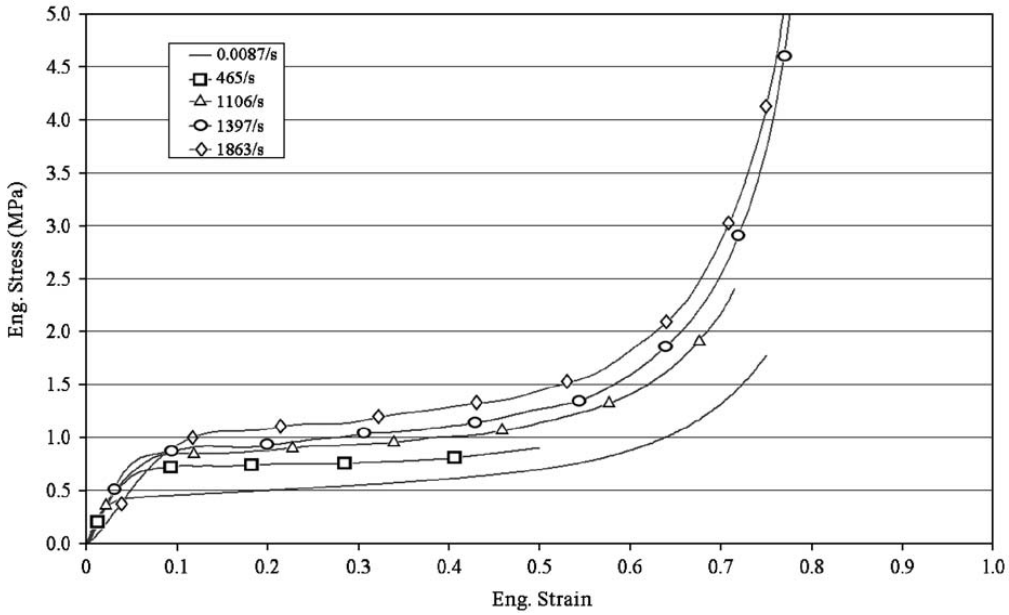

Figure 4. Compressive stress/strain responses at multiple strain rates for 61 kg/m^3 EPS foam [32].

Zhang et al. [33] conducted quasi-static and high strain rate (HSR) compression tests on microcellular PMMA foams. The experimentally determined plateau and yield stresses for the microcellular PMMA foams with various densities tested at a series of strain rates were plotted in Figures 5(a) and (b), respectively. The PMMA samples exhibited an evident strain rate sensitivity over the range of 10^{-1} s^{-1} to 10^4 s^{-1}, with increasing strain rate, the compression strength and plateau stress increased, which is consistent with the finding in the studies [29] and [31]. Furthermore, a post-yield softening phenomenon was observed in the compressive stress/strain response of

microcellular PMMA foams under dynamic testing. This phenomenon was attributed to the viscous effect due to the fluid flow through cell walls, and the overload behavior under dynamic compression. Ye et al. [24] investigated the dynamic response and failure of sandwich plates with PVC foam core. PVC foam with three different densities, namely, 80 kg/m^3, 160 kg/m^3, and 250 kg/m^3 were tested under quasi-static compressive loading with strain rates between 0.002 s^{-1} and 0.167 s^{-1}, and dynamic compression test with strain rates from 1980 s^{-1} to 3696 s^{-1}. An electromechanical universal testing machine and a modified split Hopkinson pressure bar apparatus were utilized in the quasi-static and dynamic tests, respectively. It was determined that the compressive yield stress was directly related to the foam density, and material stiffness significantly increased with the increase of strain rate. A similar Split Hopkinson Pressure Bar (SHPB) apparatus was utilized by other researchers [26-31] to investigate the compressive response of PVC foam at strain rates ranging from 400 s^{-1} to 4000 s^{-1}.

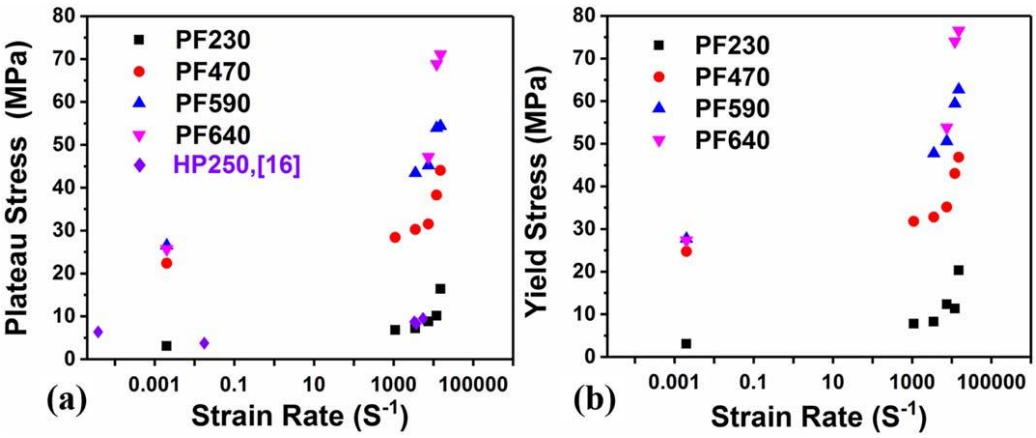

Figure 5. (a) Plateau stress and (b) yield stress with respect to strain rate for PMMA foams with densities from 230 kg/m^3 to 640 kg/m^3, and PVC foam with density 250 kg/m^3 [33].

2.4. Effect of material loading direction

The mechanical behavior of polymeric foams can vary significantly when loading in different material directions. Loading is generally considered in a direction parallel to the rise direction of the foam material and referred to accordingly. Foam rise direction is the direction that

foam cells typically elongate during its foaming and manufacturing process [2]. Loading perpendicular to the rise direction is also typically considered, but far less frequently as in the foam rise direction. Tu et al. [34] investigated the compressive responses of rigid PU foam in the foam rise direction and perpendicular to the foam rise direction under quasi-static loading. It was found that dissimilar mechanical responses occurred and were attributed to the anisotropy in the internal cellular structure that arose from the manufacturing process. The rise direction exhibited a traditional mechanical response; the stress/strain behavior exhibited three typical regions, as shown in Figure 6. An initial linear elastic response followed by a post-yield plateau region, prior to a final sharp increase in stress in the densification region. Also, compression in the PU foam rise direction resulted in a drop in stress at the start of the plateau phase: a strain-softening behavior. However, according to Tu et al. [34], no strain-softening phenomenon was observed, and the three-phase response slightly differs when loading perpendicular to the foam rise direction, the post-yield plateau is replaced by a small degree of strain hardening before densification occurs. Moreover, the experimental results show that the elastic modulus and compressive strength were significantly higher in the foam rise direction compared to the direction perpendicular to foam rise, while the yield strain was slightly lower, as illustrated in Figure 6. The different responses in the two directions indicated that the mechanical characteristics of PU foam are direction dependent and are a result of the microstructural anisotropy.

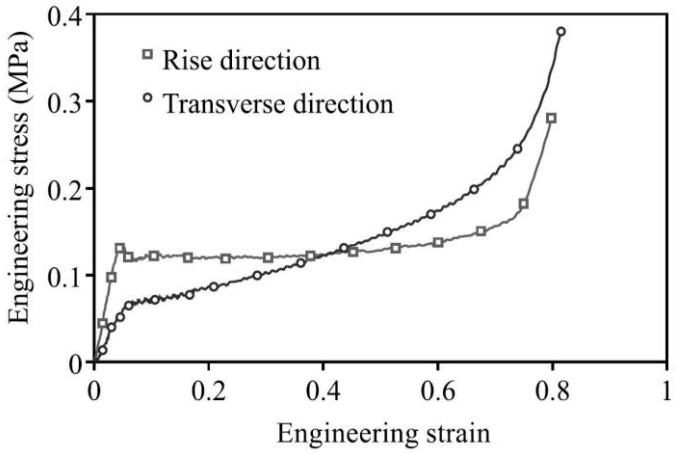

Figure 6. Compressive response of PU foam in foam rise and transverse (perpendicular to the rise) directions [34].

Gdoutos et al. [35] and Daniel el al. [36] investigated the compressive and tensile behaviors of PVC foam in the rise direction and perpendicular to the foam rise direction. Testing revealed that both the tensile and compressive strengths in the foam rise direction were considerably higher than the perpendicular direction. Shafiq et al. [37] studied the compressive behavior of PVC foam samples in three principal material directions (i.e., foam rise direction and two perpendicular to the foam rise directions) in the quasi-static regime at a strain rate of $5 \cdot 10^{-4}$ s^{-1}. The compressive responses are nearly identical in the two perpendicular to the foam rise directions, which was named transversely isotropic. Mosleh et al. [38,39] and Sakly et al. [40] investigated the anisotropic compressive behaviors of PES foam in three orthogonal directions (i.e., foam rise direction, longitudinal direction, and transverse direction) under quasi-static test at strain rates of $8 \cdot 10^{-4}$ s^{-1} and $9.5 \cdot 10^{-3}$ s^{-1}. Similar to the observations from [35-37], the PES foam exhibited an enhanced mechanical response through increased elastic modulus and compressive strength in the foam rise direction compared with the results acquired when loading in the two perpendicular directions. Moreover, the quasi-static compressive responses of PES foams were transversely anisotropic. The compressive response in the longitudinal direction was slightly enhanced in comparison to the transverse direction.

2.5. Summary of literature review

The previous investigations suggested that the compressive responses and cell deformation mechanisms of polymeric foams were associated with both the base polymer material properties and loading conditions. Foam density was shown to play a significant role in the mechanical behavior of polymeric foams. However, the mechanical properties are not solely dependent on foam density, and they are also related to foam composition and the manufacturing process.

Polymeric foams exhibited a high degree of sensitivity to strain rate. The majority of the previous studies on the strain rate effect of polymeric foams were dedicated to high strain rate testing (>1000 s^{-1}) utilizing a Split Hopkinson Pressure Bar (SHPB) apparatus [25-31]. However, to the best of the author's knowledge, no published research has investigated the compressive strain rate effect of PES foam, and very few researchers have addressed the compression response of PVC foams at the intermediate strain rates from 50 s^{-1} to 200 s^{-1}, as shown in Figure 7 [28,29,31,41-43] which is essential for the development of improved safety equipment, especially in the automotive industry where these magnitudes of strain rates are very common in traffic collisions [44,45].

Although the anisotropic responses of polymeric foams under quasi-static compressive loading are well understood [34,38-40,46-51], the effect of structural anisotropy on the foam mechanical response was scarcely investigated [52] at intermediate strain rates in comparison to the greater collection of literature on the topic of polymeric foams.

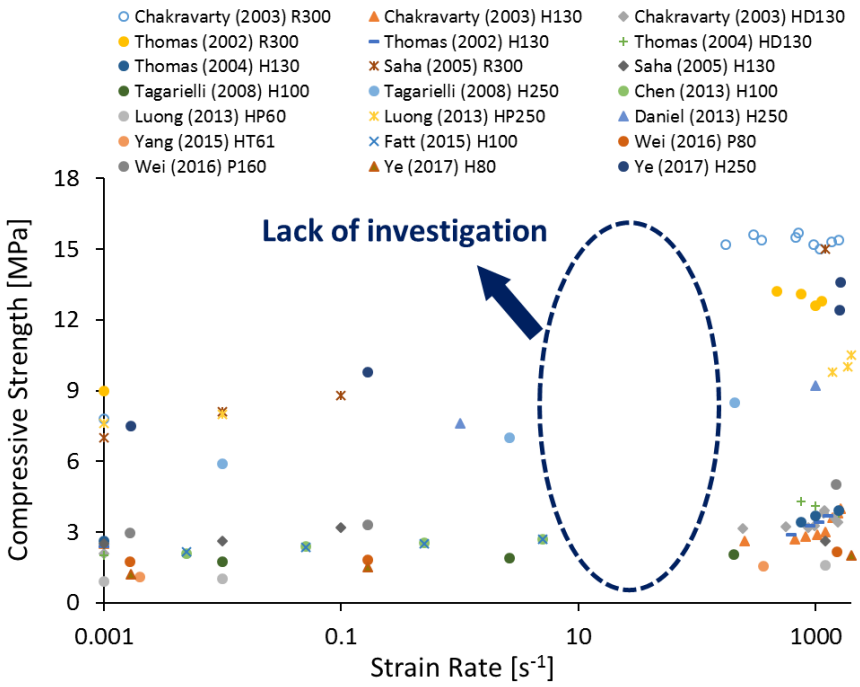

Figure 7. Summary of previous research on compressive strength of PVC foams at different strain rates (log scale) [28,29,31,41-43].

3. RESEARCH OBJECTIVES

As stated in Section 2, closed-cell polyvinyl chloride (PVC) foam was of significant interest due to its superior mechanical properties. However, few papers directly compared the compressive behaviors of closed-cell PVC foams in the intermediate strain rate range from 50 s^{-1} to 200 s^{-1}. Polyethersulfone (PES) foam is a novel material and mechanical characterization has not been investigated extensively in the open literature. Additionally, the PES foam possesses excellent FST properties and favorable mechanical characteristics; it is consequently exploited for various applications in transportation such as aircraft interiors and seating. The objective of this study was to characterize the compressive behavior of closed-cell PVC and thermoplastic PES foams considering the influence of loading direction and strain rate from the quasi-static regime to elevated strain rates, up to 200 s^{-1}.

The main objectives of this study are summarized as follows:

1. Energy dispersive x-ray spectroscope (EDS) was conducted to investigate the material compositions for each density. Scanning electron microscope (SEM) was conducted on both original and mechanically deformed foam specimens to characterize the relation between material mechanical properties and microstructural deformation.
2. Quasi-static compression testing to outline the expected engineering stress/strain behaviors and to quantify energy dissipation and maximum stress capacity for each material. The effect of foam density under quasi-static compression test was analyzed according to the mechanical performance of both PVC and PES foam specimens. PVC foams with five densities ranging from 45 to 200 kg/m^3 and PES foams with three densities ranging from 50 to 130 kg/m^3 were considered.
3. Elevated strain rate testing with a customized drop tower apparatus, the supporting part of the drop tower device, was designed to support the foam specimen. Sacrificial energy dissipation via a cutting mechanism was utilized to absorb the excess energy provided by the dropping mass and prevent overloading of the sensors and damage of the testing apparatus.
4. Dynamic compression testing with three elevated strain rates (50, 100, and 200 s^{-1}) was conducted on the PVC and PES foam specimens in three different material loading directions (i.e., parallel to foam rise direction and the two perpendicular directions) to investigate the effect of strain rate and material structural anisotropy. Engineering stress/strain behavior, compressive strength, plateau stress, and energy-absorbing capacity were obtained for each density of both foams and compared.

4. MATERIALS

PVC foam, commercially referred to as "Divinycell H", with five different densities 45, 80, 100, 130 and 200 kg/m^3, referred to as H45, H80, H100, H130, H200 groupings; PES foam, commercially referred to as "Divinycell F", with three different densities 50, 90, and 130 kg/m^3, referred to as F50, F90, and F130 groupings, respectively, were examined in this study. The numeric part in the nomenclature of the foams represents their nominal density in kg/m^3. To ensure the accuracy of the nominal density reported by the foam's manufacturer, the density of each material was measured again in accordance with ASTM D1622/D1622M-14 [17].

4.1. Material formulations

Three components are needed when making PVC foam namely, isocyanate, blowing agent, and stabilizer [53]. The three components are mixed into a plastisol that is then placed into a mold at a high temperature to initialize the blowing agent's reaction. During production, PVC particles are exposed to high temperatures to soften the polymer. Isocyanides are mixed into PVC particles to commence both chemical cross-linking and foaming [54]. During the foaming process, foam cells in shapes of polyhedrons formed, and the majority of the cells elongated in a specific direction which is the foam rise direction [53]. PVC polymer's cross-linked structure increases its modulus and strength but reduces material ductility. Therefore, the mechanical characteristics of solid PVC are not a true representative of the solid material in the PVC foam [55]. Regarding the production of PES foam, solid PES polymers are heated near its melting point and carbon dioxide is then injected to start the process of foaming. In this case, the solid constituent of the PES foam remains unchanged. Hence, the mechanical characteristics of solid material in the PES foam can be represented by the solid PES although the responses may change due to the tiny dimensions of the foam cells [55].

4.2. Test Specimens

All PVC and PES foams considered in this study were manufactured from Diab Inc and received in the form of large panels with a consistent thickness of 25.4 mm. The panel thickness direction is the foam rise direction, as indicated in Figures A1 and A2 (Appendix A). According to ASTM standard D1621-16 [15], the minimum height of the foam specimen shall be 25.4 mm, and the maximum height shall be no greater than the width of the specimen. Individual test specimens were cut from these large panels with a height of 25.4 mm, having lengths and widths approximately 50.8 mm for testing in the foam rise direction. Cubical specimens, with a length, width, and height of 25.4 mm, were cut for tests loaded in the two perpendicular to foam rise directions. Specimens with the same sizes were cut out for both the quasi-static and dynamic tests. The cutting plans of PVC foam specimens within H45 and H200 groupings are shown in the Figures A1 and A2, respectively. Individual test specimens A1-A10 were cut for tests loading in the rise (thickness) direction. Cubical specimens B1-B6 and C1-C6 were cut for tests loading in the two perpendicular to rise (thickness) directions. In order to ensure cutting surfaces are smooth and free from any tearing, a table saw and circular saw with blades having a number of 40 and 60 fine teeth, respectively, were utilized to cut out small specimens. Great care was taken when aligning and cutting the foam panels to ensure the cutting surfaces are clean and parallel. To satisfy the requirement of repeatability, three specimens were tested for each density at each strain rate and, where applicable, the average value of a specific numeric mechanical material property has been presented.

5. ELEVATED RATE TESTING APPARATUS DESIGN AND ENGINEERING

Elevated strain rate compression testing on the PVC and PES foam specimens was performed by a customized drop tower device. The dropping entity of the apparatus contained a large mass of 45.45 kg, which greatly minimized the loss of compression speed during the impact test. This resulted in the dynamic tests exhibiting an almost constant strain rate throughout the impact event. For instance, when applying 200 s^{-1} strain rate compressive loading on the specimens within the PVC H130 grouping, the strain rate negligibly decreased from 199.61 s^{-1} at the beginning to 192.48 s^{-1} when the specimen was 80% crushed. It is worth noting that maintaining a constant strain rate during intermediate strain rate testing of polymeric foams is technically challenging [56,57].

To capture the impact force with high accuracy, a PCB piezoelectric impact load cell with relatively low capacity (89 kN) but high force resolution was selected. Under elevated strain rate testing, a load cell with low capacity was susceptible to damage since the massive dropping entity generated much higher impact loads than the foam specimens could support. Therefore, an energy dissipation system was needed to limit the maximum impact force experienced by the sensor.

A patented energy dissipation system [58], utilizing a cutting mechanism, was employed to resolve this concern. As shown in Figure 8, an extruded aluminum 6061-T6 tube with an outer diameter of 63.5 mm, wall thickness of 1.5 mm, and length of 300 mm was utilized within the energy dissipation system. A cutting force of approximately 70 kN was successfully achieved with the aluminum extrusion and an 8-blade cutter with a tip width of 1.2 mm. A deflector was connected to the cutter to redirect the petalled cut wall of the extrusion after cutting a certain depth. The cutter and deflector were fastened together with a standard 6.35 mm fastener. Prior to inserting the cutter/extrusion assembly into the three-jaw chuck, an approximate 5 mm precut of the tube

was made with careful alignment to ensure concentricity was maintained during the dynamic test. The mass of the 8-blade cutter and deflector were measured as 0.71 kg and 2.18 kg, respectively. When cutting occurs during the impact test, the entire energy dissipation system translated parallel to the dropping entity, along with the specimen after full compaction of the foam specimen was achieved and without overloading the load cell utilized to measure the foam crushing force. Therefore, the relative displacement between the impact plate and specimen support was the true compressed displacement of the specimen. A 380 mm long aluminum c-channel with a web thickness of 12.7 mm was fastened to the cutter/deflector assembly utilizing a 6.35 mm set screw, and the displacement of the c-channel was measured as the cutting displacement. Displacements of the dropping entity and c-channel were measured by two noncontact laser displacement transducers.

Due to the small cross-sectional area of the load cell, conducting the dynamic test with a foam specimen fabricated with standard dimensions (50. 8 mm × 50.8 mm × 25.4 mm) on the top surface of the load cell was impossible. Therefore, a supporting plate with a size larger than the cross-section of the foam specimen was implemented, as illustrated in Figure 8. Since the supporting plate needed to be fastened on the top surface of the load cell and would move downwards with the specimen during the cutting process, the dynamic force generated by the supporting plate was included in the loading detected by the load cell during the dynamic test. Therefore, minimizing the mass while preserving the structural stiffness of the supporting plate was critical. To investigate the difference between the compressive loads provided by the impact plate and the force detected by the load cell, dynamic tests in which the supporting plate with various geometric and material combinations was simulated utilizing the explicit finite element analysis (FEA) package LS-DYNA, as summarized in the following section.

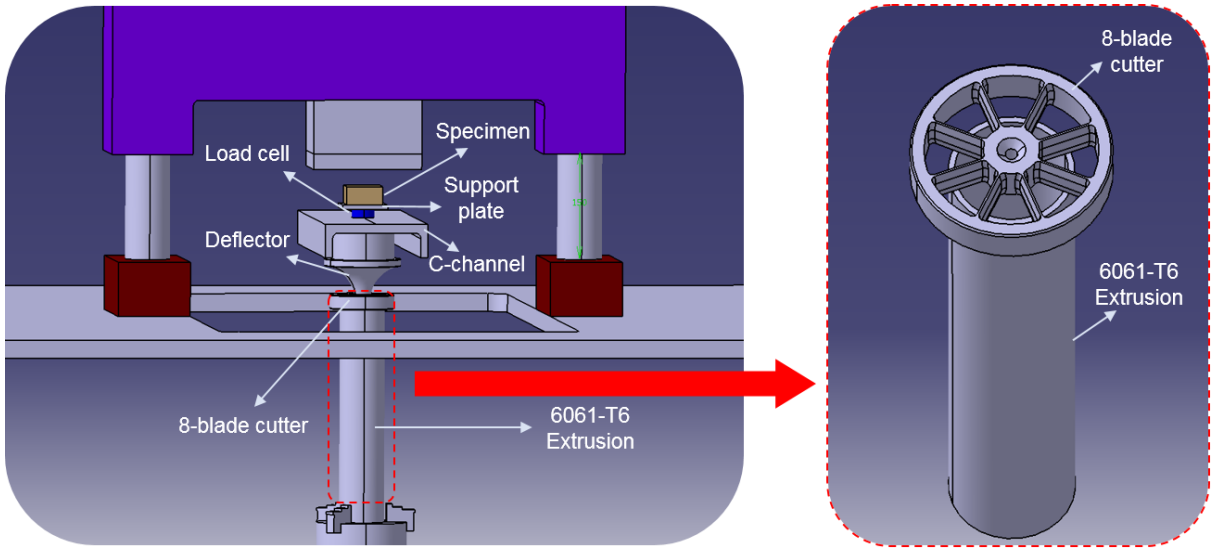

Figure 8. Schematic of the elevated strain rate compression testing apparatus.

5.1. Finite element model (FEM) of the apparatus

FEA was carried for the dynamic testing apparatus considering the highest strain rate of interest for this research (200 s^{-1}). Foam specimens within H200 and H45 groupings which have the highest and lowest densities were considered to constrain the analysis to the most conservative cases. The finite element (FE) mesh and keyword deck were generated by LS-PrePost. All simulations were completed utilizing the finite element software LS-DYNA. Details of the FEM and simulation results are provided below.

Since the simulation of the cutting process is computationally expensive and time-consuming [59,60], a spring element was applied to mimic the cutting mechanism and support the aluminum c-channel, as shown in Figure 9. The experimental load/displacement responses from the cutting of an aluminum 6061-T6 extrusion with the dimension described in the previous section were input into the material model of the spring element. To further increase the efficiency of the FEA, the dropping entity (including the impact plate) and deflector were modeled as simple rigid plates with only one solid element in the thickness direction, as illustrated in Figure 9. As these two parts were fabricated from 4140 steel (an alloy with high yield strength in

comparison to the other components) and negligible deformation was expected, simplifying their geometries in the FEM did not significantly influence the desired simulation results from the components of interest. The FEM of other components, namely, the aluminum c-channel, load cell, supporting plate, and foam specimen were generated according to their true geometries and dimensions. The primary objective of this FEA was to select a suitable supporting plate which would not significantly influence the dynamic mechanical response data captured by the load cell. Therefore, a supporting plate with different geometries and composed of two different materials, 6061-T6 aluminum and carbon fiber, were considered in the simulation.

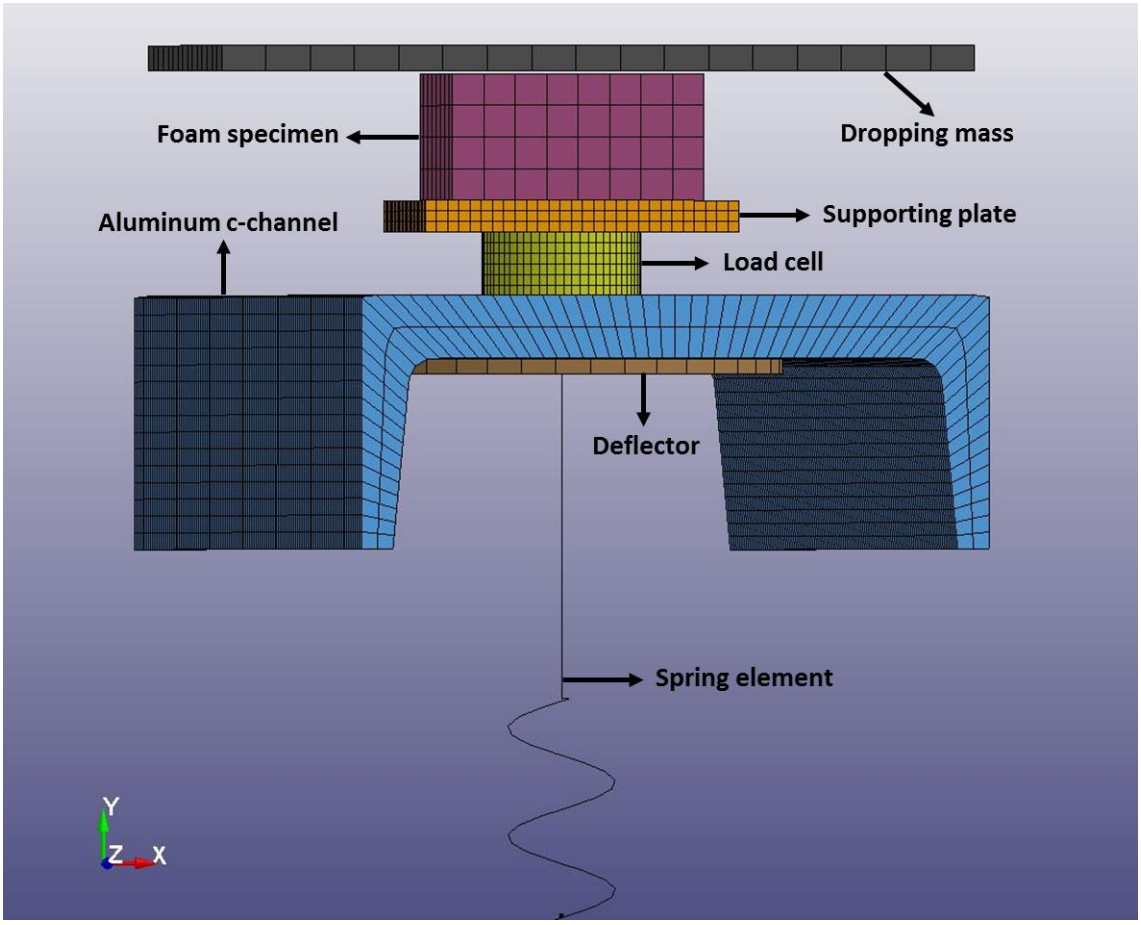

Figure 9. FEM of the elevated strain rate compression test.

5.1.1 Element discretization

Except for a discrete element which was utilized for simulating the cutting process via a nonlinear spring, the models of the dropping mass, foam specimen, supporting plate, load cell, aluminum c-channel, and deflector were all generated with hexahedron solid elements. To add the large mass of the dropping crosshead in the simulation, an element named "ELEMENT_MASS_PART" in LS-DYNA [61] with a translational mass of 45.45 kg was tied to the dropping mass. As the foam model was fully crushed and hence experienced a large deformation, a fully integrated, selectively reduced (S/R) solid element section was employed for solid elements within the foam model to prevent hourglassing. To increase the simulation efficiency without reducing accuracy, a fully integrated, S/R solid element formulation intended for elements with poor aspect ratio was selected for the solid elements within all other components.

5.1.2 Material models

Since closed-cell PVC and PES foams investigated in this study were rigid foams and they would not fully recover their initial shapes after being crushed, MAT_063 (MAT_CRUSHABLE_FOAM) in LS-DYNA [61] was selected to model the foam specimens. As the compressive response of PVC and PES foams under the 200 s^{-1} strain rate loading has not been previously investigated, experimental load/displacement responses of the foam specimens within H45 and H200 groupings from the quasi-static test were input into this material card. The piezoelectric impact load cell (model #:200C20) was constructed with stainless steel which possesses a stiffness of 11 kN/μm. Therefore, MAT_001 (MAT_ELASTIC) in LS-DYNA [61] was selected for the load cell model. Parameters (density, modulus of elasticity, and Poisson's ratio) required for this material model are available from the product specifications provided by the sensor supplier PCB Piezotronics [62]. To investigate the load-bearing capacity of the

supporting plate, a non-iterative plasticity simple plastic strain failure material model, MAT_013 (MAT_ISOTROPIC_ELASTIC_FAILURE) in LS-DYNA [61], was selected. Elements with this material model can experience both elastic and plastic deformations. An optional variable "ETAN", namely plastic hardening modulus, could be input into this material model to define the plastic deformation region. Since the maximum stress experienced by the supporting plate during the impact test (simulation) was significantly less than the compressive yield stress of both carbon fiber and 6061-T6 aluminum materials considered in this study, the default value of "0" for plastic hardening modulus was applied. As previously indicated in the apparatus design, two possible materials (6061-T6 aluminum and carbon fiber) were considered for the supporting plate. The mechanical properties of these two materials were input into this material model through a universal input deck and substituted between simulations. A piecewise linear isotropic plasticity material model based on the von Mises yield criterion, MAT_024 (MAT_PIECEWISE_LINEAR_PLASTICITY), was utilized to model the elastoplastic behavior of the 6061-T6 aluminum c-channel. Effective stress versus effective plastic strain data for the material 6061-T6 aluminum was input into this material model. MAT_020 (MAT_RIGID) and MAT_S03 (SPRING_ELASTOPLASTIC) were utilized to model the rigid components (impact plate and deflector) and approximated the cutting tool, respectively. More details of each material model utilized in the FEA are shown in Appendix B.

5.1.3 Contact algorithms

Segment based contact, namely the AUTOMATIC_SURFACE_TO_SURFACE algorithm from LS-DYNA [61], was applied between the impact plate and foam specimen, and between the foam specimen and supporting plate. The impact plate was defined as the master entity in the contact definition, and the foam specimen was defined as the slave entity since the impact plate

was modeled with a rigid material. The supporting plate was set as the master in the contact between the foam specimen and the supporting plate. During this two-way contact, both slave and master nodes were checked for penetration through the master and slave segments, respectively, by the additional option card "SOFT=2" with default parameters to invoke penalty-based contact in which the contact stiffness is inversely proportional to the time step of the simulation. Therefore, the contact force can be adjusted, and the penetration can be prevented by changing the time scale factor. Furthermore, in order to avoid undesirable oscillation in the contact forces, a viscous damping coefficient of 0.20 was applied following the recommendations of the LS-DYNA User's Manual [61]. In the experimental test, the supporting plate was fastened on the upper surface of the load cell, with the load cell assembly and supporting plate fastened on the upper surface of the aluminum c-channel. The contact algorithm "TIED_NODES_TO_SURFACE" was applied between the supporting plate, load cell, and aluminum c-channel to approximate the fastening mechanisms implemented in the apparatus. Nodes appearing on the lower and upper surfaces of the load cell were defined as two different node sets. Segments on the lower surface of the supporting plate and the upper surface of the aluminum c-channel were defined as two segment sets. In this tied contact, the node sets were always set as the slave and were constrained to move with the master surfaces (segment sets); there was no presence of penetration. A similar contact algorithm named TIED_SURFACE_TO_SURFACE was applied between the aluminum c-channel and the deflector. In this contact, segments on the lower surface of the aluminum c-channel and upper surface of the deflector were defined as the slave and master, respectively.

5.1.4 Initial conditions and simulation environment

Since the energy dissipation system was fixed on a three-jaw chuck in the experimental test, correspondingly in the simulation the lower node of the spring element was fully constrained of

both displacement and rotation in *x*, *y*, *z* directions. An initial velocity of 5 m/s was assigned to the impact plate, which resulted in a compressive strain rate of approximately 200 s^{-1} within the foam specimen. Due to the geometrical, material, and contact nonlinearities associated with the problem studied, an explicit time integration scheme was chosen for simulation of the dynamic test. All FEA was performed with LS-DYNA, utilizing shared memory processing (SMP), with double precision solver (Revision # 105896). Data of loadings provided by the impact plate and detected by the load cell from the simulation results were output at 100 kHz. Results of the simulation of various configurations are compared and listed in section 5.3.

5.2. FEM of different supporting plates

5.2.1 Aluminum supporting plate

Due to the relatively low density and high strength of aluminum alloys, a 63.5 mm × 63.5 mm aluminum 6061-T6 plate with a thickness of 6.35 mm was simulated first to support a foam specimen with standard size (50.8 mm × 50.8 mm × 25.4 mm) as shown in Figure 10(a) (configuration 1). The mass of the aluminum supporting plate was approximately 70 g.

To further reduce the mass of the supporting plate, a tapered aluminum 6061-T6 plate with a thickness of 6.35 mm was simulated in configuration 2, as shown in Figure 10(b). The widths of the upper surface and bottom square surface of the tapered aluminum plate were 63.5 mm and 38.1 mm, respectively. The mass of the tapered aluminum 6061-T6 supporting plate was approximately 40 g.

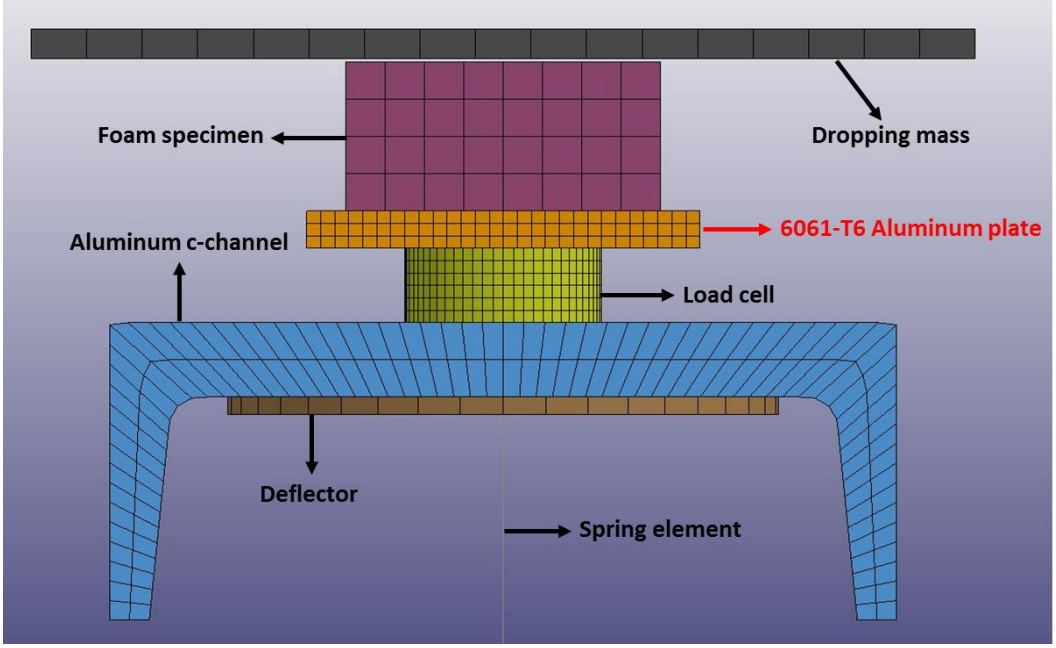

(a)

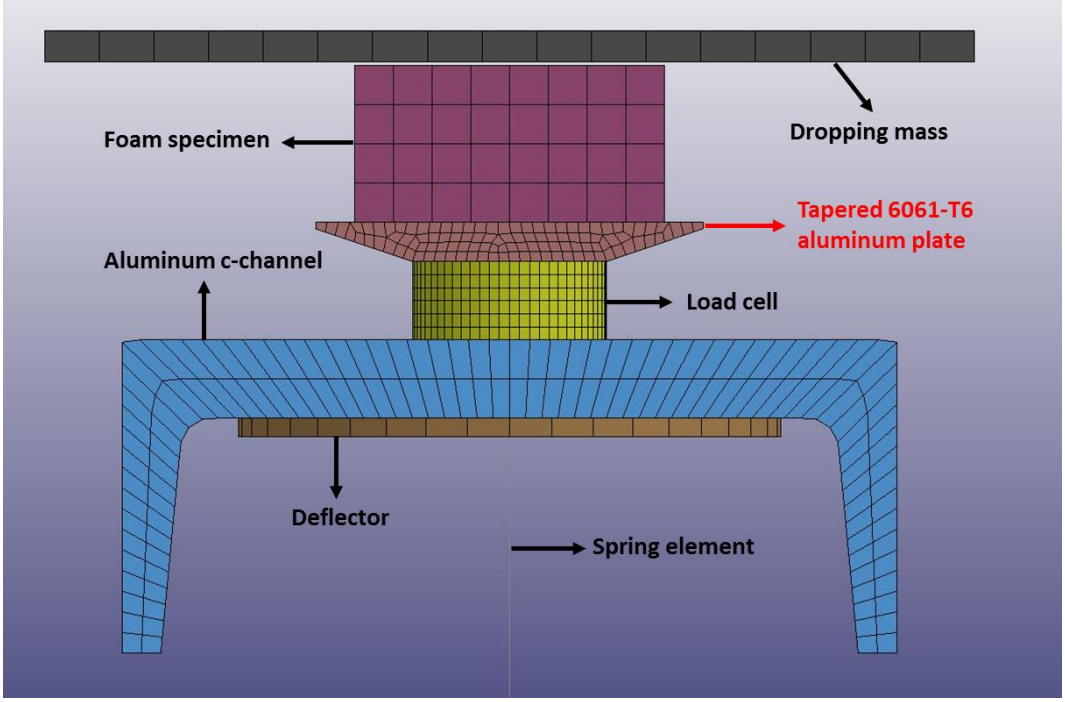

(b)

Figure 10. FEM of the dynamic compression test with an (a) aluminum supporting plate (configuration 1) and (b) tapered aluminum supporting plate (configuration 2).

5.2.2 Carbon fiber supporting plate

Many composite materials possess lower densities and higher yield strengths than aluminum alloys. A 63.5 mm × 63.5 mm × 6.35 mm composite plate, comprised of ultra-strength

lightweight carbon fiber sheet, supplied by McMaster-Carr, was selected as an alternative supporting plate, as shown in Figure 11 (configuration 3). The material properties of the carbon fiber sheet are summarized in Table 3 [63]. Except for the supporting plate, material models all other components were consistent between simulations. The mass of the carbon fiber supporting plate was approximately 30 g.

Table 3. Mechanical properties of 6.35 mm thick carbon fiber sheet [63].

Material	Carbon fiber sheet
Thickness (inches)	0.25
Density (kg/m^3)	1384.0 - 1854.5
Tensile Strength (MPa)	827.4 - 1206.6
Compressive Strength (MPa)	517.1 - 882.5
Flexural Strength (MPa)	613.6 - 1199.7

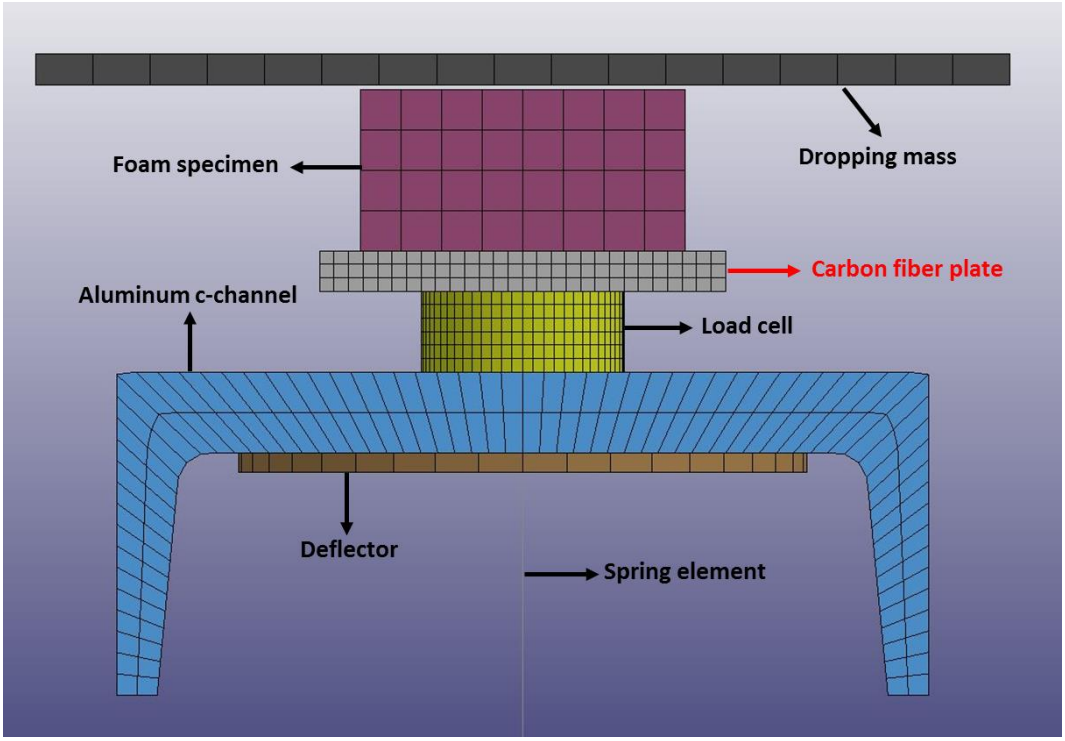

Figure 11. Simulation of the dynamic compression test with a carbon fiber supporting plate (configuration 3).

5.3. Results of the FEA

Impact forces provided by the impact plate and detected by the load cell, obtained from the simulation of foam specimens within H45 grouping at 200 s^{-1} strain rate, are presented in Figures 12(a) and (b), respectively. Figure 12(b) illustrates the plateau region of the impact force provided by the impact plate and the force detected by the load cell in configuration 1, 2, and 3. As shown in Figure 12(a), the impact force generated by the impact plate in different configurations are almost identical. However, the force detected by the load cell in different configurations deviates slightly, especially in the plateau region shown in Figure 12(b). Due to the lower density (smaller mass) of the carbon fiber plate, it is observed that the variation between the impact force and the force measured by the load cell in configuration 3 is the lowest of the configurations.

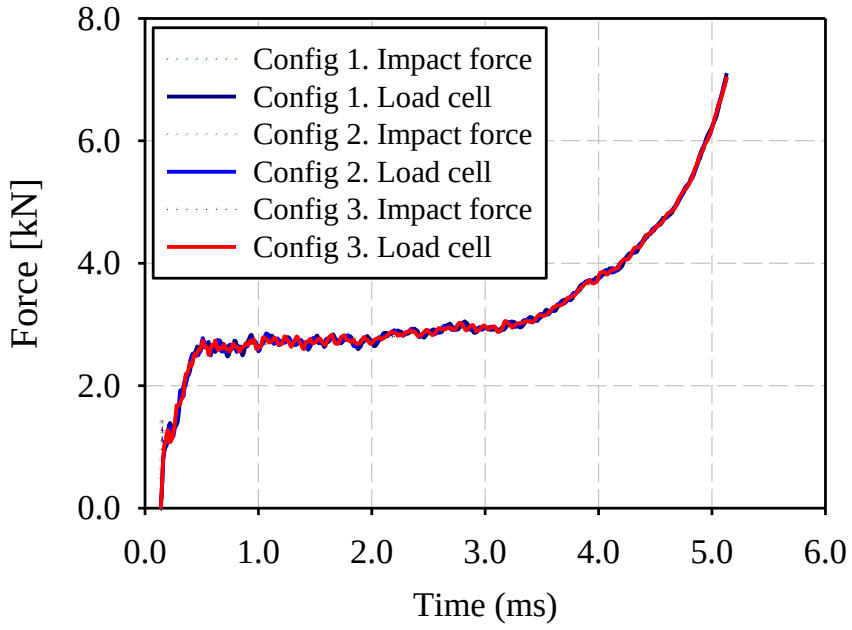

(a)

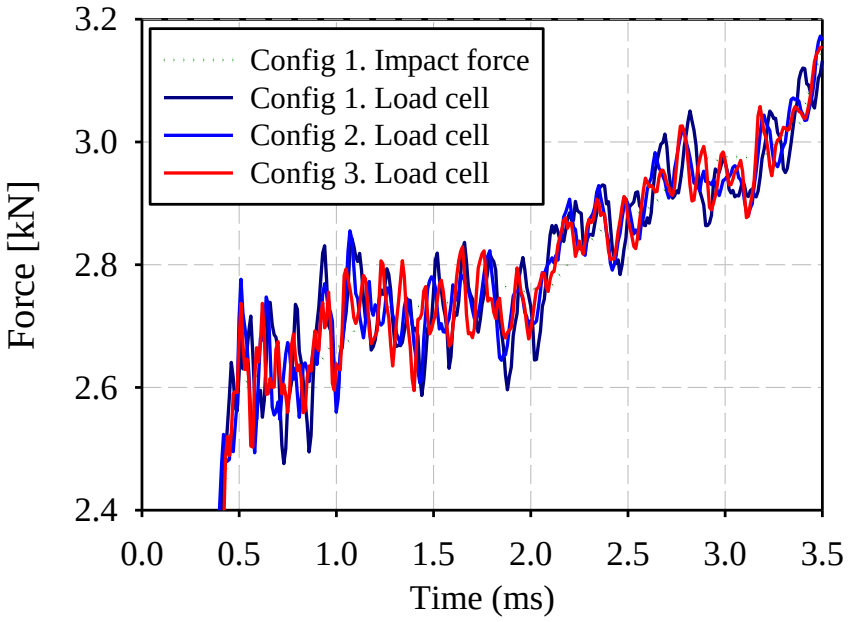

(b)

Figure 12. (a) Results of impact forces provided by the impact plate and detected by the load cell in configurations 1 to 3 from the simulation of compression of PVC foam specimens within H45 grouping at 200 s^{-1} strain rate; (b) simulation results of the forces within the plateau region.

Similar observations are shown in Figures 13(a) and (b), which illustrate the results of the simulation of the foam specimen within H200 grouping under 200 s^{-1} strain rate. From both Figures 13(a) and (b), it is observed that the degree of variation between the impact forces provided by the impact plate and detected by the load cell is lower in comparison to the H45 grouping. This is because the foam specimen with a higher density within the H200 grouping can bear much higher loads than their H45 counterparts. The effect of the dynamic forces generated by the supporting plate reduced for specimens within the H200 grouping. Again, simulation of configuration 3 in which the carbon fiber plate was utilized to support H200 foam specimens displayed the smallest variations between the impact force and the force detected by the load cell.

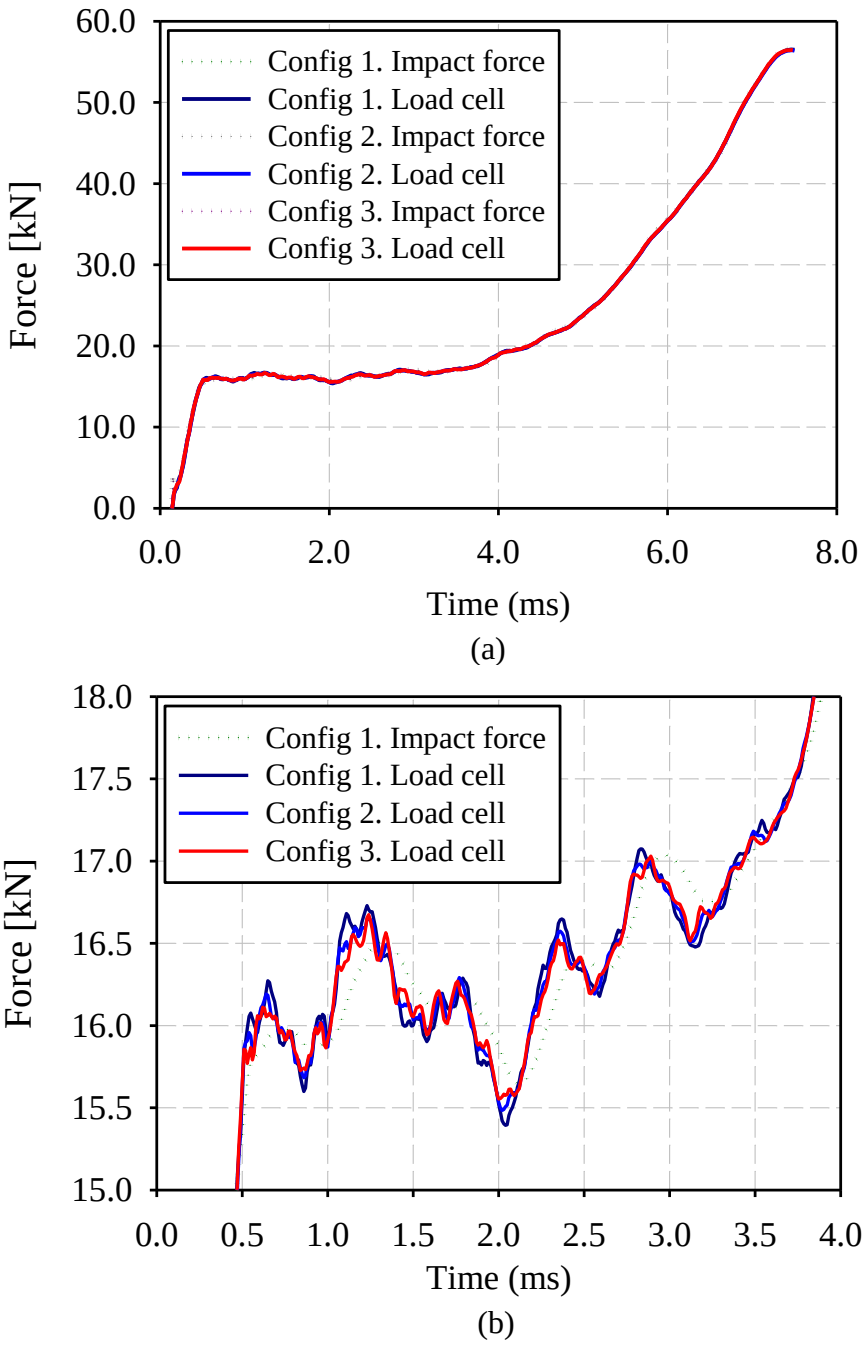

Figure 13. (a) Results of impact forces generated by the impact plate and detected by the load cell in different configurations for the simulation of PVC foam specimens within H200 grouping at 200 s^{-1} strain rate and (b) simulation results of the forces in the plateau region.

To quantify the variations between the impact forces provided by the impact plate and detected by the load cell in the simulation, the average error, e, and validation metric, V, were

calculated for the simulation of each configuration, as defined in [64]. Equations (5) and (6) present the absolute calculation of the average error e and validation metric V.

$$e = \frac{1}{T}\int_0^T \left|\frac{Load\ cell(t) - Impact\ force(t)}{Impact\ force(t)}\right| dt \tag{5}$$

$$V = 1 - \frac{1}{T}\int_0^T \tanh\left|\frac{Load\ cell(t) - Impact\ force(t)}{Impact\ force(t)}\right| dt \tag{6}$$

Table 4 shows the results of the average error and validation metric between the impact force and the force detected by the load cell in each configuration. For both H45 and H200 foam specimens, the average error continuously decreased from configurations 1 to 3. Correspondingly, the validation metric increased. This was expected as the vibration and dynamic effect of the supporting plate would increase with the increase of its mass. Due to the lower load-bearing capacity of the foam specimen within H45 grouping, the dynamic effect of the supporting plate seemed to influence the results more than the specimen within the H200 grouping. This was proved by the increased average error and decreased validation metric value of H45 grouping than H200 grouping at each configuration. From Table 4, it was observed that configuration 3, in which the carbon fiber plate was utilized as the supporting plate, shows the smallest average error and largest validation metric. Therefore, the 63.5 mm × 63.5 mm × 6.35 mm carbon fiber plate was selected to support the PVC and PES foam specimens in the experimental test.

Table 4. Validation results of different simulation configurations for the 200 s^{-1} strain rate tests.

Foam groupings	Configuration	Average error e	Validation Metric V
H45	1	0.029	0.976
	2	0.023	0.981
	3	0.020	0.984
H200	1	0.021	0.988
	2	0.019	0.990
	3	0.011	0.992

6. EXPERIMENTAL TESTING METHODOLOGIES

6.1. EDS analysis

To better understand the material compositions of the PVC and PES foams. EDS analysis was conducted on specimens within H45, H80, H100, and H130 groupings for PVC foam and F50, F90, and F130 groupings for PES foam. During the EDS analysis, electron beams were generated by the FEI Quanta 200 Field Emission Gun (FEG) which was utilized in the SEM analysis as well. X-rays given off by a test specimen were detected by an EDAX Octane detector which was incorporated with a silicon drift detector (SDD). Signals from the detector were analyzed by TEAM Software (version 4.0.2). One cubic centimeter foam specimens were examined in the EDS analysis. Two areas from the interested surface of a specimen were considered as shown in Figure C1 (Appendix C). When the EDS analysis was completed, a report including the spectrum of chemical composition (Figures C2-C5), weight percent and atomic percent of each element detected from the specimen was generated for both areas by the TEAM software.

6.2. SEM analysis

SEM images were acquired for specimens as received and after quasi-static and dynamic compression tests using an FEI Quanta 200 field emission gun (FEG) environmental scanning electron microscope (SEM). As the foam materials are non-conductive, low vacuum mode with a chamber pressure of 70 Pa was applied. A relatively low accelerating voltage of 12 kV for the primary electron beam was selected to prevent damaging the foam materials. Cubic specimens with approximate dimensions 1 cm by 1 cm by 1 cm and cuboid specimens with approximate dimensions 1 cm by 0.5 cm by 0.5 cm were cut from untested and tested foam specimens, respectively. A scalpel blade was applied to make sure that the cutting surfaces were as clean as possible. To prevent contamination, any contact with the surface of interest was avoided.

6.3. Quasi-static compression testing

Uniaxial quasi-static compressive test was conducted in accordance with ASTM standard D1621-16 [15] on an electromechanical MTS machine having a model number LPS-504 which is equipped with a 50 kN load cell, as shown in Figure 14. Three material loading directions, one parallel to foam rise direction and two perpendicular to the foam rise directions were considered. The compressive displacement of the specimen was measured according to the upper platen movement after it contacted the specimen while the lower platen was fixed. Data from the load cell and displacement of the upper platen was acquired using a computer-controlled data acquisition system. Loading and unloading forces, and displacement measurements were recorded at a sampling rate of 20 Hz. The tests were completed at a constant crosshead speed of 5 mm/min at room temperature. A high-resolution camera, providing images at 1038 by 1388 pixels^2, was set up to capture the material deformation during the test.

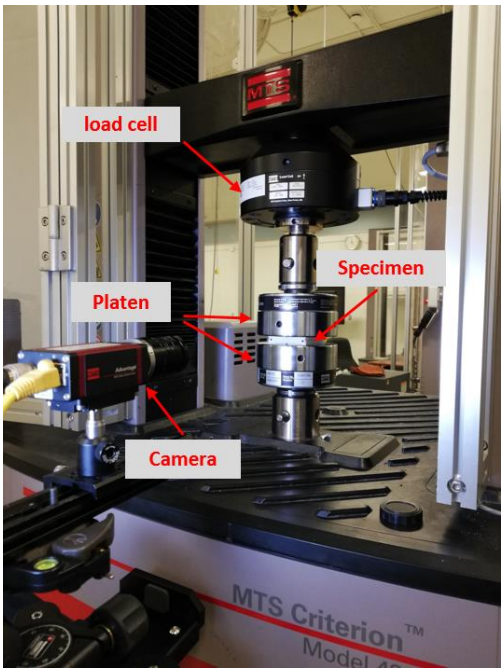

Figure 14. Setup of quasi-static compression test

6.4. Elevated strain rate compression testing

The patented energy dissipation system described in Section 5 was incorporated into a customized drop tower device to conduct the elevated strain rate tests, as shown in Figures 15(a) and (b). A schematic diagram of the dynamic compressing test set up is shown in Figure 16. The drop tower system consisted of a dropping entity, two guide posts which the dropping entity linearly translates along, and a steel support column equipped with a 3-jaw chuck. The dropping entity included a steel block and a 100 mm thick steel plate as the impacting plate. To control the lift height of the dropping entity, a desktop computer with custom-developed software was used. The highest dropping height can result in the maximum impact speed of approximately 7.0 m/s.

As previously described in Section 5, the relative displacement between the impact plate and the specimen support plate was the true compressing displacement of the specimen. The displacement of the dropping entity and c-channel was measured by two micro-epsilon noncontact laser displacement transducers with ranges of 300 mm (model # optoNCDT ILD2300-300) and 100 mm (model # optoNCDT 1607-100), respectively. The piezoelectric impact load cell (model # 200C20), having a range of 89 kN, was manufactured by PCB Piezotronics Inc. The load cell was fastened on the top surface of the c-channel. According to the results of the FEA in Section 5, the 63.5 mm × 63.5 mm × 6.35 mm (thickness) carbon fiber plate was selected and fastened on the top surface of the load cell to support the foam specimen during the impact test. The lightweight yet stiff characteristics of the carbon fiber would result in very little inertial forces arising during impact so that the measured force from the load cell was an excellent measure of the contact force between the 4140 steel impacting plate and the foam specimen.

Analog voltage output from the laser displacement transducer was measured by a National Instruments NI9215, 4 channel, 16 bit, analog input module, which was incorporated into a National Instruments NI9174 CompactDAQ data acquisition system. The output from the piezoelectric load cell was measured using a National Instruments NI9233 module which incorporated integrated electronic piezoelectric (IEPE) signal conditioning. The measurements from the two laser displacement transducers and load cell through the NI9215 and NI9233 modules were recorded using a laptop computer equipped with National Instruments LabVIEW 2019 data acquisition software. For all impact tests, a consistent data sampling rate of 50 kHz was used.

The mass of the load cell and aluminum c-channel was 0.43 kg and 3 kg, respectively. A Photron SA4 high-speed camera was used for capturing the visual observations of the foam deformation during the dynamic test. A frame rate of 10000 frames/s and a shutter speed of 1/35000 s were utilized. Images were obtained with a resolution of 768 by 512 pixels^2. A NI9401 high-speed digital input/output module incorporated into the CompactDAQ system was used to synchronize the data acquisition between the transducer and high-speed camera triggering system. Within the custom-developed LabVIEW 2019 code, timing for appropriate triggering, based on measurements from the 300 mm laser displacement transducer, was implemented for transducer data acquisition and digital signal output to activate and synchronize the high-speed camera.

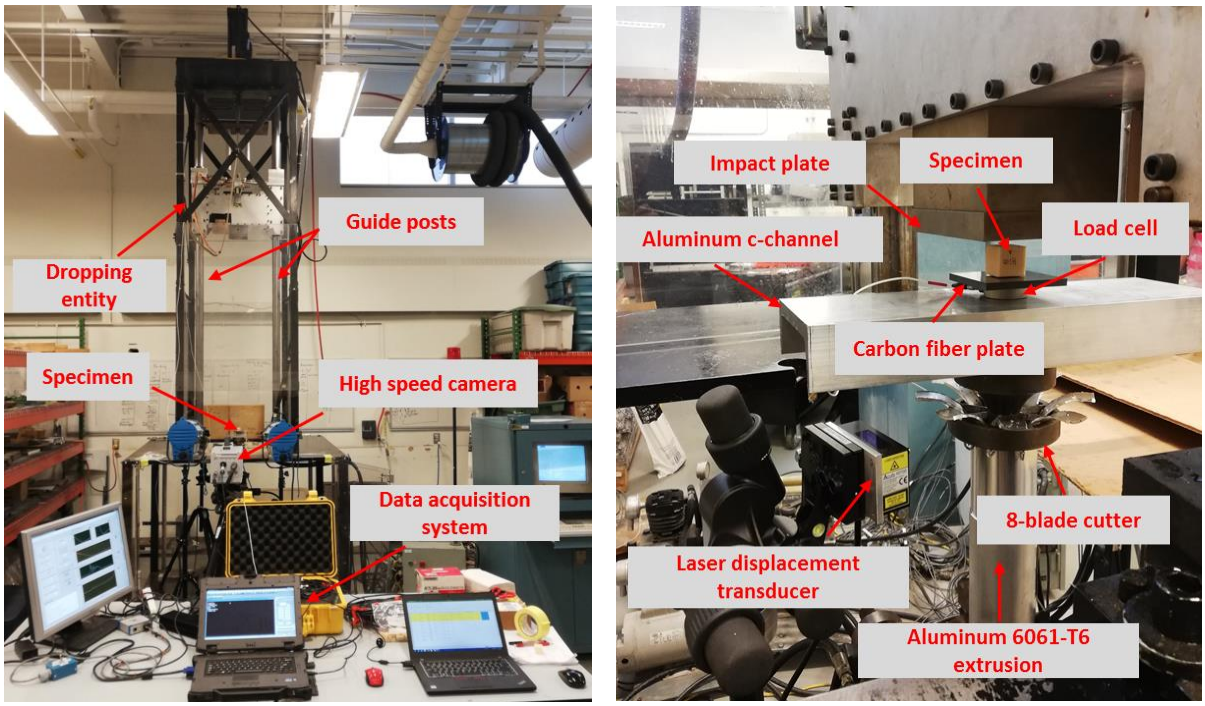

(a) (b)

Figure 15. The drop tower system (a) and support (b) of a specimen for the dynamic compression test.

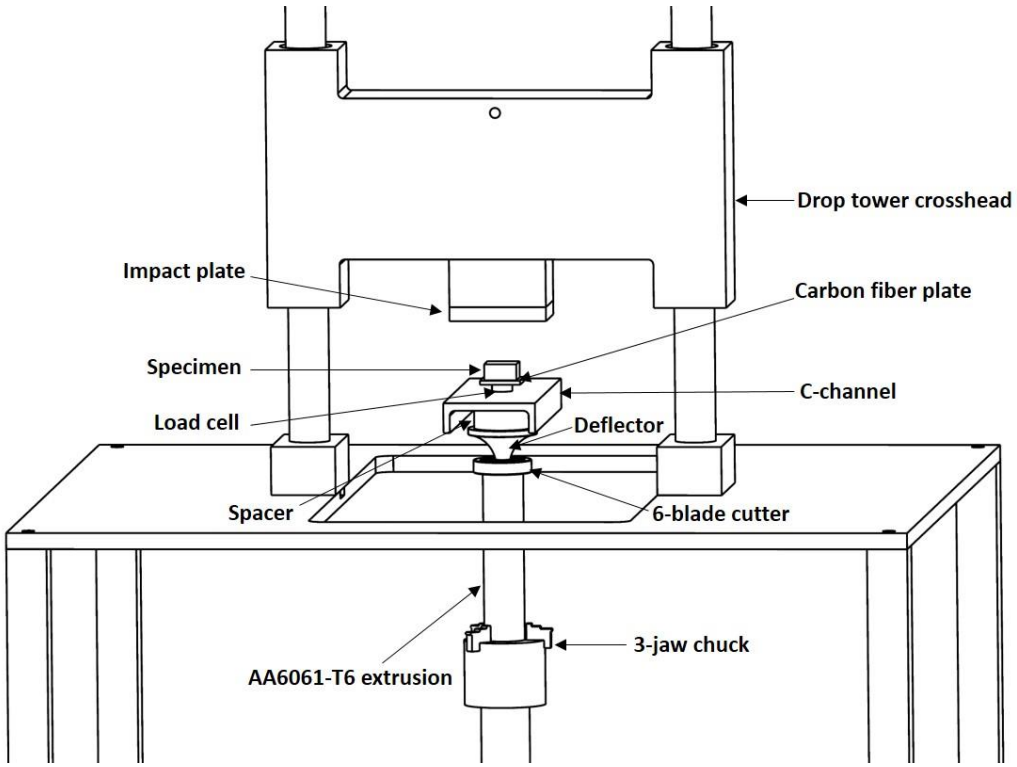

Figure 16. Schematic diagrams for the dynamic compression test setup.

7. RESULTS & DISCUSSION

7.1. Observations of EDS analysis

As shown in Table 5, four elements, namely, carbon (C), nitrogen (N), oxygen (O), and chlorine (Cl) were detected from the EDS testing results of all four PVC foam densities. The averaged weight percent of each element detected are shown in Table 5. As expected, the share of carbon (C) is high; about half of the total specimen weight. This is due to PVC being a repeating hydrocarbon chain connecting carbon and hydrogen atoms in its base elemental form, as shown in Figure 17(a). The hydrocarbon chains also feature elemental chlorine-to-carbon-bonds. The weight percent of chlorine was 31.29% to 36.28% for the four different foam densities. Other than the elements carbon (C) and chlorine (Cl) that from the base PVC material itself, PVC foams can also have extra elements within their composition. For instance, nitrogen and carbon dioxide can be used as foaming/blowing agents for foam production. Small amounts of nitrogen (N) and oxygen (O) were detected in the PVC foams, as indicated in Table 5.

In terms of PES foams, four elements carbon (C), oxygen (O), silicon (Si), and sulfur (S) were detected for specimens within F50 and F90 groupings. However, the amount of silicon (Si) was only 0.41% and 0.22% in weight for F50 and F90 specimens, respectively. The tiny amount of the silicon (Si), which is a component of sand, may have come from soil impurities. No silicon (Si) element was detected from the PES foam specimen within the F130 grouping. The weight percent of each element detected from PES foam is shown in Table 6. As PES molecular structure consists of aromatic rings, as shown in Figure 17(b), and carbon (C) accounted for more than half of the specimen weight for the PES foam. The aromatic rings are alternatively connected with ether and sulfone groups, and sulfur and oxygen stand for about 20% in weight, as shown in Table 6.

With the relatively large standard deviation of the results and the small variation of the amount of each element at different foam densities, it can be concluded that the amount of each element detected for PVC and PES foams with different densities are quite consistent. The consistent portions of the elements of the PVC and PES foams at different densities indicate that the foam solid material composition does not change with the increase of foam density.

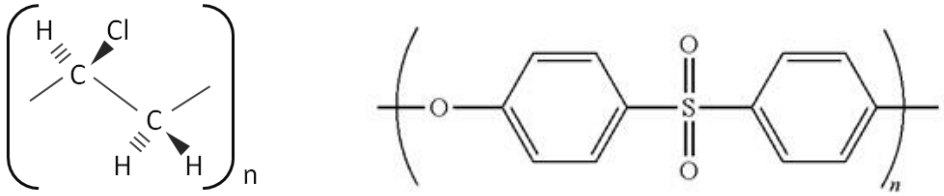

(a) (b)

Figure 17. Molecular structures of (a) PVC and (b) PES polymers.

Table 5. Weight percent (%) and standard deviation (S.D) of the chemical composition of PVC foam.

	C	S.D.	N	S.D.	O	S.D.	Cl	S.D.
H45	54.40	3.19	4.25	0.55	5.08	0.69	36.28	4.42
H80	53.95	0.09	4.48	0.13	3.98	0.04	37.61	0.01
H100	56.92	0.46	5.74	1.47	3.92	0.59	33.43	2.52
H130	57.85	0.25	6.47	0.11	4.40	0.21	31.29	0.35

Table 6. Weight percent (%) and standard deviation (S.D) of the chemical composition of PES foam.

	C	S.D.	O	S.D.	Si	S.D.	S	S.D.
F50	56.97	0.10	19.94	1.21	0.41	0.00	22.69	1.11
F90	58.60	0.48	20.52	0.86	0.22	0.07	20.67	0.45
F130	61.13	0.32	20.07	0.73	0.00	0.00	18.82	0.40

7.2. Observations of SEM analysis

SEM images of the PVC and PES foam specimens were acquired prior to and after the compression tests. The SEM images can be used to identify and investigate the main microstructural characterization and deformation mechanisms that cause mechanical degradation of the foam material. An isometric view of a typical foam specimen used in the SEM imaging is shown in Figure 18 along with SEM images of planes A, B, and C illustrating the polygonal structure of the foam cells appearing on the cutting surface. In addition, the loading direction, in the negative *z*-axis direction, is also indicated. When loading parallel to foam rise direction, plane A is perpendicular to the load axis, planes B and C are parallel to the loading direction. SEM images obtained from planes A and B of original and tested PVC foam specimens within H200 grouping and PES foam specimens within F130 grouping are shown in Figures 19 and 20, respectively. Details of the SEM analysis including foam cell size, cell shape anisotropy, and cell wall thickness for both PVC and PES foams with various densities are shown in the following subsections.

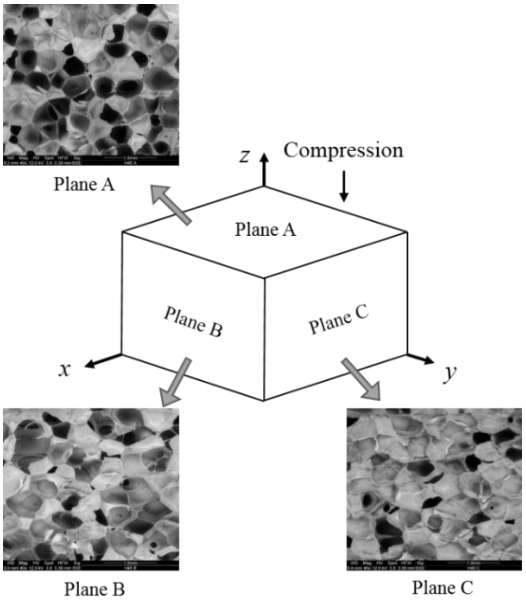

Figure 18. Isometric view of cubical foam specimen for SEM Analysis; foam rise direction is along with the positive direction of z-axis.

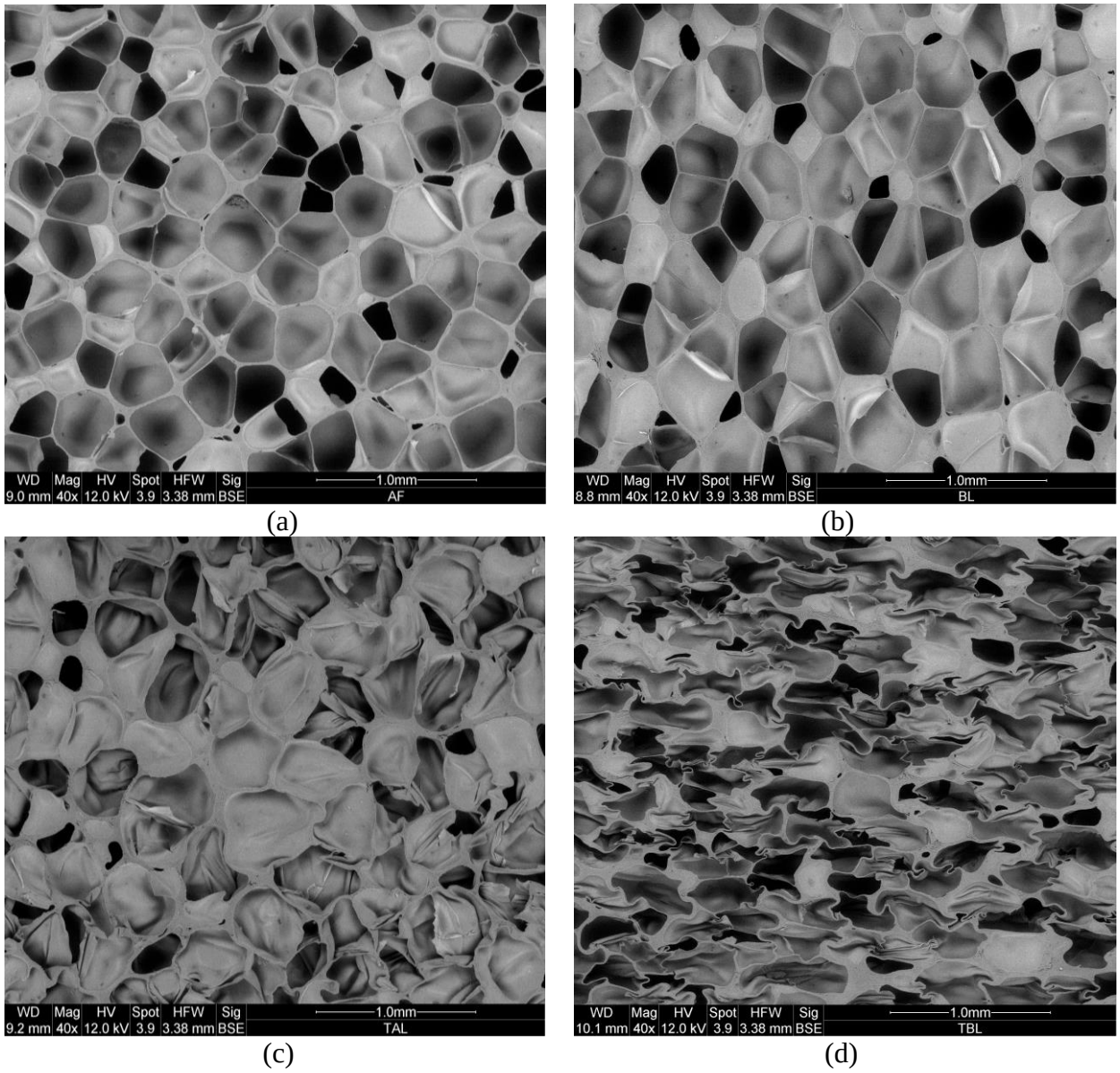

Figure 19. SEM images of (a) plane A, (b) plane B of an untested specimen within H200 grouping; (c) plane A and (d) plane B of a specimen within H200 grouping after quasi-static loading in the foam rise direction.

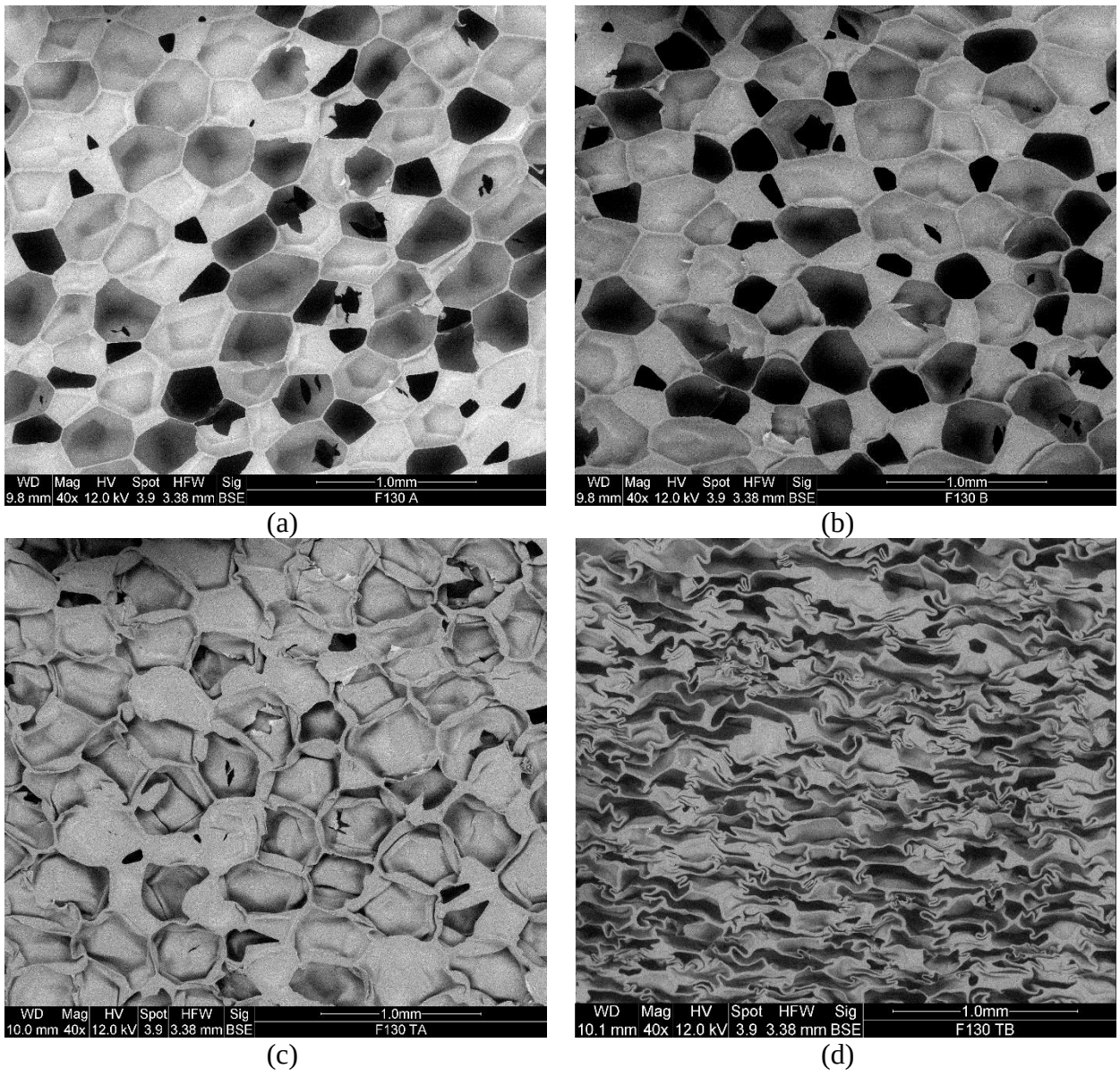

Figure 20. SEM images of (a) plane A, (b) plane B of an untested specimen within F130 grouping; (c) plane A and (d) plane B of a specimen within F130 grouping after quasi-static loading in the foam rise direction.

7.2.1 Cell size and shape anisotropy

Anisotropy in the cell shape is defined as the ratio of the largest cell dimension to the smallest (shape anisotropy, R). The typical value of R for polymeric foams is 1.3, but it can vary from 1 (isotropic) to more than 10 (highly anisotropic) [50].

Applying the intersecting line method from the ASTM D 3576-15 [65] protocol from SEM images of foam samples, the shape anisotropy value, R, has been measured for both PVC and PES foam cells. Horizontal and vertical lines were drawn on the SEM image. Cell sizes in the horizontal and vertical directions (d_H and d_V, respectively) were obtained by dividing the line length to the number of cells intersecting with the line and multiplying the resultant figure by 1.623 [65]. The measurements were repeated for each plane (i.e., A, B, and C). Shape anisotropy R was calculated by dividing the larger cell size to the smaller one for all three planes (A, B, and C) of each foam density. The results are presented in Table 7. Both PVC and PES foam cells show substantial variation in cell sizes, which requires measuring a large number of cells to obtain an accurate average cell size value. Therefore, two images with the lowest possible magnification (27 X) of each plane of each density (total 48 images) were measured by using the SEM image measuring software Scandium, corresponding to more than 700 cells being measured for each plane to ensure the accuracy of the measurements. SEM images of specimens within H130 and F130 groupings, from the A and B planes, with the horizontal and vertical intersecting lines are shown in Figures D1 and D2 (Appendix D) as an example.

Cell dimensions of foams from Table 7 indicate that PVC and PES foam specimens have similar horizontal and vertical cell diameters on plane A. Correspondingly, the shape anisotropy appearing on plane A is quite close to unity. However, cells on planes B and C, which are parallel to the foam rise direction, have different dimensions in the horizontal and vertical directions resulting in shape anisotropy of the cells on planes B and C of PVC foam with all densities and PES foam with the lowest density (F50 grouping) being significant as shown in Table 7. This indicates that the cells elongated in the foam rise direction during the foaming process. Although shape anisotropy of cells on planes B and C of PES foam specimens within F90 and F130

groupings are evident, the anisotropic levels are relatively lower compared with other densities. Moreover, comparing cell dimensions at different foam densities, both PVC and PES foam cell sizes on A plane (as a representative for general cell size) are not simply dependent on foam densities. In other words, the cell sizes of PVC and PES foams do not continuously increase or decrease with the increase of foam density.

Table 7. Cell dimensions on planes A, B, and C of PVC and PES foams with different densities.

Grouping		Plane	Horizontal diameter d_H (μm)	Vertical diameter d_V (μm)	R
PVC foam	H45	A	496.61	498.10	1.00
		B	513.19	681.58	1.33
		C	500.19	689.81	1.38
	H80	A	345.65	335.84	1.03
		B	340.86	463.01	1.36
		C	339.84	439.18	1.29
	H100	A	449.99	456.66	1.01
		B	425.48	601.46	1.41
		C	445.17	666.89	1.50
	H130	A	366.32	372.16	1.02
		B	358.87	514.25	1.43
		C	406.45	613.94	1.51
	H200	A	431.28	425.92	1.01
		B	398.71	573.15	1.44
		C	392.37	568.74	1.44
PES foam	F50	A	498.35	485.80	0.97
		B	455.42	737.78	1.62
		C	459.78	780.79	1.70
	F90	A	425.17	469.41	1.08
		B	436.35	482.04	1.22
		C	503.40	478.33	1.15
	F130	A	570.89	612.55	1.07
		B	534.76	587.91	1.09
		C	523.83	644.72	1.23

7.2.2 Cell edge thickness

Cell edge thickness appearing on planes A, B, and C of the PVC and PES foams with different densities were measured, and the results are shown in Table 8. Approximately 80 measurements were randomly taken on the SEM image of each plane. Examples of the measurement of cell edge thickness on planes A and B of specimens within H130 and F130 groupings are shown in Figures D3 to D6 (Appendix D). From Table 8, the cell edge thickness measured on planes A, B, and C of each density are quite consistent and all of them increase with increasing foam density. For PVC foam specimens ranging from H45 to H200 groupings and PES foam specimens ranging from F50 to F130 groupings, the average cell edge thickness increased from 7.44 μm and 6.87 μm to 20.41 μm and 10.25 μm, respectively. At comparable densities, the cell wall thicknesses of PVC foam are larger than those of the PES foam. Moreover, large standard deviation values show substantial variation in cell edge thickness. The value of the standard deviation increases with the increase of foam density as well. From the SEM images of tested specimens, it is seen that the major cell deformation mechanism for both PVC and PES foams was the formation of, and rotation along, plastic hinges, as shown in Figures 19(d) and 20(d). Therefore, the majority of compressive energy was absorbed through the plastic bending of cell edges. With constant cell sizes, thicker edges can better resist elastic bending in the elastic region and plastic collapse in the plateau region than thin edges. At higher densities, both PVC and PES foam shows thicker cell edges than that of lower densities, which is the most likely reason that higher densities show superior compressive properties, such as increased elastic modulus, compressive strength, plateau stress, and energy absorption.

Table 8. Cell wall thickness on planes A, B, and C of untested PVC and PES foams.

Grouping		Plane	Cell wall thickness *t* (μm)	S.D. of measurement on one SEM image	Average cell wall thickness *t* of Planes A, B, and C (μm)
PVC foam	H45	A	7.48	4.01	7.44
		B	7.42	3.69	
		C	7.43	3.33	
	H80	A	8.89	5.48	8.84
		B	8.65	4.06	
		C	8.97	4.75	
	H100	A	12.00	5.57	11.9
		B	11.66	7.47	
		C	12.05	6.25	
	H130	A	14.00	6.83	13.86
		B	14.09	5.87	
		C	13.48	5.81	
	H200	A	20.51	10.72	20.41
		B	20.57	12.04	
		C	20.14	12.09	
PES foam	F50	A	7.02	3.70	6.87
		B	6.46	3.71	
		C	7.14	2.75	
	F90	A	8.12	3.62	8.16
		B	8.25	3.91	
		C	8.11	4.35	
	F130	A	10.17	4.62	10.25
		B	10.40	4.81	
		C	10.17	5.37	

7.3. Mechanical responses of PVC and PES foams

7.3.1 Consistency of observations from repeated tests

Tests were repeated three times for each density of PVC and PES foams in each loading direction for the 0.003 s^{-1} quasi-static, 50 s^{-1} and 100 s^{-1} dynamic tests. Considering the potential of damage or overloading of transducers when testing at the highest strain rate, two repeated tests were conducted for specimens subjected to dynamic compressive tests at 200 s^{-1}. The results of all repeated tests are very consistent for all densities. For example, the consistency of the results of PVC foam specimens within H45 grouping and PES foam specimens within F50 grouping under quasi-static strain rate are shown in Figures 21(a) and (c), respectively. The consistency of the results of PVC foam specimens within H200 grouping and PES foam specimens within F90 grouping under 100 s^{-1} strain rate tests are shown in Figures 21(b) and (d), respectively. Specimens A1-A3 were loaded in the foam rise direction, specimens B1-B3 and C1-C3 were loaded perpendicular to the foam rise directions (loading on planes B and C, respectively). Both loading and unloading stress/strain responses of the three repeated tests under quasi-static tests are very consistent. For the dynamic tests, the high level of consistency in stress/strain responses prior to the densification region was also evident. However, the degree of consistency was influenced, typically in the dynamic tests at 200 s^{-1} strain rate, when the sacrificial energy dissipation experiences significant cutting (typically greater than 3 mm). This influence was observed only within the unloading phase of the stress/strain responses in the dynamic tests. Moreover, the unloading phase in dynamic tests was not the pure unloading phase of the specimen but included the fluctuation and rebound associated with the energy dissipation device. However, the results of repeated dynamic tests for all materials were still considered consistent.

As shown in Figures 21(a) to (d), the compressive behavior of PVC and PES foams in the foam rise direction (loading on plane A) is different from observations acquired from specimens with loading perpendicular to the foam rise directions (loading on planes B or C). However, the compressive responses of PVC foam in the two perpendicular to foam rise directions (loading on planes B or C) are almost identical. On the contrary, the compressive responses of PES foam in the two perpendicular to foam rise directions (loading on planes B or C) are evidently different, especially under elevated strain rate tests. This was most likely caused by different cell structural anisotropy on planes B and C. Therefore, tests with loading on plane B were discussed as loading in perpendicular to foam rise direction and compared with the compressive behavior in the foam rise direction for PVC foam. However, compressive responses of the PES foam when loading on planes B and C were considered separately.

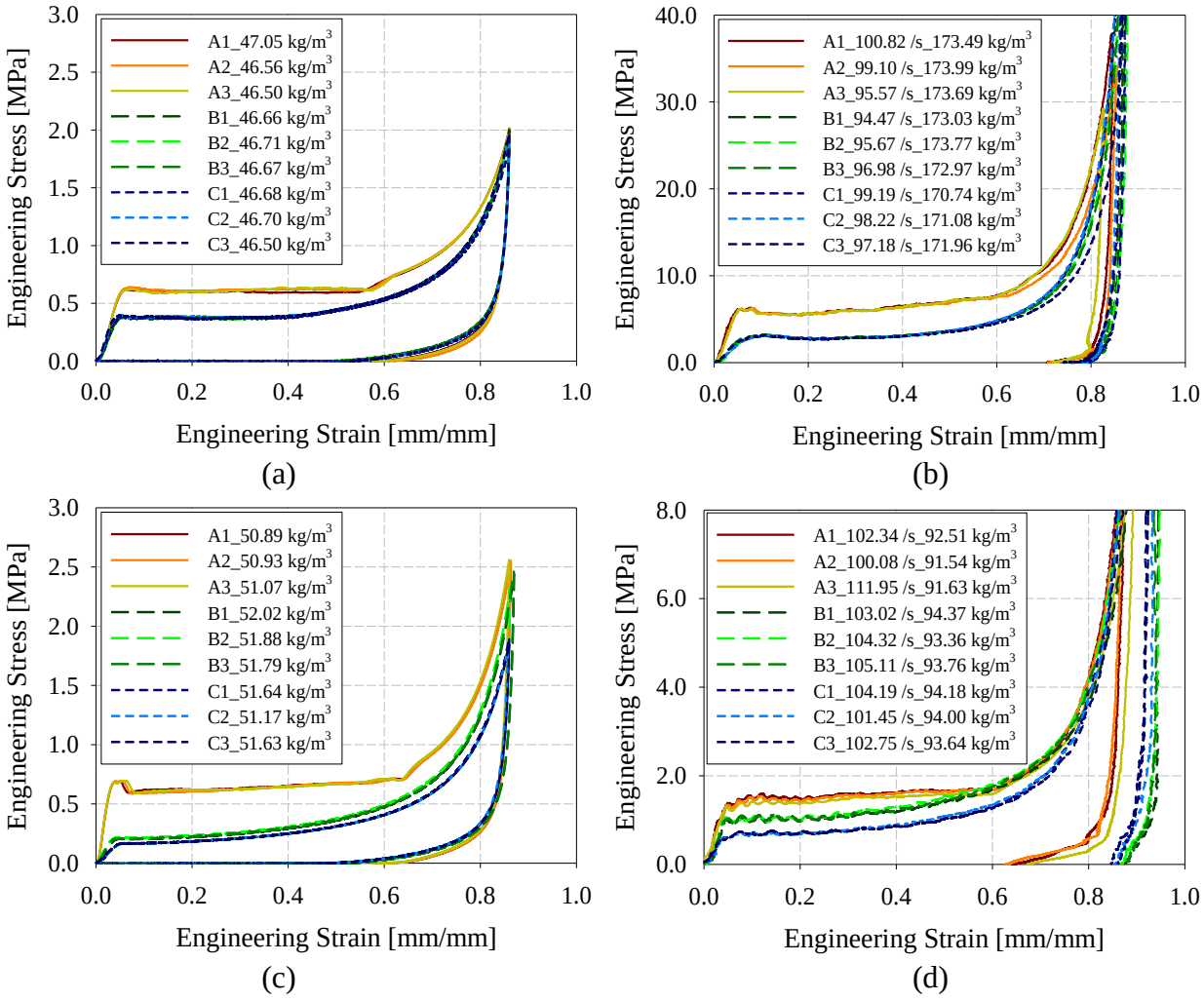

Figure 21. Stress/strain responses of repeated tests in three different loading directions under quasi-static test on specimens within (a) PVC H45 and (c) PES F50 groupings, dynamic test on specimens within (b) PVC H200 and (d) PES F90 groupings at strain rate of about 100 s^{-1}.

7.3.2 Effect of foam density under quasi-static test

Stress/strain responses for PVC and PES foams with different densities under quasi-static compression test at 0.003 s^{-1} strain rate are shown in Figures 22 and 23, respectively. Typical compressive stress/strain responses for cellular material were observed for both PVC and PES foam specimens. Three regions (elastic, plateau, and densification) can be distinguished in the graphs.

Comparing graphs (a) and (b) in Figures 22 and 23, it is observed that both PVC and PES foams have enhanced compressive behaviors in the foam rise direction compared to the

perpendicular foam rise direction as evident in an increased modulus of elasticity, compressive strength, and plateau stress. Except for specimens within the H80 grouping, compressive behaviors of the PVC and PES foams with other densities improved with the increase of foam density in both the foam rise direction and perpendicular to the foam rise directions. Also, the extent of the plateau region, within the strain domain, decreased with increasing foam density. This was consistent with the typical compressive behavior of polymeric foams as observed by [2]. However, the H80 grouping illustrated slightly enhanced compressive behavior than the specimens within the H100 grouping when loading perpendicular to the foam rise direction. This observation can be justified based on the SEM analysis results considering the higher shape anisotropy factor for specimens within H100 grouping (R=1.46) compared to H80 grouping (R=1.33), as shown in Table 7. Foam with higher shape anisotropy factor showed more reduction in compressive strength when loading perpendicular to the foam rise direction.

As illustrated in Section 7.3.1, the compressive behaviors of PVC foam specimens are almost identical in the two perpendicular to foam rise directions (loading on planes B or C). Therefore, tests with loading on plane B are shown in Figure 22(a) only as of the compressive response in perpendicular to the foam rise direction. However, as shown in Figure 23(b), the compressive responses of PES foam specimens enhanced when loading on plane B compared with loading on plane C, and the enhancement was even more significant at higher densities. The different compressive responses of the PES foam appeared in different transverse directions were most likely attributed to the different cell structural anisotropy in these two directions, as illustrated in Table 7. Furthermore, a strain hardening phenomenon was observed at the highest densities of both PVC (H200 grouping) and PES (F130 grouping) foams, and it is seen the stress gradually

increases with the increase of strain in the plateau region, giving a linear plateau region. This phenomenon can be associated with a combination of cell edges plastic bending and collapse [19].

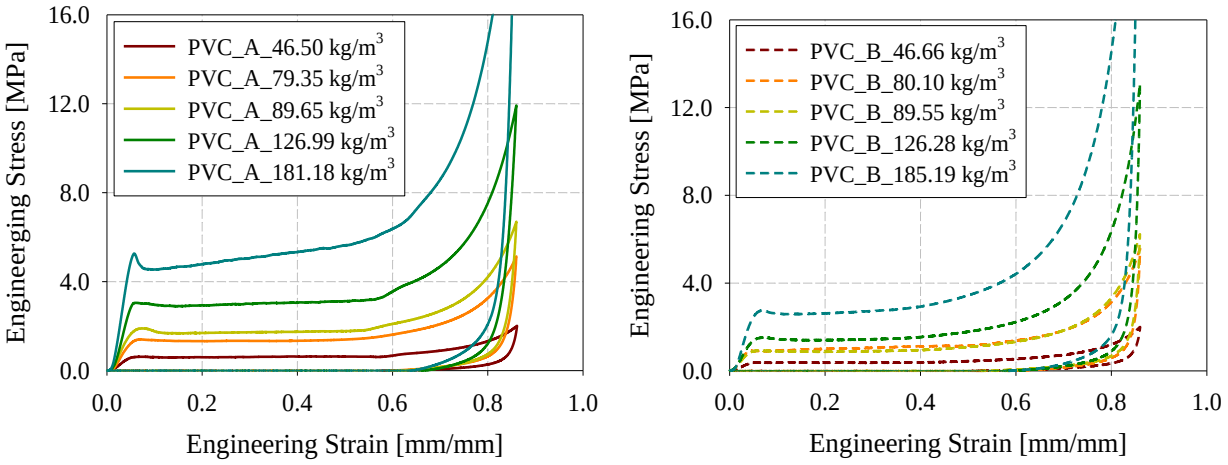

Figure 22. Stress/strain responses of PVC foam with different densities loading in (a) foam rise direction and (b) perpendicular to foam rise direction under quasi-static test.

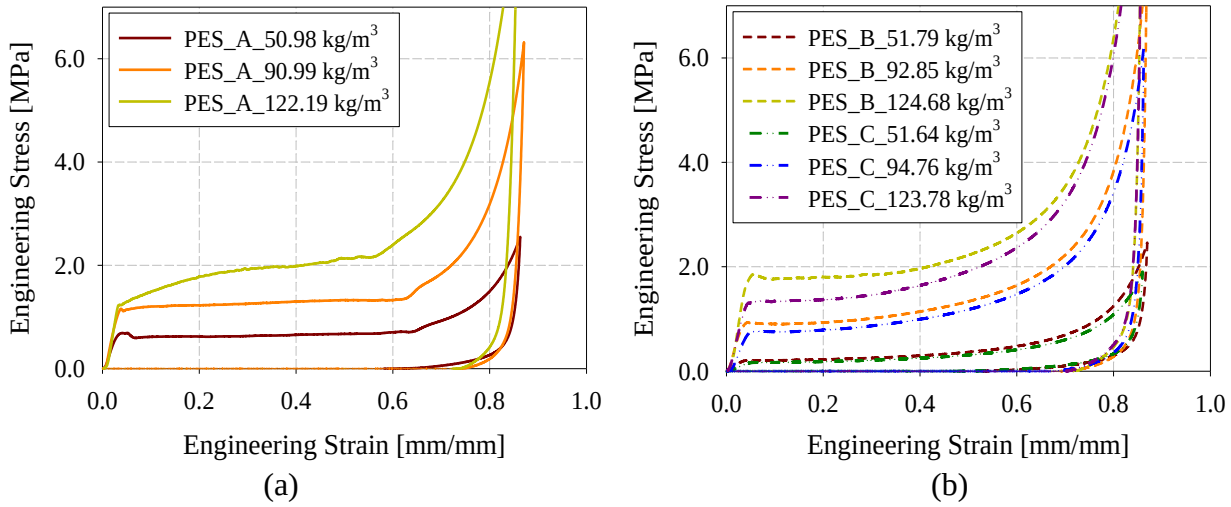

Figure 23. Stress/strain responses of PES foam with different densities loading in (a) foam rise direction and (b) perpendicular to foam rise directions under quasi-static test.

7.3.3 Effect of strain rate

Compressive stress/strain responses of PVC foam specimens within the H45 through H200 groupings and PES foam specimens within F50 through F130 groupings, loaded in the foam rise direction and perpendicular to the rise directions at different strain rates, are shown in Figures 24(a) to (j) and 24(a) to (h), respectively. Since the compressive responses of the PVC foam specimens in the two perpendicular directions (loading on planes B and C) were nearly identical, stress/strain responses from tests loaded on plane B were selected to represent the compressive behavior for PVC foam in the perpendicular direction as displayed in Figure 24. However, the stress/strain responses from tests loaded on planes B and C are shown in Figure 25 for PES foam. All the dynamic stress/strain data presented in this thesis were directly obtained from the data acquisition system without filtering. The rationale behind providing the nonfiltered data was to avoid any numerical altered information and not influence the original data for mechanical material characterization. Compressive strength and energy absorbed per unit volume with respect to strain rate for each density of the PVC and PES foams loaded in the foam rise direction and perpendicular on plane B are shown in Figures 26 and 27, respectively.

No significant strain rate influence for PVC foam specimens at the lowest density (H45 grouping) was evident when loading parallel to the foam rise direction at elevated strain rates. However, a slight strain rate effect is shown for this PVC foam density when loading perpendicular to the foam rise direction, as shown in Figure 24(b). For specimens in the H80 grouping, an evident strain rate effect appears at 100 s^{-1} strain rate tests by an observed increase in compressive strength and plateau stress when loading parallel to the foam rise direction. As illustrated in Figure 26(a), the compressive strength of specimens within the H80 grouping increased from 1.372 MPa at the quasi-static test to 1.753 MPa at 100 s^{-1}. However, there is no significant difference between the

compressive stress/strain responses at 100 s^{-1} and 200 s^{-1} strain rate tests. With the increase of foam density, the strain rate effect became more evident when loading in the foam rise direction. For specimens within H100 and H130 grouping, the compressive strength continuously increased from 1.908 MPa and 3.061 MPa at the quasi-static test to 2.557 MPa and 3.818 MPa at the elevated strain rate tests of approximately 200 s^{-1}, respectively. However, the level of increase between 100 s^{-1} and 200 s^{-1} strain rate tests is not significant. For the highest density material grouping (H200 grouping), a strain rate effect was quite evident through the observed increase in the stress/strain response at higher strain rate tests. However, no significant difference between the 50 s^{-1} and 100 s^{-1} strain rate tests was observed. Negligible increase in compressive strength was also observed for the specimens within H45, H80, H100, and H130 groupings from testing at strain rates approximately equal to 100 s^{-1} to 200 s^{-1} with loading parallel to the rise direction. On the contrary, when loading perpendicular to the foam rise direction, an increase in the compressive strength was shown for the specimens in H45, H80, H100, and H130 groupings from 100 s^{-1} to 200 s^{-1} strain rate tests.

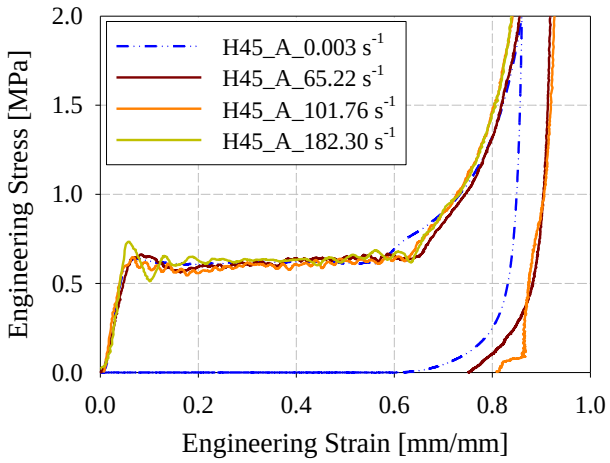
H45_A_0.003 s-1
H45_A_65.22 s-1
H45_A_101.76 s-1
H45_A_182.30 s-1
Engineering Stress [MPa]
Engineering Strain [mm/mm]
0.0
0.5
1.0
1.5
2.0
0.0
0.2
0.4
0.6
0.8
1.0

(a)

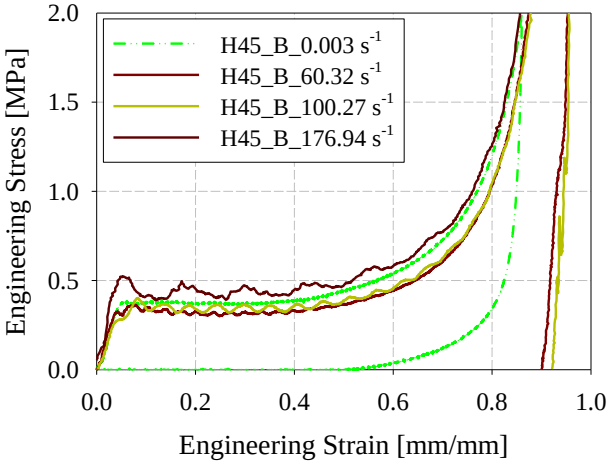
H45_B_0.003 s-1
H45_B_60.32 s-1
H45_B_100.27 s-1
H45_B_176.94 s-1
Engineering Stress [MPa]
Engineering Strain [mm/mm]
0.0
0.5
1.0
1.5
2.0
0.0
0.2
0.4
0.6
0.8
1.0

(b)

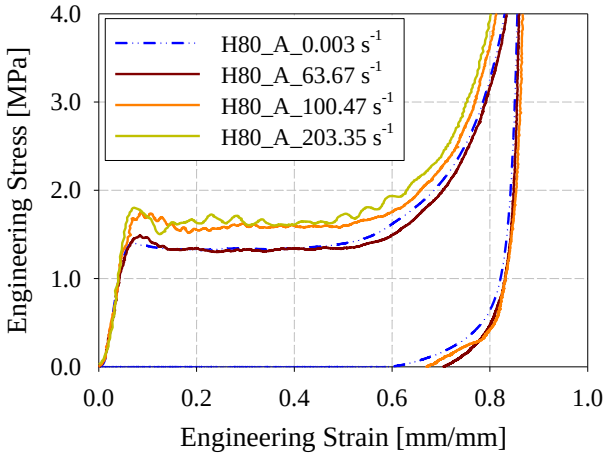
H80_A_0.003 s-1
H80_A_63.67 s-1
H80_A_100.47 s-1
H80_A_203.35 s-1
Engineering Stress [MPa]
Engineering Strain [mm/mm]
0.0
1.0
2.0
3.0
4.0
0.0
0.2
0.4
0.6
0.8
1.0

(c)

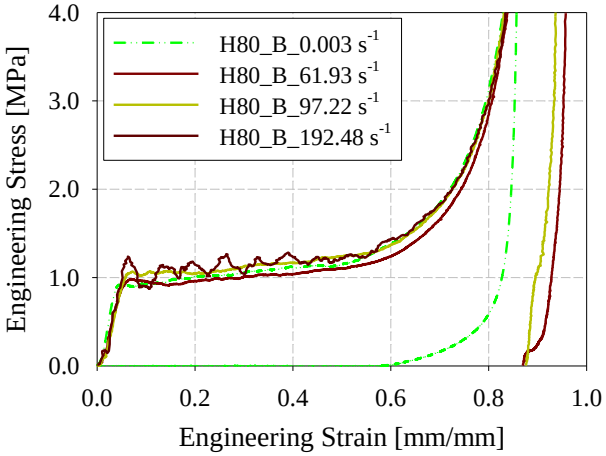
H80_B_0.003 s-1
H80_B_61.93 s-1
H80_B_97.22 s-1
H80_B_192.48 s-1
Engineering Stress [MPa]
Engineering Strain [mm/mm]
0.0
1.0
2.0
3.0
4.0
0.0
0.2
0.4
0.6
0.8
1.0

(d)

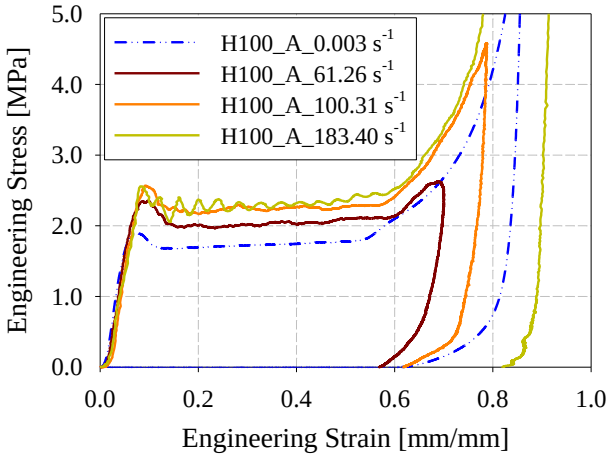
H100_A_0.003 s-1
H100_A_61.26 s-1
H100_A_100.31 s-1
H100_A_183.40 s-1
Engineering Stress [MPa]
Engineering Strain [mm/mm]
0.0
1.0
2.0
3.0
4.0
5.0
0.0
0.2
0.4
0.6
0.8
1.0

(e)

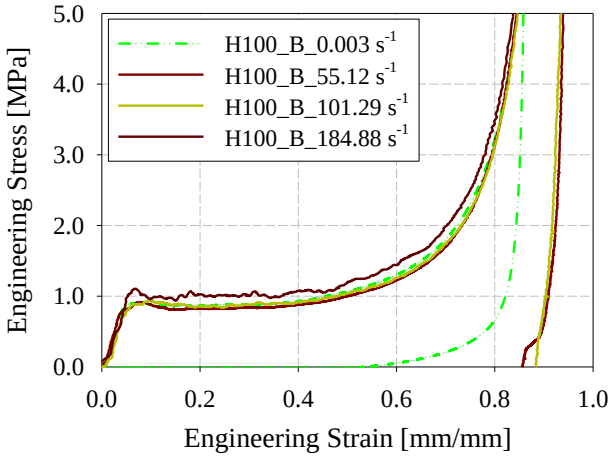
H100_B_0.003 s-1
H100_B_55.12 s-1
H100_B_101.29 s-1
H100_B_184.88 s-1
Engineering Stress [MPa]
Engineering Strain [mm/mm]
0.0
1.0
2.0
3.0
4.0
5.0
0.0
0.2
0.4
0.6
0.8
1.0

(f)

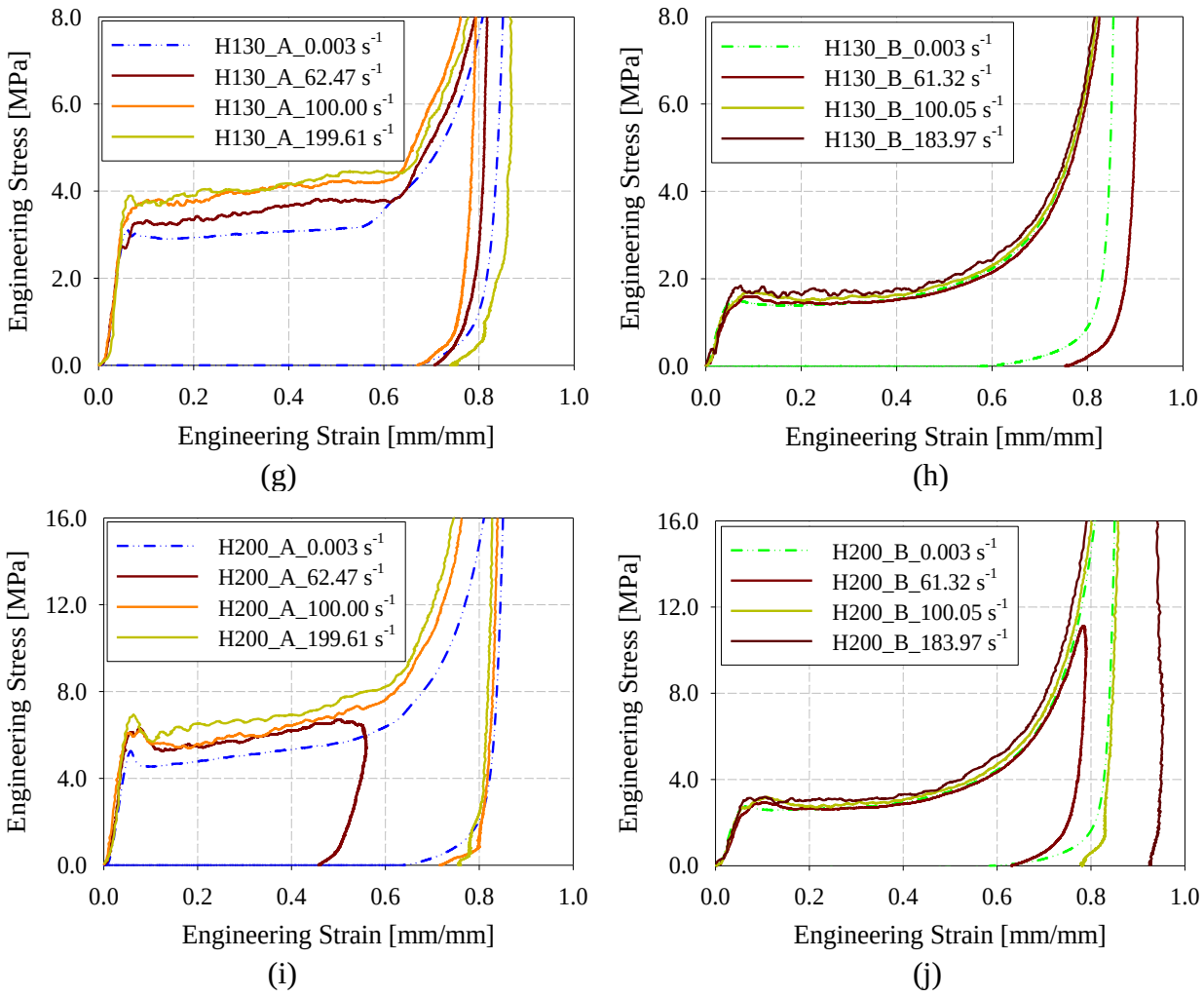

Figure 24. Stress/strain responses of PVC foam (H45 - H200 groupings) in the rise direction (left-hand-side graphs) and perpendicular to the rise direction (right-hand-side graphs) under quasi-static and elevated strain rate tests.

Regarding the PES foam specimens, an evident strain rate effect started to appear at the lowest density (F50 grouping) when loading in the foam rise direction at the strain rate of about 50 s^{-1}, as illustrated in Figure 25(a). However, with the continuous increase of the strain rate from 50 s^{-1} to 200 s^{-1}, no significant continuous increase in strain rate effect was observed. Additionally, no significant strain rate influence was observed when loading perpendicular to the foam rise direction, as shown in Figures 25(b) and (d). With increasing the foam density, the strain rate effect became more evident for the PES foam specimens within F90 and F130 groupings. Continuous

enhancement in the stress/strain responses was observed with the increasing strain rates from the quasi-static test to 200 s^{-1} strain rate tests for F90 grouping when loading in the foam rise direction. This could also be observed by the compressive strength extracted from the stress/strain responses as shown in Figure 26(c). Compressive strength of PES foam specimens within F90 grouping continuously increased from 1.164 MPa at the quasi-static test to 1.545 MPa at the 200 s^{-1} strain rate test. The highest magnitude of strain rate effect was observed between the quasi-static and 50 s^{-1} strain rate tests for the F130 grouping, where the compressive strength suddenly increased from 1.330 MPa to 2.134 MPa as displayed in Figure 26(c). With the continuous increase of strain rates from 50 s^{-1} to 200 s^{-1}, the compressive strength of F130 grouping gradually increased from 2.134 MPa to 2.335 MPa. Similar to specimens within the F50 grouping, no significant strain rate effect was observed when loading perpendicular on planes B or C of specimens within the F90 and F130 groupings. The slightly negative strain rate effect observed for specimens within the F90 grouping loaded on plane C most likely resulted from the slight variation of specimens' densities. Although no significant strain rate effect was observed for PES foam when loading perpendicular to the foam rise directions, transversely anisotropic compressive behaviors were clearly observed when loading in the two different perpendicular directions under the elevated strain rates tests.

The fluctuation observed in the stress/strain responses of PVC specimens within the H45 and H80 grouping and PES specimens within the F50 and F90 groupings, most likely associated with the lack of filtering, especially when loading perpendicular to the rise direction at approximately 200 s^{-1} strain rate, may play a minor role in the accurate measurement of the compressive strength values for specimens within these groupings and reported in Figures 26(b) and (d).

Overall, there is no significant strain rate influence on the compressive stress/strain responses when loading perpendicular to the foam rise direction for both the PVC and PES foams. When loading parallel to the foam rise direction, the strain rate effect was more evident for PVC and PES foams with higher densities.

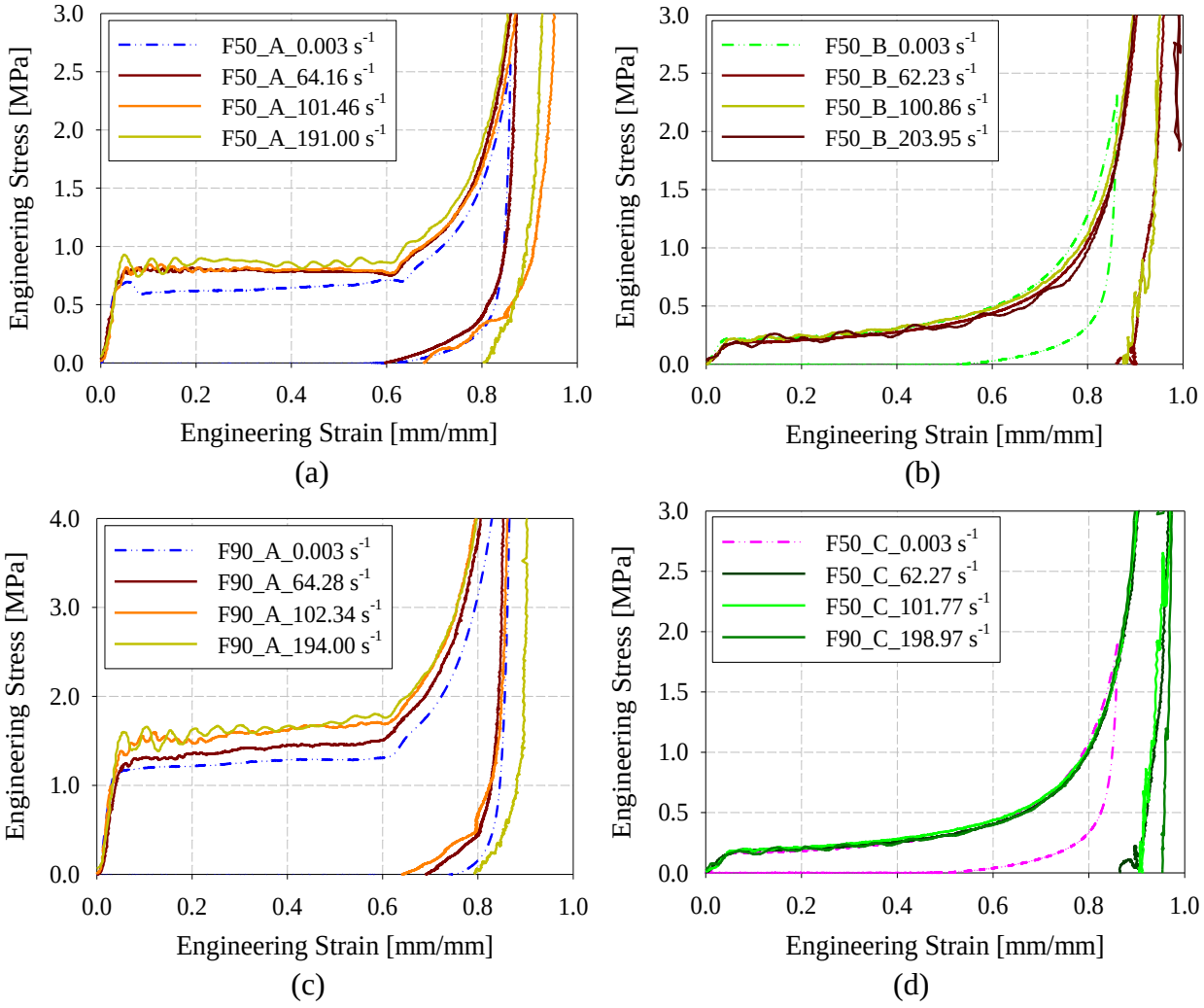

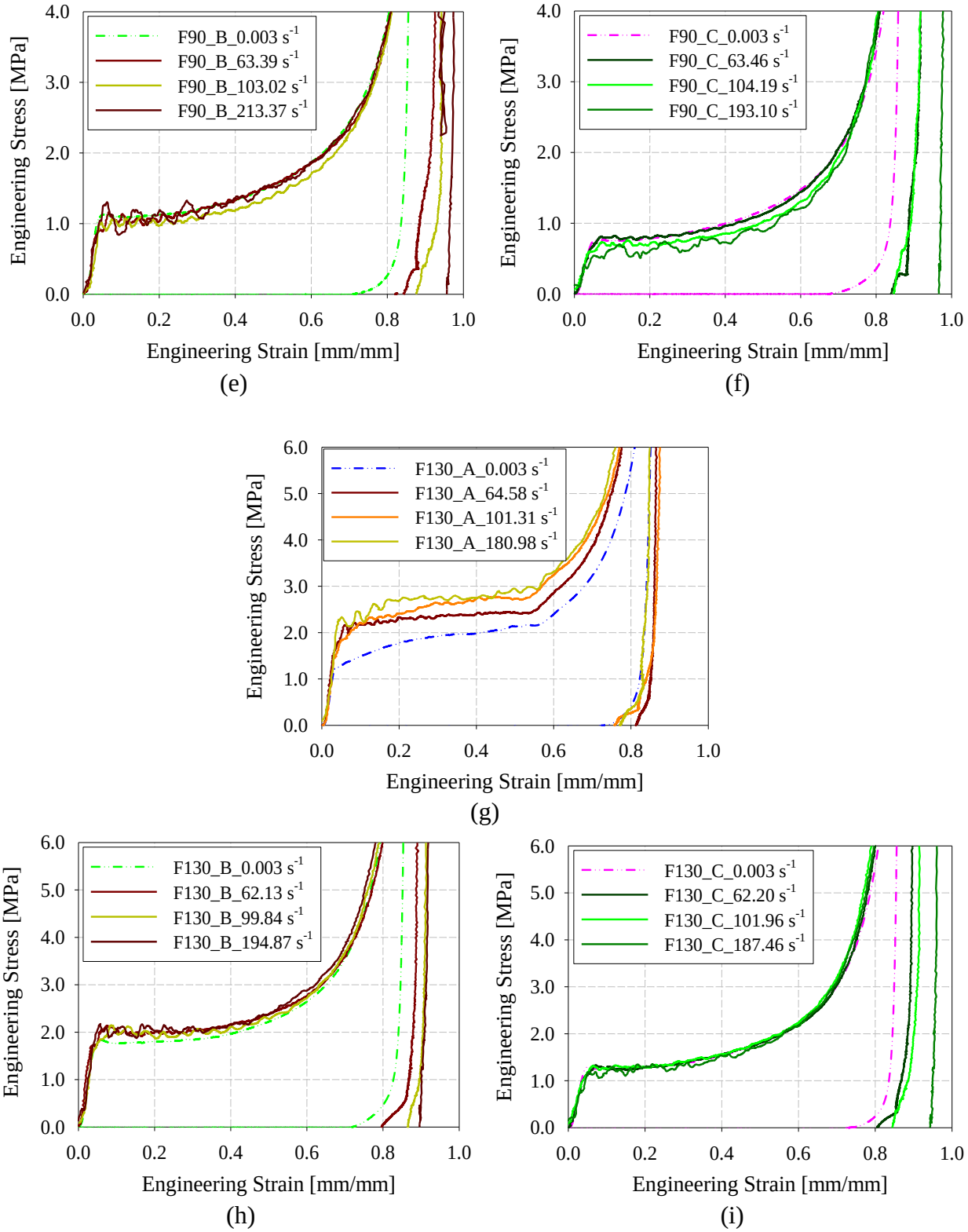

Figure 25. Stress/strain responses of PES foam (F50-F130 groupings) loaded in (a), (c), (g) foam rise direction (loaded on plane A) and (b), (e), (h) loaded on planes B and (d), (f), (i) loaded on plane C under quasi-static and elevated strain rate tests.

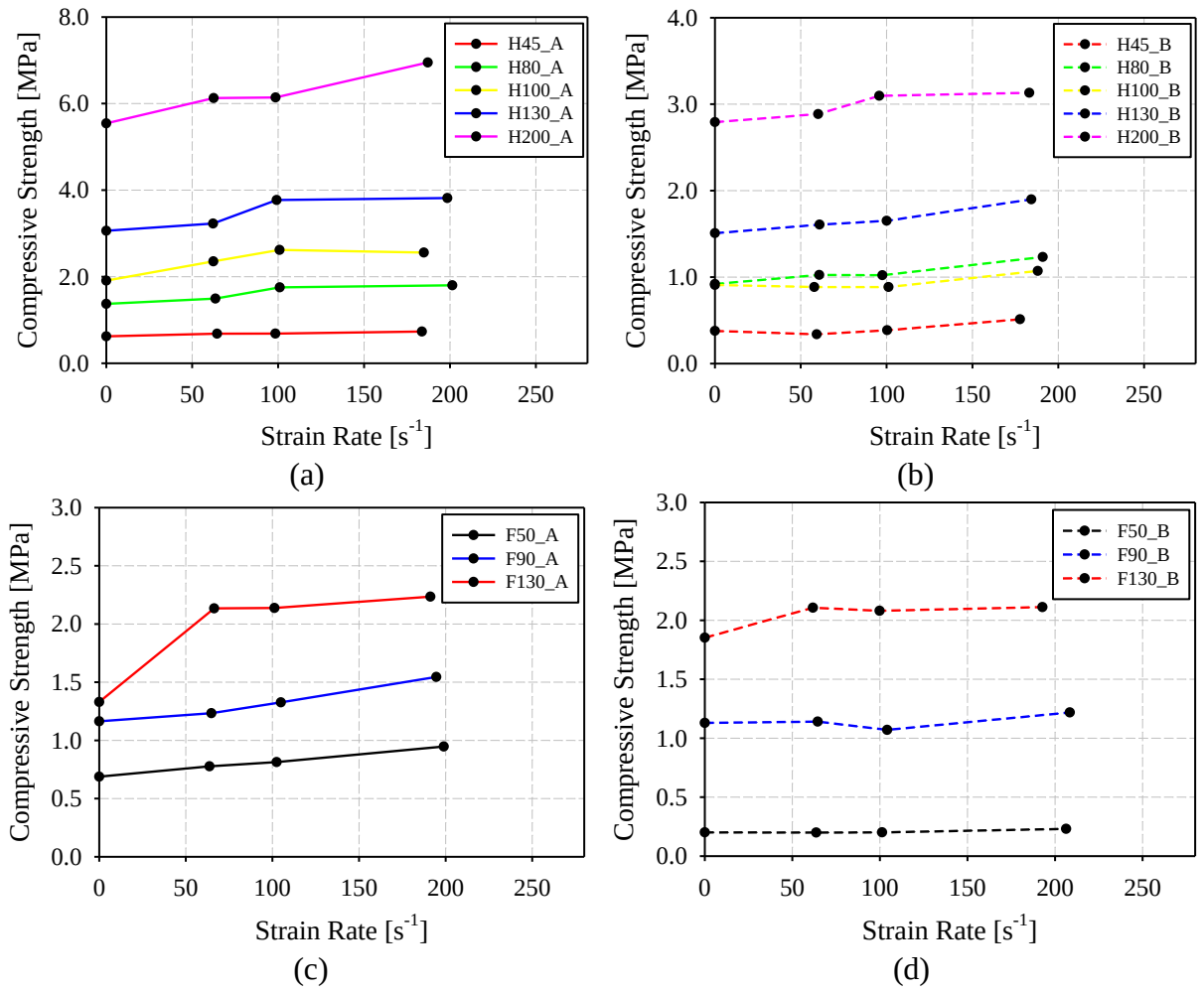

Figure 26. Compressive strength versus strain rate of PVC and PES foams with various densities loading in (a) (c) foam rise direction (loaded on plane A) and (b) (d) perpendicular to foam rise directions (loaded on plane B).

Figure 27 illustrates the energy absorbed per unit volume for each density of the PVC and PES foams at various strain rates considered in this investigation. The maximum strain achieved for the highest density, specimens within the H200 grouping, at 62.47 s^{-1} strain rate tests was 0.55. This magnitude of strain was used to compute the energy absorption per unit volume for all densities under all different strain rate tests. However, the energy absorbed per unit volume for specimens with the highest density, tested at a strain rate approximately equal to 50 s^{-1} (highlighted point in Figure 27(a)), was slightly underestimated as the densification region had not been achieved. A similar trend with compressive strength illustrated in Figure 26 was observed for the energy

absorption per unit volume. As indicated in the previous section 7.3.2, due to a higher shape anisotropy factor of foam cells within the H100 category, the PVC foam specimens within H80 grouping illustrated slightly enhanced energy absorbing capacity than specimens within the H100 category when loading perpendicular to the foam rise direction. The effect of shape anisotropy dominates the effect of foam density on the mechanical response of specimens within H80 and H100 groupings when loading perpendicular to the foam rise direction.

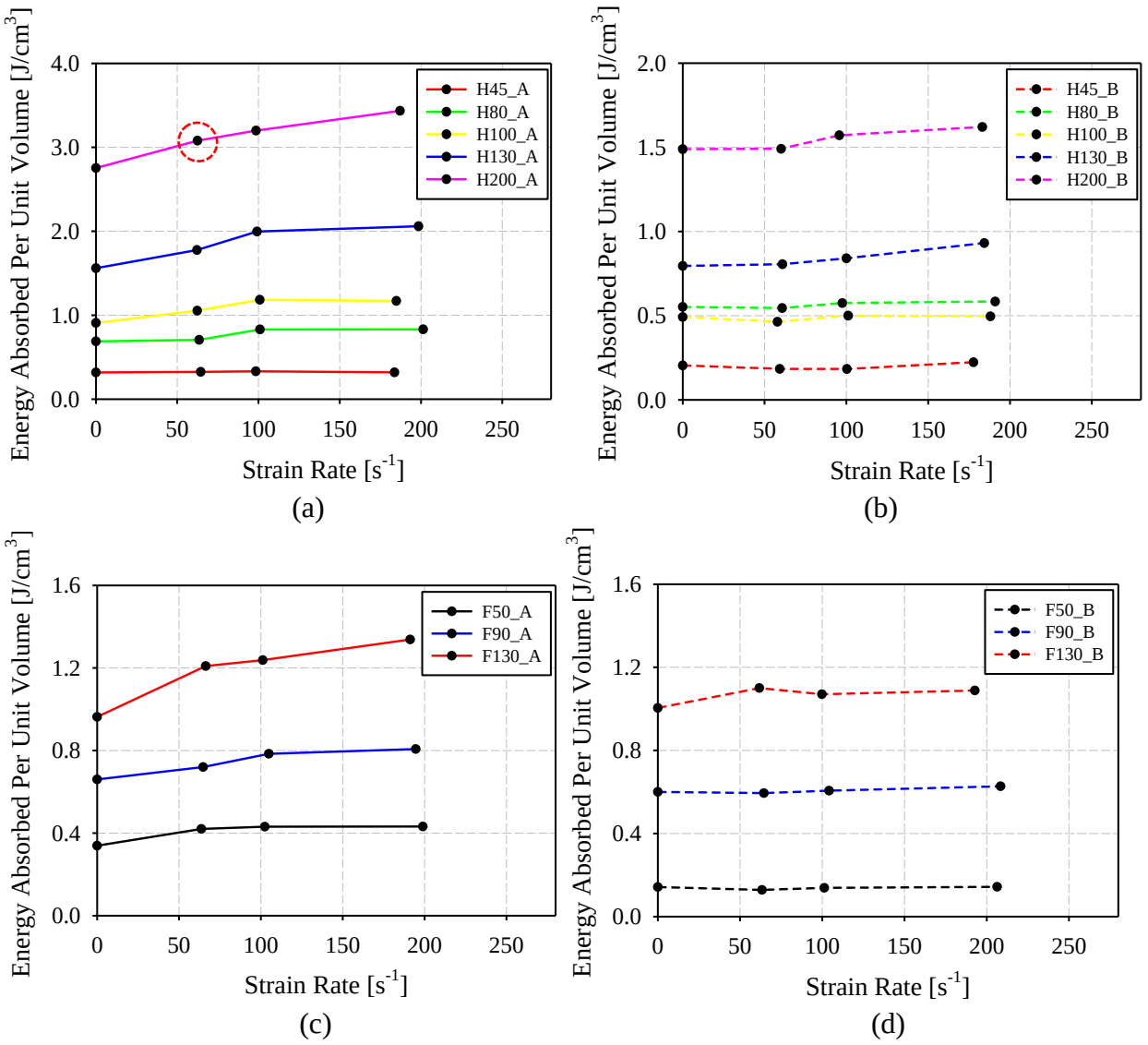

Figure 27. Energy absorbed per unit volume to 0.55 strain versus strain rate of PVC and PES foams with various densities loading in (a) (c) foam rise direction and (b) (d) perpendicular to foam rise direction.

7.4. Deformation uniformity

Both PVC and PES foam specimens with different densities showed localized deformation when loading parallel to the foam rise direction. This localized layer-by-layer deformation was also observed when loading on plane B of PES foam specimens within the F130 grouping, in which a slight strain rate effect appeared in this perpendicular direction. This localization phenomenon was found to be not rate dependent. In other words, loading parallel to the rise direction of PVC and PES foams, and perpendicular on plane B of PES foam specimens within the F130 grouping resulted in localized deformation under all quasi-static and elevated strain rate tests. This rate independency was also observed for the uniform deformation response of the PVC foam specimens when loading perpendicular to the foam rise direction, and PES foam specimens within the F130 grouping loaded perpendicular on plane C.

A number of successive images of different stages of deformation of PVC and PES foam specimens loaded parallel and perpendicular to the foam rise directions under the 200 s^{-1} strain rate tests are shown in Figures 28 to 31, respectively. Red and blue arrows are marked in these figures to represent localized and non-localized deformation regions, respectively. Highly localized layer-by-layer deformation of PVC foam specimen within H130 grouping and PES foam specimen within F130 grouping, when loading parallel to the foam rise direction, is indicated in Figures 28(a) and (b), respectively. In contrast, the deformation was more uniform when loading perpendicular to the rise direction of PVC foam and perpendicular on plane C of PES foam, as illustrated in Figures 29 and 31, respectively. This localized deformation can be one of the reasons for the higher level of rate sensitivity of PVC and PES foam specimens when loading parallel to the foam rise direction. To elaborate further, the actual local strain rate is significantly higher than the nominal strain rate in the locally deformed regions of the specimen. Consequently, an enhanced

rate effect would be observed on the macro-mechanical response of the specimen with localized deformation. A number of other successive images of different stages of the deformation of PVC and PES foam specimens when loading parallel to the foam rise direction and perpendicular to the rise direction are shown in Appendix E.

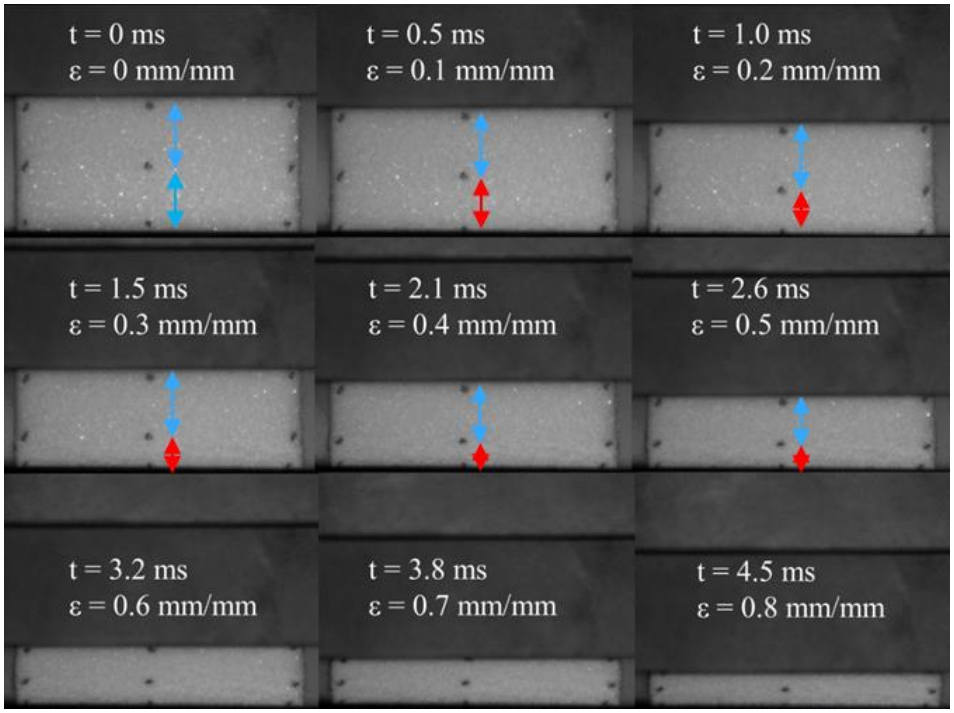

(a)

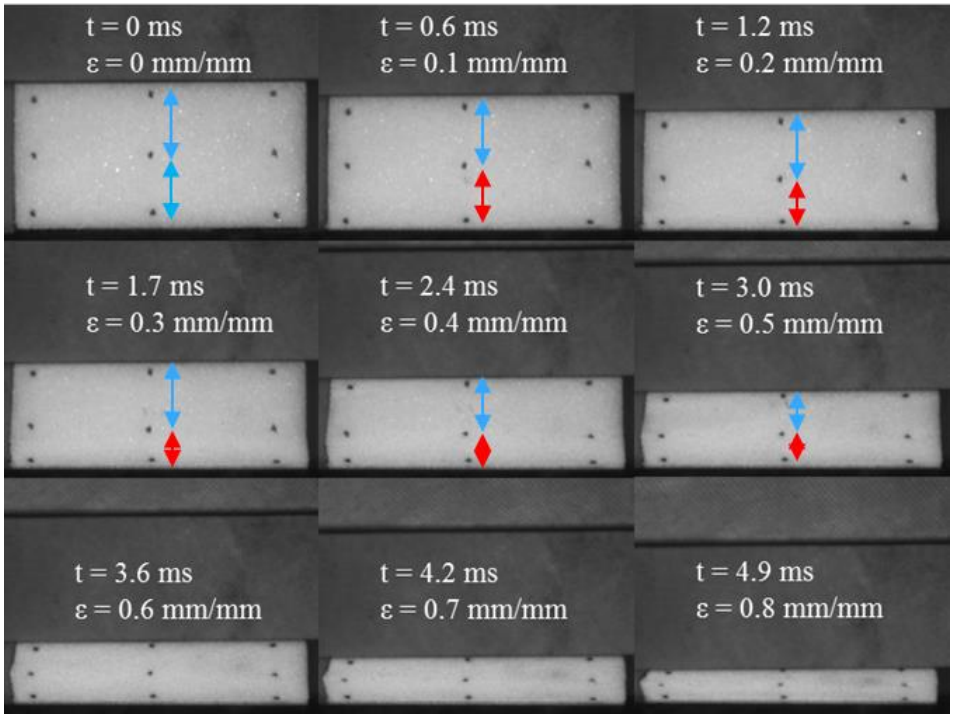

(b)

Figure 28. Successive images of different stages of the deformation of samples within (a) H130 and (b) F130 groupings when loading parallel to the foam rise direction with a strain rate of 200 s^{-1}; red and blue arrows represent the localized and non-localized deformation regions, respectively.

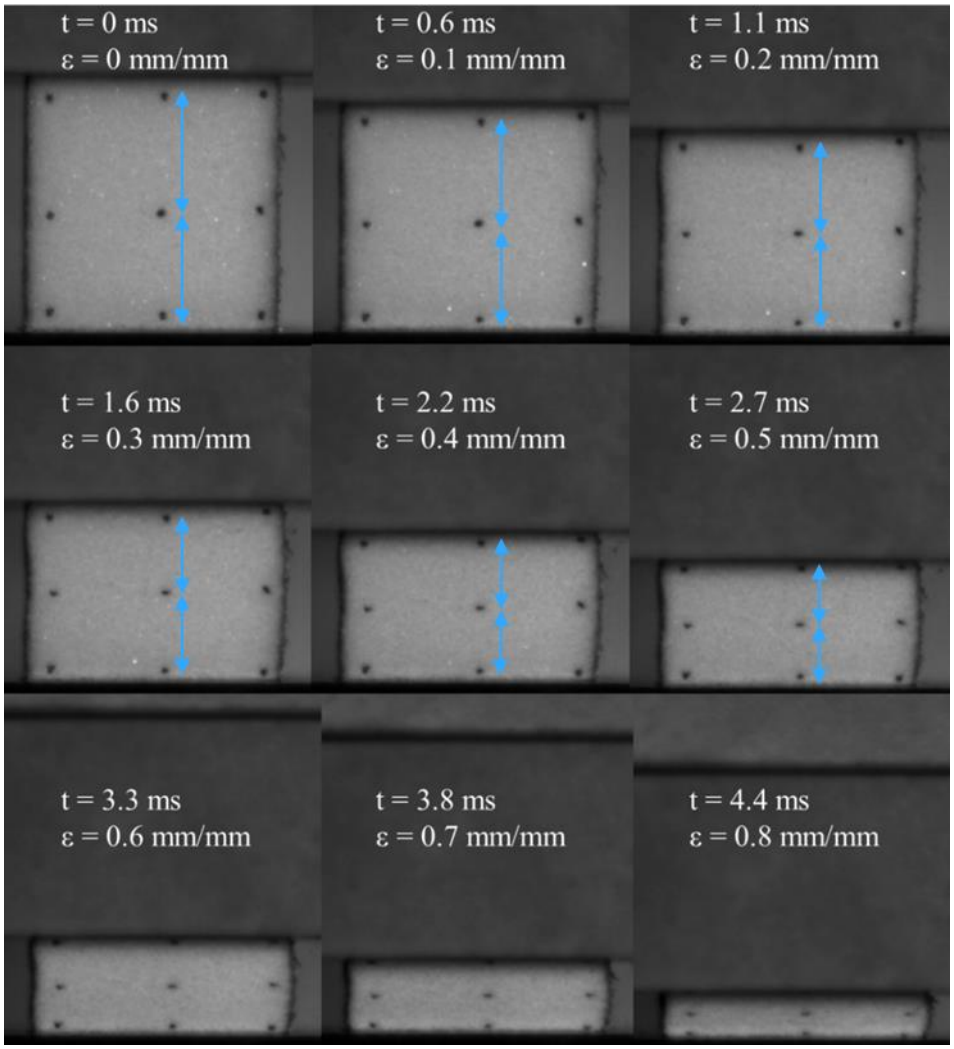

Figure 29. Successive images of different stages of the deformation of a sample within H130 grouping when loading perpendicular on plane B with a strain rate of 200 s^{-1}; blue arrows represent the non-localized deformation regions.

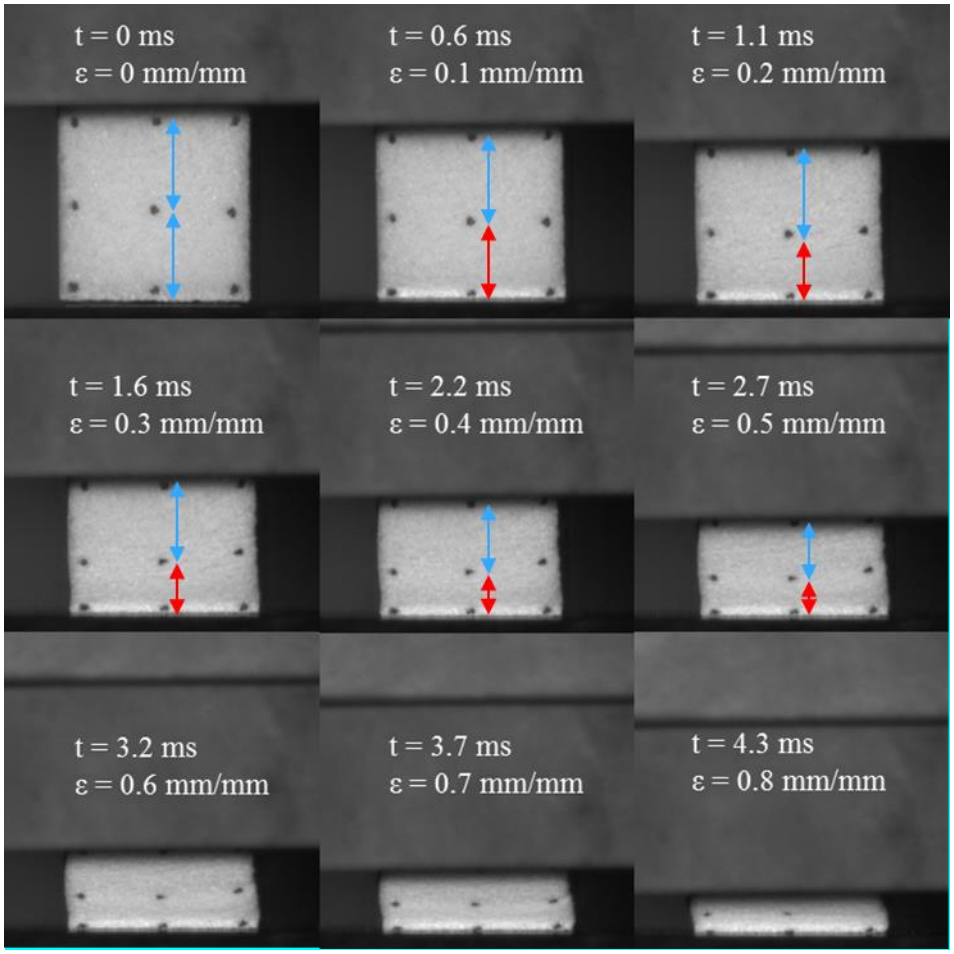

Figure 30. Successive images of different stages of the deformation of a sample within F130 grouping when loading perpendicular on plane B with a strain rate of 200 s^{-1}; red and blue arrows represent the localized and non-localized deformation regions, respectively.

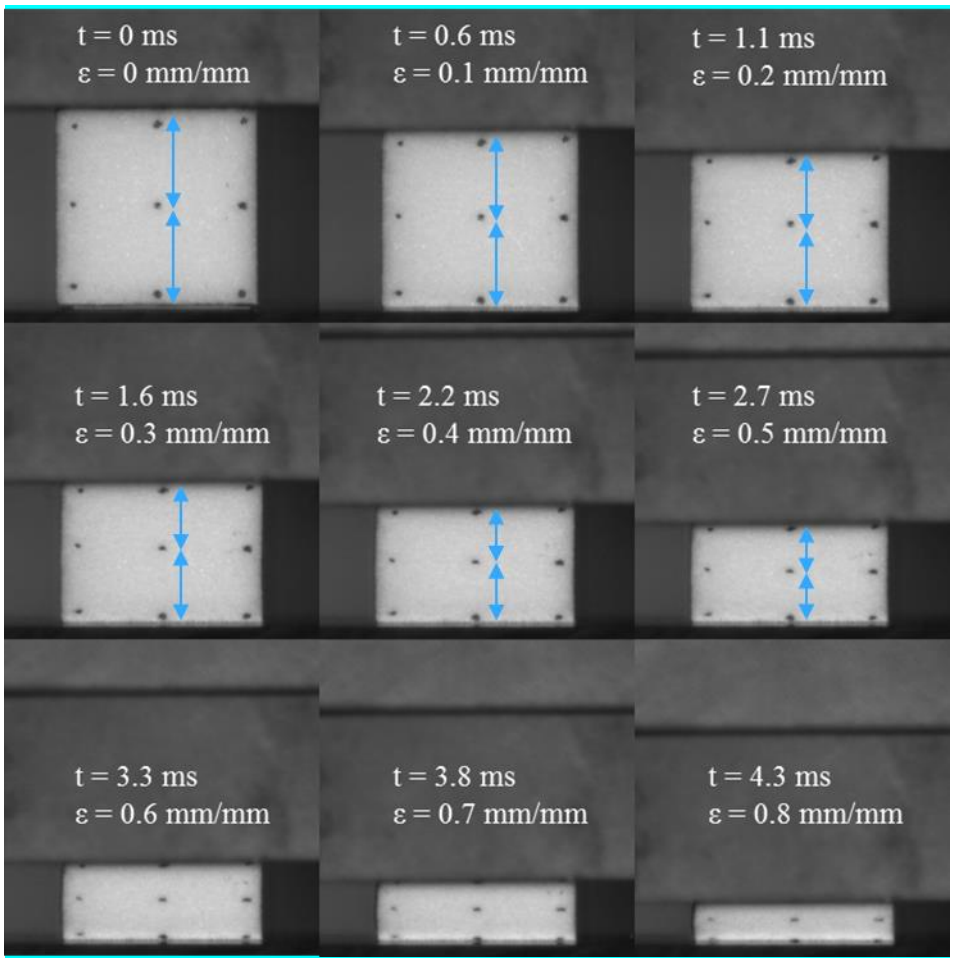

Figure 31. Successive images of different stages of the deformation of a sample within F130 grouping when loading perpendicular on plane C with a strain rate of 200 s^{-1}; blue arrows represent the non-localized deformation regions.

8. CONCLUSIONS

In this thesis, the compressive mechanical material behaviors of PVC foam with five different densities ranging from 45 to 200 kg/m^3 and PES foam with three different densities ranging from 50 to 130 kg/m^3 have been studied in three different loading directions (parallel and perpendicular to the foam rise direction) under quasi-static and elevated strain rate tests. Engineering stress/strain responses, compressive strength, and energy absorption capacity of each density under each strain rate test from 0.003 to 200 s^{-1} have been obtained and compared against each other. EDS and SEM analysis have been conducted to investigate the material composition and cell microstructure characteristics. The following conclusions can be drawn from this research:

1. For both quasi-static and dynamic tests, PVC and PES foams exhibited enhanced compressive behaviors when loading parallel to the foam rise direction, compared with findings from tests where loading was perpendicular to the foam rise direction. For instance, when loading in the foam rise direction at the strain rate of 200 s^{-1}, the compressive strength of PVC and PES foams with the same density of 130 kg/m^3 increased 87% and 14%, respectively, compared with the tests loading perpendicular on plane B. When loading in two different perpendicular directions (loading on planes B and C), the compressive responses of PVC foam specimens were nearly identical. In contrast, PES foam specimens exhibited transversely anisotropic behaviors. The magnitudes of the transverse anisotropy of PES foam were more evident at higher densities.

2. For both PVC and PES foams, a material strain rate effect was observed through increased compressive strength, plateau stress, and energy absorbing capacity, and it is more evident at higher densities when loading in the foam rise direction. For example, from the quasi-static to 200 s^{-1} strain rate tests, the energy absorbed per unit volume for PVC foam specimens within H200 grouping and PES foam specimens within F130 grouping increased about

51% and 62%, respectively. No significant strain rate effect was observed for both PVC and PES foams when loading perpendicular to the foam rise directions. However, a slight strain rate effect was observed for PES foam specimens within F130 grouping when loading perpendicular on plane B, which most likely resulted from the structural anisotropy of foam cells. Moreover, no significant strain rate influence on elastic modulus was observed for both PVC and PES foams considered in this study.

3. Through SEM analysis, cell sizes of both PVC and PES foams were found not to depend on foam density. However, the cell edge thickness continuously increased with the increase of foam density. For both quasi-static and dynamic tests, plastic hinges are the primary deformation mechanism for the PVC and PES foam cell edges. At comparable densities, PVC foam cells possess larger cell edge thickness than PES foam by approximately 30 %, which is the main reason that PVC foam specimens exhibited superior compressive behaviors than PES foam specimens at comparable densities.

4. A highly localized rate-independent deformation mechanism was observed for both PVC and PES foam specimens with all different densities when loading parallel to the foam rise direction. This localized deformation mechanism was also observed from the tests when loading perpendicular on plane B of PES foam specimens within the F130 grouping. In contrast, a rate-independent uniform deformation mechanism was observed for the PVC foam specimens when loading perpendicular to the foam rise direction (loading on planes B and C) and PES foam specimens within the F130 grouping loaded perpendicular on plane C. Since the loading directions where localized deformation occurred were very consistent with the loading directions where the strain rate effect appeared, the localized deformation is most likely the reason for the higher level

of rate sensitivity of PVC and PES foam samples when loading in the material directions mentioned above.

9. RECOMMENDATIONS FOR FUTURE WORK

By observing the compressive stress/strain responses of the rigid PVC and PES foams at elevated strain rates tests up to 200 s^{-1}, an evident strain rate effect was found for both foams when loading in the foam rise direction. Foam density and material loading directions play a significant role in the compressive behaviors of these two foams. Based on the knowledge and findings, the following recommendations are provided for future investigations into this topic with the potential to improve the material characterization of these two polymeric foams.

1. Although the compressive behaviors of the PVC and PES foams at elevated strain rates up to 200 s^{-1} have been studied in this research, the strain rate effect of these two polymeric foams at strain rates ranging from 200 s^{-1} to 500 s^{-1} was scarcely investigated. Since strain rates up to 500 s^{-1} are quite common in traffic collisions, it is highly recommended to further characterize the material compressive behaviors of PVC and PES foams at those strain rates.

2. Many researchers have investigated the analytical model of the compressive responses of polymeric foams under quasi-static test. However, very few researchers [2] studied an analytical model predicting the compressive behaviors of polymeric foams considering both the strain rate and cell structural anisotropy effects. An analytical model considering these two effects will significantly contribute to this topic.

3. Cell sizes and edges thickness have been measured on the foam specimens as received, and the primary deformation mechanism (plastic hinges) under both quasi-static and elevated strain rate tests have been observed based on 2D SEM images. To further understand the relationship between the deformation mechanism and strain rate effect, 3D images obtained from Computed Tomography (CT) might be employed in the future.

REFERENCES

[1] S-T. Lee, C.B. Park, and N.S. Ramesh, Polymeric foams science and technology. CRC Press: Boca Raton, 2007.

[2] L.J. Gibson and M.F. Ashby, Cellular solids: structure and properties. Cambridge university press, 1999.

[3] J. Zhang and M.F. Ashby, Mechanical selection of foams and honeycombs used for packaging and energy absorption, Journal of Materials Science, Vol. 29, 1994, pp. 157-163.

[4] M. Avalle, G. Belingardi, and R. Montanini, Characterization of polymeric structural foams under compressive impact loading by means of energy-absorption diagram, International Journal of Impact Engineering, Vol. 25, 2001, pp. 455-472.

[5] A.G. Mamalis and D.P. Papapostolou, Experimental investigation of strain rate effects on the crushing characteristics of composite sandwich panels, International Journal of Crashworthiness, Vol. 15, No. 6, 2010, pp. 581-603.

[6] A.K. Toksoy and M. Güden, The optimization of the energy absorption of partially Al foam-filled commercial 1050H14 and 6061T4 Al crash boxes, International Journal of Crashworthiness, Vol. 16, No. 1, 2011, pp. 97-109.

[7] International Transport Forum (2019), Road Safety Annual Report 2019, OECD Publishing, Paris.

[8] M. Colloca, G. Dorogokupets, N. Gupta and M. Porfiri, Mechanical properties and failure mechanisms of closed-cell PVC foams, International Journal of Crashworthiness, Vol. 17, No. 3, 2012, pp. 327-336.

[9] A. Saeid and S.L. Donaldson, Experimental and finite element evaluation of debonding in composite sandwich structure with core thickness variations, Advances in Mechanical Engineering, Vol. 8(9), 2016, pp. 1-18.

[10] B.J. Lansing. Mechanical and physical characterization of foams made of gelatinized starch and pre-polymer polyurethane. Rochester, New York: College of Applied Science and Technology, 2016.

[11] A.G. Mamalis, K.N. Spentzas, D.E. Manolakos, M.B. Ioannidis, and D. P. Papapostolou, Experimental investigation of the collapse modes and the main crushing characteristics of composite sandwich panels subjected to flexural loading, International Journal of Crashworthiness, Vol. 13, No. 4, 2008, pp. 349-362.

[12] Q. Wang, Z. Fan, H. Song, and L. Gui, Experimental and numerical analysis of the axial crushing behavior of hat sections partially filled with aluminum foam, International Journal of Crashworthiness, Vol. 10, No. 5, 2010, pp. 535-543.

[13] 13DIAB products-Divinycell (2004) DIAB Group. http://www.diabgroup.com/en-GB/Products-and-services/Core-Material/Divinycell-F Accessed 2019.

[14] D. Ruan, M.A. Kariem, and I.G. Crouch, High strain rate and specialised testing, The Science of Armour Materials, 2017, pp. 581-637.

[15] ASTM Standard D1621-16, 2016, Standard test methods for compressive properties of rigid cellular plastics, ASTM International, West Conshohocken, PA 19428-2959. United States.

[16] Q.M. Li, I. Magkiriadis, and J.J. Harrigan, Compressive strain at the onset of densification of cellular solids, Journal of Cellular Plastics, Vol. 42, 2006, pp. 371-391.

[17] ASTM Standard D1622/D1622M-14, 2018, Standard test method for the apparent density of rigid cellular plastics, ASTM International, West Conshohocken, PA 19428-2959. United States.

[18] T. Thomas, H. Mahfuz, L.A. Carlsson, K. Kanny, and S. Jeelani, Dynamic compression of cellular cores: temperature and strain rate effects, Composite Structures, Vol. 58, 2002, pp. 505-512.

[19] M.C. Saha, H, Mahfuz, U.K. Chakravarty, M. Uddin, M.E. Kabir, and S. Jeelani, Effect of density, microstructure, and strain rate on compression behavior of polymeric foams, Materials Science and Engineering A, Vol. 406, 2005, pp. 328-336.

[20] M. Thirumal, D. Khastgir, N.K. Singha, B.S. Manjunath, and Y.P. Naik, Effect of foam density on the properties of water blown rigid polyurethane foam, Journal of Applied Polymer Science, Vol. 108, 2008, pp. 1810-1817.

[21] A. Deb and N.D. Shivakumar, An experimental study on energy absorption behavior of polyurethane foams, Journal of Reinforced Plastics and Composites, Vol. 28, 2009, pp. 3021-3026.

[22] J.V. Mane, S. Chandra, S. Sharma, H. Ali, V.M. Chavan, B.S. Manjunath, and R.J. Patel, Mechanical property evaluation of polyurethane foam under quasi-static and dynamic strain rates-An experimental study, Procedia Engineering, Vol. 173, 2017, pp. 726-731.

[23] H. Zhao, Testing of polymeric foams at high and medium strain rates, Polymer Testing, Vol. 16, 1997, pp. 507-516.

[24] N. Ye, W. Zhang, D. Li, W. Huang, W. Xie, X. Huang and X. Jiang, Dynamic response and failure of sandwich plates with PVC foam core subjected to impulsive loading, International Journal of Impact Engineering, Vol. 109, 2017, pp. 121-130.

[25] W. Chen, F. Lu, and N. Winfree, High-strain-rate compressive behavior of a rigid polyurethane foam with various densities, Experimental Mechanics, Vol. 42, 2001, pp. 65-73.

[26] H. Mahfuz, W.A. Mamun, A. Haque, S. Turner, H. Mohamed, and S. Jeelani, An innovative technique for measuring the high strain rate response of sandwich composites, Composite Structures, Vol. 50, 2000, pp. 279-285.

[27] U. Chakravarty, H. Mahfuz, M. Saha, and S. Jeelani, Strain rate effect on sandwich core materials: An experimental and analytical investigation, Acta Materialia, Vol. 51, 2003, pp. 1469-1479.

[28] I.M. Daniel, J. Cho, and B.T. Werner, Characterization and modeling of strain-rate-dependent behavior of polymeric foams, Composite: Part A, Vol. 45, 2013, pp. 70-78.

[29] D.D. Luong, D. Pinisetty, and N. Gupta, Compressive properties of closed-cell polyvinyl chloride foams at low and high strain rates: Experimental investigation and critical review of state of the art, Composite: Part B, Vol. 44, 2013, pp. 403-416.

[30] Z. Wei and Y, Nan, High strain rate and quasi-static compression behavior and energy absorption characteristics of PVC foam, Challenge Journal of Structural Mechanics, Vol. 2(4), 2016, pp. 212-215.

[31] V.L. Tagarielli, V.S. Deshpande, and N.A. Fleck, The high strain rate response of PVC foams and end-grain balsa wood, Composites Part B: Engineering, Vol. 39, 2008, pp. 83-91.

[32] S. Outllet, D. Cronin, and M. Worswick, Compressive response of polymeric foams under quasi-static medium and high strain rate conditions, Polymer Testing, Vol. 25, 2006, pp. 731-743.

[33] R. Zhang, L. Zhang, J. Zhang, G. Luo, D. Xiao, Z. Song, M. Li, Y. Xiong, and Q. Shen, Compressive response of PMMA microcellular foams at low and high strain rates, Journal of Applied Polymer Science (2018), APP. 46044.

[34] Z.H. Tu, V.P.W. Shim, and C.T. Lim, Plastic deformation modes in rigid polyurethane foam under static loading, International Journal of Solids and Structures. Vol. 38, 2001, pp. 9267-9279.

[35] E.E. Gdoutos, I.M. Daniel and K.-A. Wang, Compression facing wrinkling of composite sandwich structures, Mechanical of Materials, Vol, 35, 2003, pp. 511-522.

[36] I.M. Daniel, E.E. Gdoutos, K.-A. Wang, and J.L. Abot, Failure modes of composite sandwich beams, International Journal of Damage Mechanics, Vol. 11, 2002, pp. 309-334.

[37] M. Shafiq, R.S. Ayyagari, M. Ehaab, and M. Vural, Multiaxial yield surface of transversely isotropic foams: part II —Experimental, Journal of the Mechanics and Physical of Solids, Vol. 76, 2015, pp. 224-236.

[38] Y. Mosleh, K.V. Bosche, M.A. Rodriguez-Perez, J.V. Sloten, J. Ivens, and I. Verpoest, Development of anisotropic foams and characterization methods for bicycle helmets, Conference: Composite week, Leuven, Belgium. 2003.

[39] Y. Mosleh, K.V. Bosche, B. Depreitere, J.V. Sloten, I. Verpoest, and J. Ivens, Effect of polymer foam anisotropy on energy absorption during combined shear-compression loading, Journal of Cellular Plastics, Vol. 54(3), 2018, pp. 597-613.

[40] A. Sakly, A. Laksimi, H. Kebir, and S. Benmedakhen, Experimental and modelling study of low velocity impacts on composite sandwich structures for railway applications, Engineering Failure Analysis, Vol. 68, 2016, pp. 22-31.

[41] P. Yang, S.S. Shams, A. Slay, B. Brokate, and R. Elhajjar, Evaluation of temperature effects on low velocity impact damage in composite sandwich panels with polymeric foam cores, Composite Structures, Vol. 129, 2015, pp. 213-223.

[42] L. Chen and M.S. Fatt, Transversely isotropic mechanical properties of PVC foam under cyclic loading, Material Science, Vol. 48, 2013, pp. 6786-6796.

[43] M.S. Fatt and L. Chen, A viscoelastic damage model for hysteresis in PVC H100 foam under cyclic loading, Journal of Cellular Plastics, Vol. 51(3), 2015, pp. 269-287.

[44] P.K.C. Wood and C.A. Schley. Strain Rate Testing of Metallic Materials and their modelling for use in CAE based Automotive Crash Simulation Tools (Recommendations and Procedures). First published by iSmithers, Shawbury, Shrewsbury, Shropshire, SY4 4NR, UK. 2009.

[45] P.KC. Wood, C.A. Schley, S. Kenny, T. Dutton, M. Bloomfield, R. Bardenheier, and J.R.D. Smith. Validation performance of automotive materials at high strain rate for improved crash design. 2006.

[46] N-C. Fahlbusch, L. Joachim, and W.B. Grenestedt, Effective failure behavior of an analytical and a numerical model for closed-cell foams, International Journal of Solids and Structures, Vol. 97–98, 2016, pp. 417-430.

[47] V. Srivastava and R Srivastava, On the polymeric foams: modeling and properties, Journal of Materials Science, Vol. 49, 2014, pp. 2681-2692.

[48] M. Marvi-Mashhadia, C.S. Lopesa, J. LLorca, Effect of anisotropy on the mechanical properties of polyurethane foams: An experimental and numerical study, Mechanics of Materials, Vol. 124, 2018, pp. 143-154.

[49] W-Y Jang, A.M. Kraynik, and S. Kyriakides, On the microstructure of open-cell foams and its effect on elastic properties, International Journal of Solids and Structures, Vol. 45, 2008, pp. 1845-1875.

[50] V. Bernardo, E. Laguna-Gutierrez, A. Lopez-Gil, and M.A. Rodriguez-Perez, Highly anisotropic crosslinked HDPE foams with a controlled anisotropy ratio: Production and characterization of the cellular structure and mechanical properties, Materials and Design, Vol. 114, 2017, pp. 83-91.

[51] Y. Sun, X. Zhang, Z. Shao, and Q.M. Li, Image-based correlation between the meso-scale structure and deformation of closed-cell foam, Materials Science & Engineering A, Vol. 688, 2017, pp. 27-39.

[52] E. Linul, D.A. Şerban, L. Marsavina, and T. Sadowski, Assessment of collapse diagrams of rigid polyurethane foams under dynamic loading conditions, Archives of Civil and Mechanical Engineering, Vol. 17, 2017, pp. 457-466.

[53] E.E. Saenz, L.A. Carlsson, and A. Karlsson, In suit analysis of crack propagation in polymer foams, Journal of Material Science, Vol. 46, 2011, pp. 5487-5494.

[54] E.E. Saenz, L.A. Carlsson, and A. Karlsson, Characterization of fracture toughness G_c of PVC and PES foams, Journal of Materials Science, Vol. 46, 2011, pp. 3207-3215.

[55] E.E. Saenz, L.A. Carlsson, and A.M. Karlsson, In suit analysis of fatigue crack propagation in polymer foams, Engineering Fracture Mechanics, Vol. 101, 2013, pp. 23-32.

[56] J. Shen, G. Lu, and D. Ruan, Compressive behavior of closed-cell aluminum foams at high strain rates, Composites: Part B, Vol. 41, 2010, pp. 678-685.

[57] O. Weißenborn, C. Ebert, and M. Gude, Modelling of the strain rate dependent deformation behavior of rigid polyurethane foams, Polymer Testing, Vol. 54, 2016, pp. 145-149.

[58] S.Y. Jin, W. Altenhof, and T. Kapoor, An experimental investigation into the cutting deformation mode of AA6061-T6 round extrusions, Thin-Walled Structures, Vol. 44, 2006, pp. 773-786.

[59] M. Bondy, M.R. Jensen, J. Magliaro, and W. Altenhof, Finite element modeling of a novel cutting deformation mode of AA6061-T6 tubes employing higher order Lagrangian element formulations, International Journal of Impact Engineering, Vol. 110, 2016, pp. 288-298.

[60] A. Majumder, W. Altenhof, S.Y. Jin, T. Kapoor, and D. Green, Simulation of the axial cutting deformation of AA6061-T6 round tubes utilizing Eulerian and mesh free finite element formulations, SAE International Journal of Material and Manufacturing, Vol. 1, 2008, pp. 525-536.

[61] LSTC. LS-DYNA keyword manual. Vol. I. Livermore (CA): Livermore Software Technology Corporation (LSTC); 2015.

[62] Specifications of piezotronics impact load cell (model #: 200C20) from PCB Piezotronics Inc. https://www.pcb.com/products?m=200C20 Accessed 2019.

[63] Material properties of Ultra-Strength Lightweight Carbon Fiber Sheet from McMaster-Carr. https://www.mcmaster.com/carbon-fiber-sheets Accessed 2019.

[64] W.L. Oberkampf and T.G. Trucano, Verification and validation in computational fluid dynamics, Progress in Aerospace Science, Vol. 38, 2002, pp. 209-272.

[65] ASTM Standard D3576-15, 2019, Standard test method for cell size of rigid cellular plastics, ASTM International, West Conshohocken, PA 19428-2959. United States.

APPENDICES

Appendix A: Preparation of test specimens

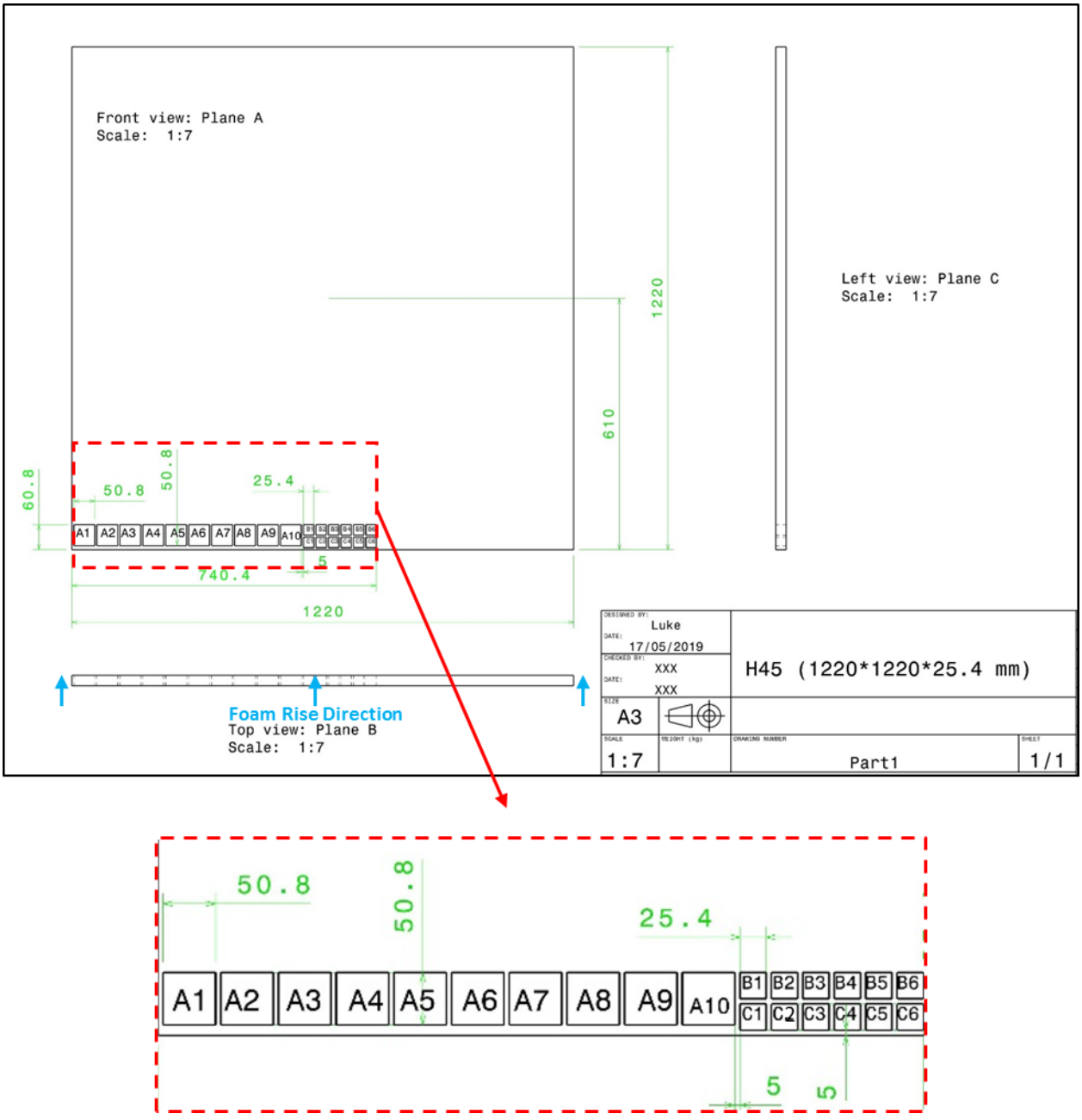

Figure A 1. Cutting plan of PVC foam specimens within the H45 grouping; foam rise direction is indicated in the top view of the foam panel.

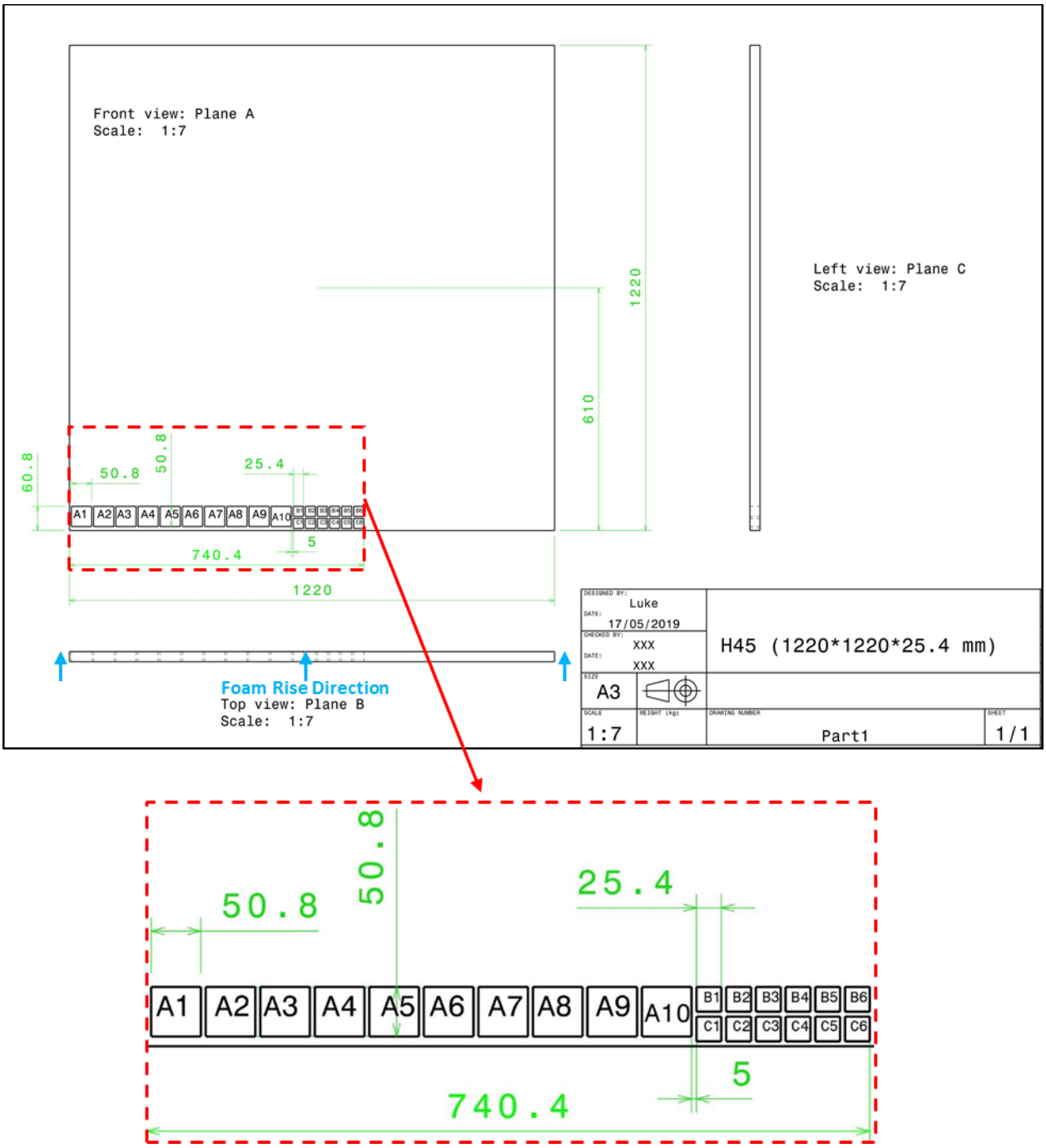

Figure A 2. Cutting plan of PVC foam specimens within the H200 grouping; foam rise direction is indicated in the top view of the foam panel.

Appendix B: Material models for FEA

*MAT_CRUSHABLE_FOAM_TITLE
THIS IS THE MATERIAL MODEL FOR FOAM SPECIMEN (BASE UNITS: kg, mm, s)

$#	mid	ro	e	pr	lcid	tsc	damp
	1	2.0E-07	145100	-0.001	1	0.1	0.25

*DEFINE_CURVE_TITLE
COMPRESSIVE STRESS/STRAIN DATA OBTAINED FROM QUASI-STATIC TEST OF PCV FOAM SPECIMEN WITHIN H200 GROUPING (BASE UNITS: kg, mm, s)

$#	lcid	sidr	sfa	sfo	offa	offo	dattyp	lcint
	1	0	1	1	0	0	0	0

$#	a1	o1
	0	0
	0.0081	113.59
	0.0145	615.18
	0.0202	1318.27
	0.0291	2583.45
	0.03544	3518.82
	0.04361	4568.1
	0.05831	5394.22
	0.10331	5395
	0.30854	5395.2
	0.52257	5872.83
	0.58909	6460.71
	0.6633	7844.63
	0.74474	10870.99
	0.795	14915.93
	0.83044	20068.84
	0.859	26859.5
	0.88	150000
	0.99	2000000

*MAT_PIECEWISE_LINEAR_PLASTICITY_TITLE
THIS IS THE MATERIAL MODEL FOR AA6061-T6 (BASE UNITS: kg, mm, s)

$#	mid	ro	e	pr	sigy	etan	fail	tdel
	2	2.70E-06	6.81E+07	0.35	271500	0	1.0E+21	0
$#	c	p	lcss	lcsr	vp			
	0	0	2	0	0			
$#	eps1	eps2	eps3	eps4	eps5	eps6	eps7	eps8
	0	0	0	0	0	0	0	0
$#	es1	es2	es3	es4	es5	es6	es7	es8
	0	0	0	0	0	0	0	0

*DEFINE_CURVE_TITLE
EFFECTIVE STRESS VERSUS EFFECTIVE PLASTIC STRAIN DATA FOR AA6061-T6 (BASE UNITS: kg, mm, s)

$#	lcid	sidr	sfa	sfo	offa	offo	dattyp	lcint
	2	0	1	1	0	0	0	0
$#		a1	o1					
		0	271564.3					
		6.11E-04	283788					
		0.00225	291531					
		0.005	295856.3					
		0.00887	299423.7					
		0.01387	303390.5					
		0.01998	308138.6					
		0.02721	313673.5					
		0.03556	319943.5					
		0.04503	326897.2					
		0.05562	334257.3					
		0.06733	341386.6					
		0.08016	347734.9					
		0.09411	353516.7					
		0.10918	358394.7					

*MAT_RIGD _TITLE
THIS IS THE MATERIAL MODEL FOR RIGID COMPONENTS (BASE UNITS: kg, mm, s)

$#	mid	ro	e	pr	n	couple	m	alias
	3	2.70E-06	6.81E+07	0.35	0	0	0	
$#	cmo	con1	con2					
	0	6	7					
$#	lco or	a1	a2	a3	v1	v2	v3	
	0	0	0	0	0	0	0	

*MAT_ELASTIC _TITLE
THIS IS THE MATERIAL MODEL FOR LOAD CELL COMPONENT CONSIDERED IN THIS ANALYSIS (BASE UNITS: kg, mm, s)

$#	mid	ro	e	pr	da	db	not	used
	4	8.72E-06	1.23E+08	0.29	0	0	0	

*MAT_ISOTROPIC_ELASTIC_FAILURE_TITLE
THIS IS THE MATERIAL MODEL FOR CARBON FIBER SUPPORTING PLATE CONSIDERED IN THIS ANALYSIS (BASE UNITS: kg, mm, s)

$#	mid	ro	g	sigy	etan	bulk
	5	1.66E-06	2.60E+07	689000	0	1.6E+08
$#	epf	prf	rem	trem		
	0.01	0	0	0		

*MAT_SPRING_ELASTOPLASTIC_TITLE
THIS IS THE MATERIAL MODEL FOR SPRING ELEMENT CONSIDERED IN THIS ANALYSIS (BASE UNITS: kg, mm, s)

$#	mid	k	kt	fy
	6	7.0E+07	0	7.0E+07

Appendix C: EDS analysis

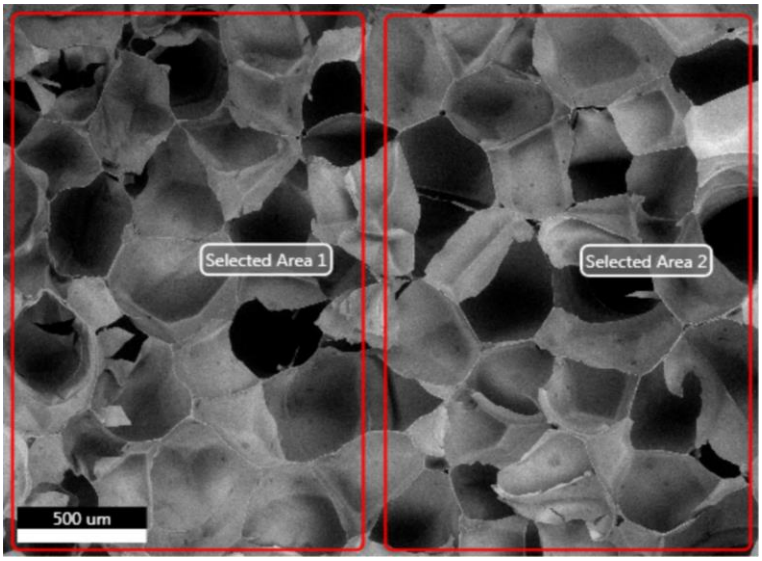

Figure C 1. Areas 1 and 2 selected for EDS analysis of PVC foam H45 at 100× magnification.

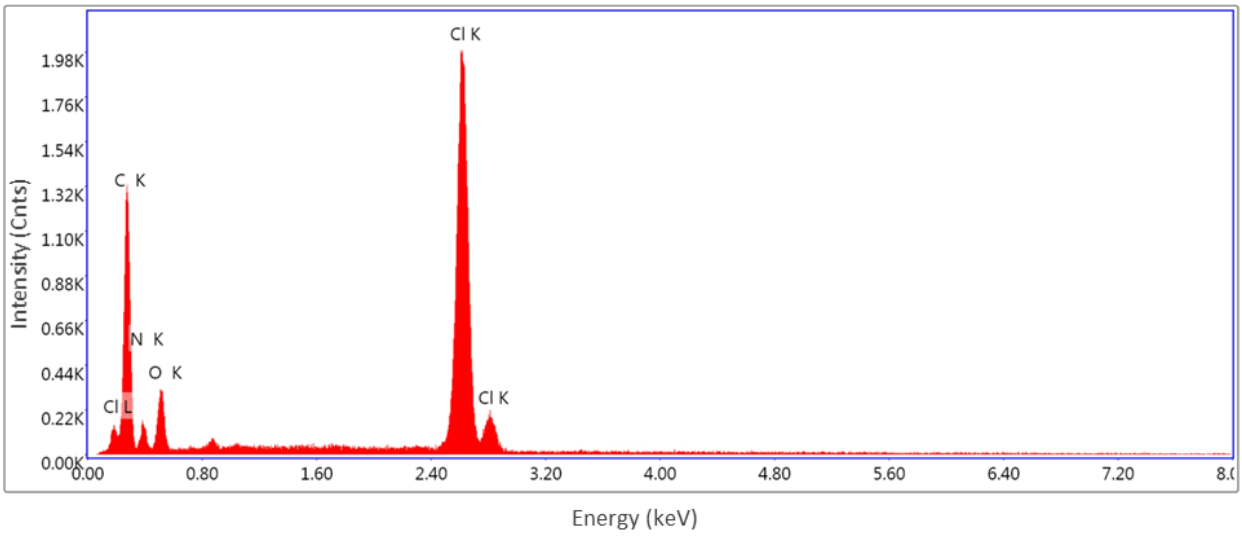

Figure C 2. The spectrum of Area 1 of a PVC foam (H45) specimen.

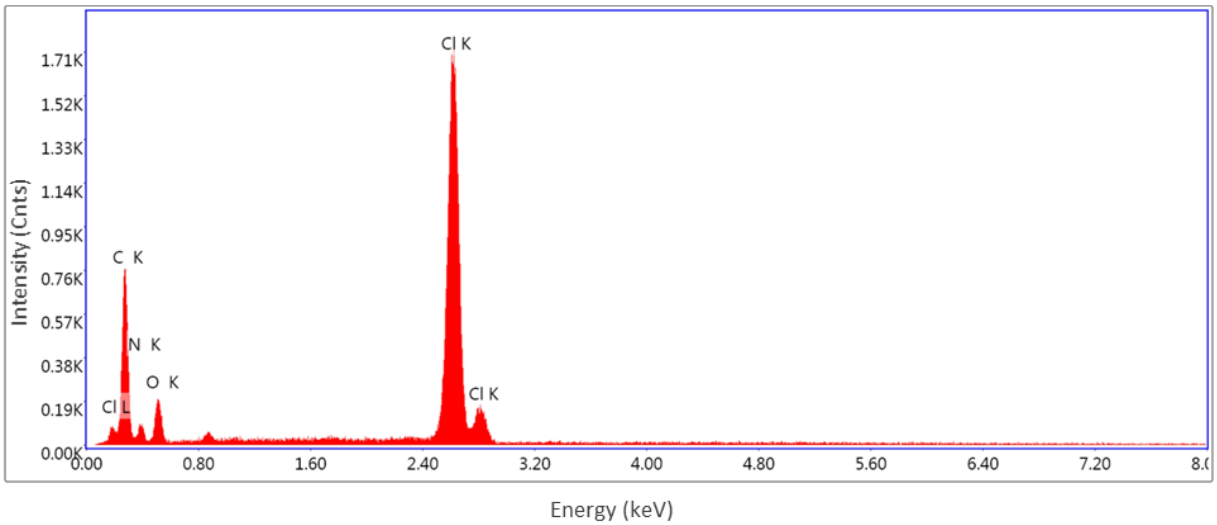

Figure C 3. The spectrum of Area 2 of a PVC foam (H45) specimen.

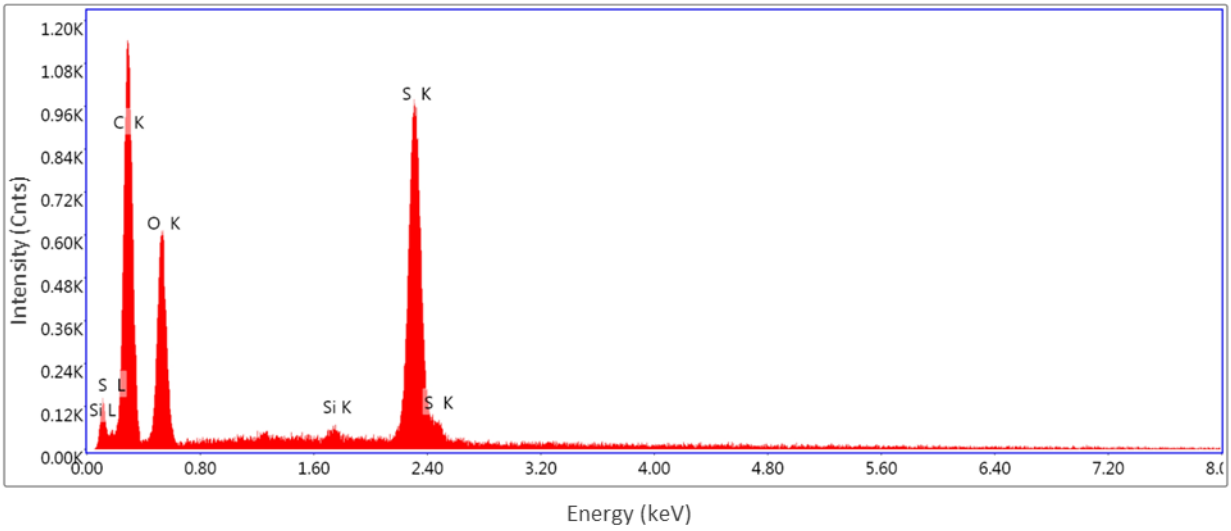

Figure C 4. The spectrum of Area 1 of a PES foam (F50) specimen.

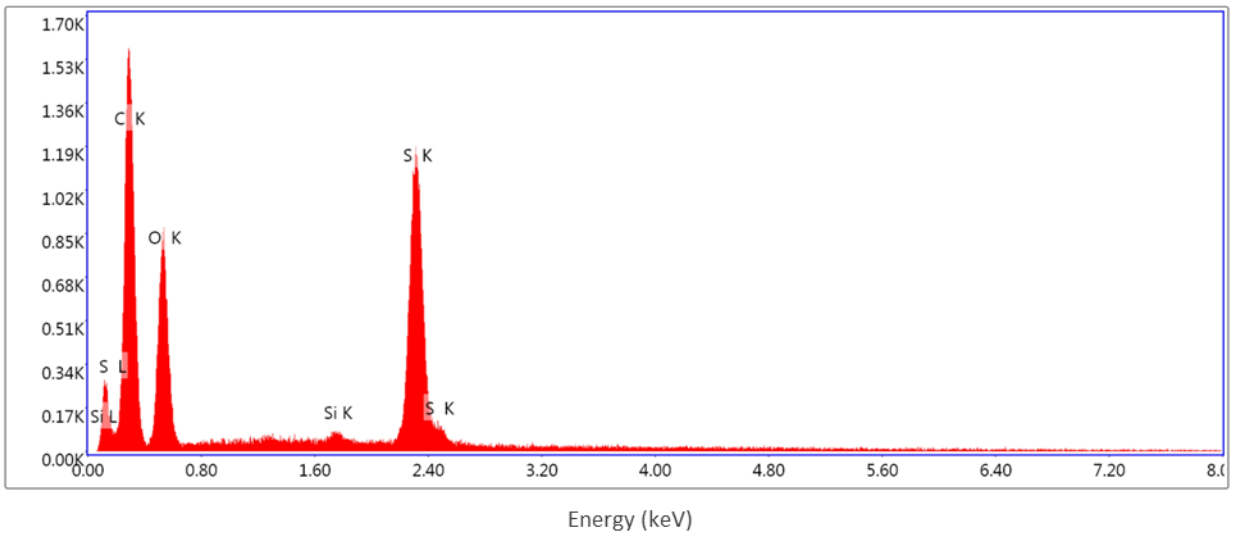

Figure C 5. The spectrum of Area 2 of a PES foam (F50) specimen.

Due to the surface of foam materials not being perfectly flat, some x-rays generated in a specimen were unable to escape from the random distribution of cell walls. All the x-rays absorbed within the specimen cannot be detected. This was the reason that a slight difference in weight percent and atomic percent of a specific element detected in Area 1 and 2. Generally, the results of EDS analysis on Area 1 and 2 of all PVC and PES foam specimens considered in this research are consistent.

Appendix D: SEM analysis

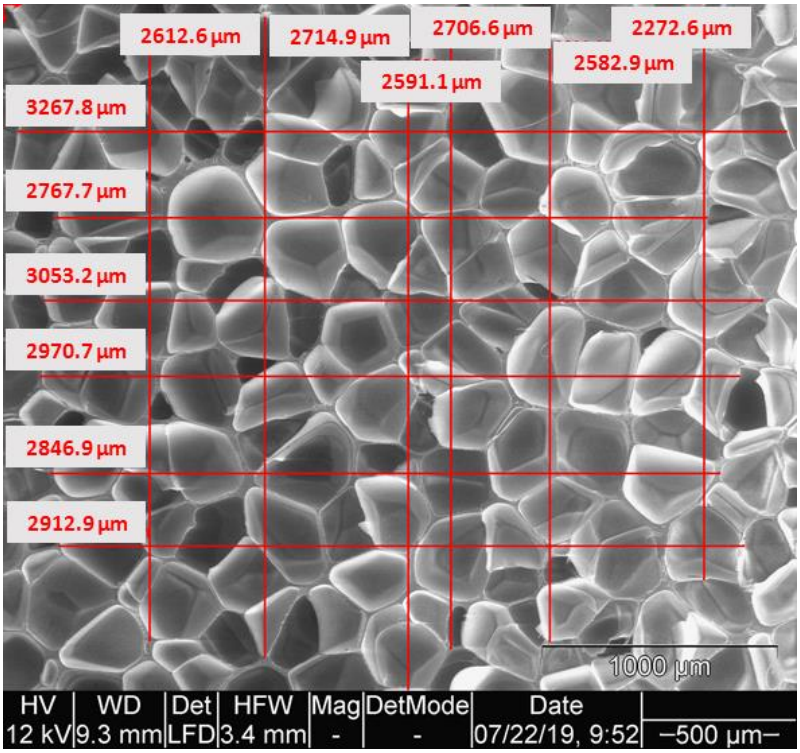

(a)

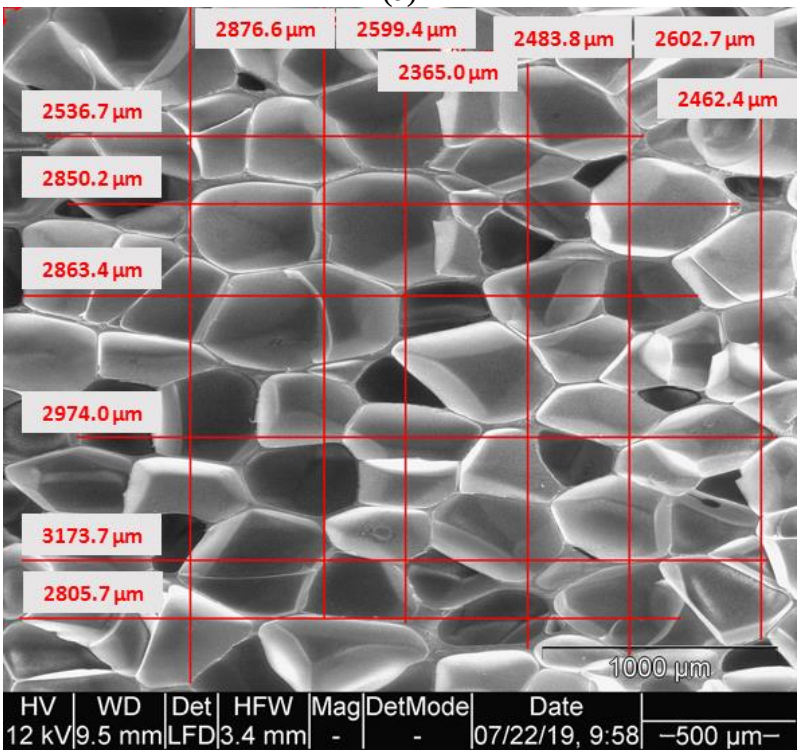

(b)

Figure D 1. SEM images of a specimen within the H130 grouping with the horizontal and vertical intersecting lines on (a) plane A and (b) plane B.

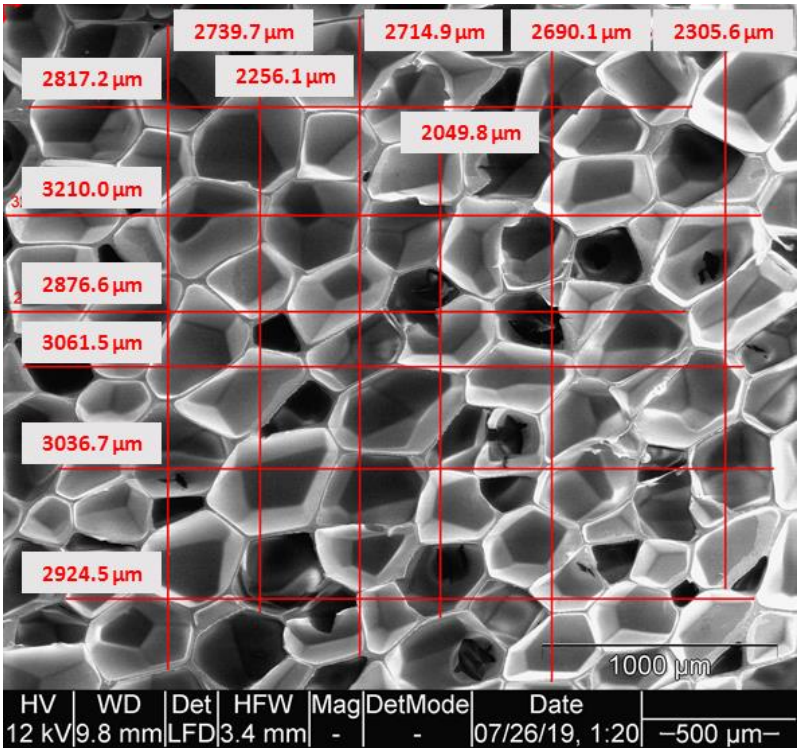

(a)

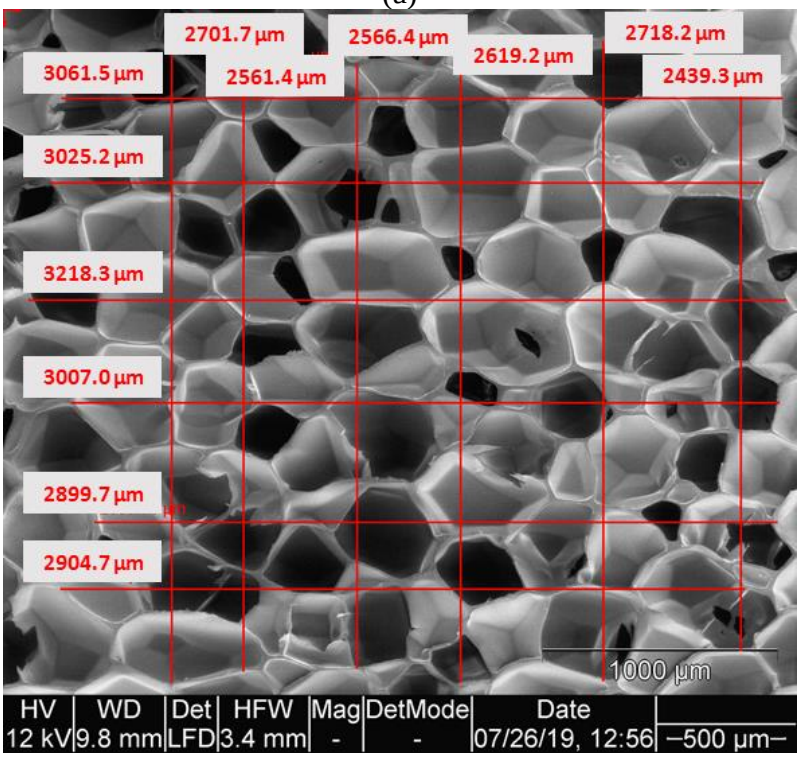

(b)

Figure D 2. SEM images of a specimen within the F130 grouping with the horizontal and vertical intersecting lines on (a) plane A and (b) plane B.

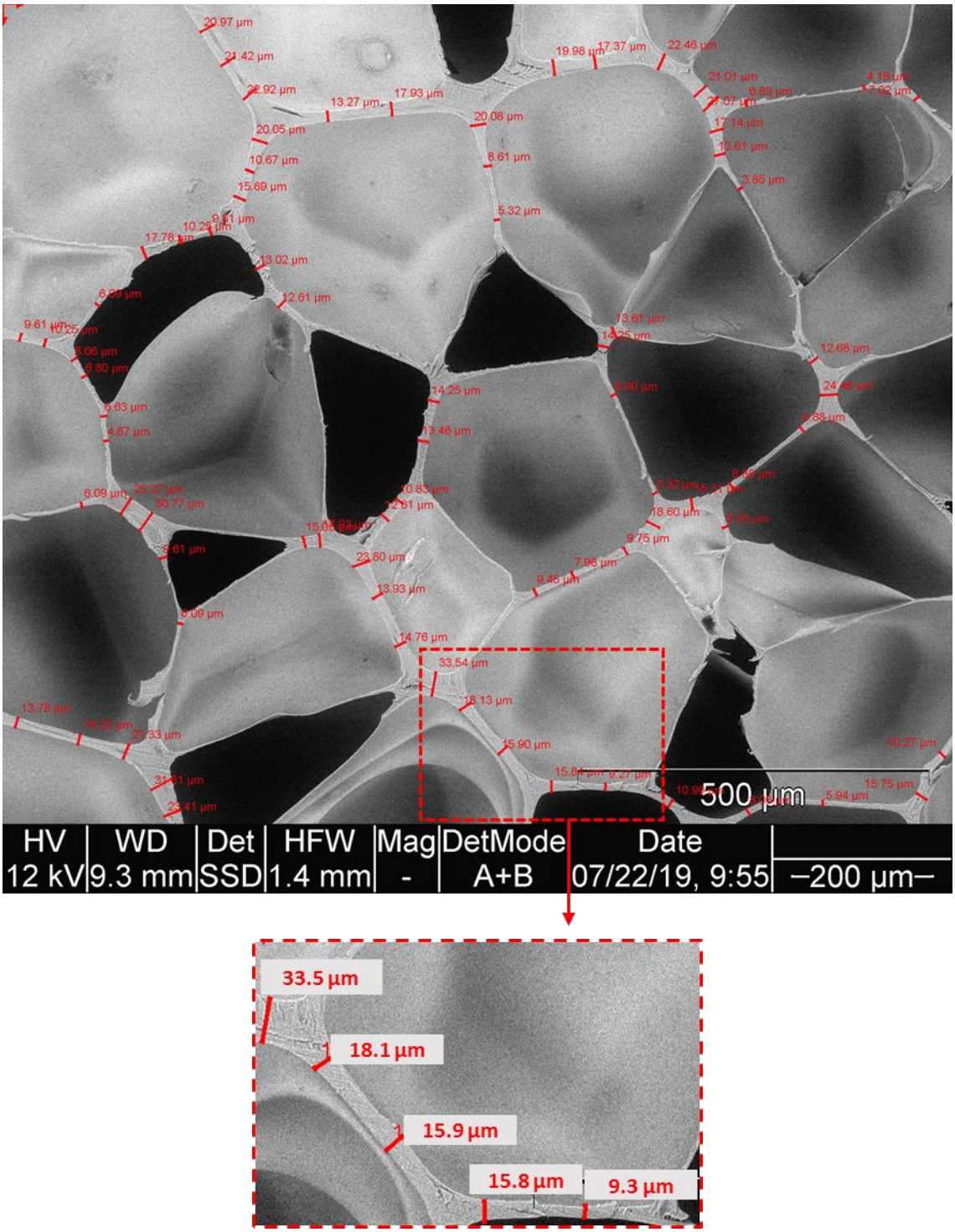

Figure D 3. Cell wall (edge) thickness measurement on plane A of a specimen within the H130 grouping.

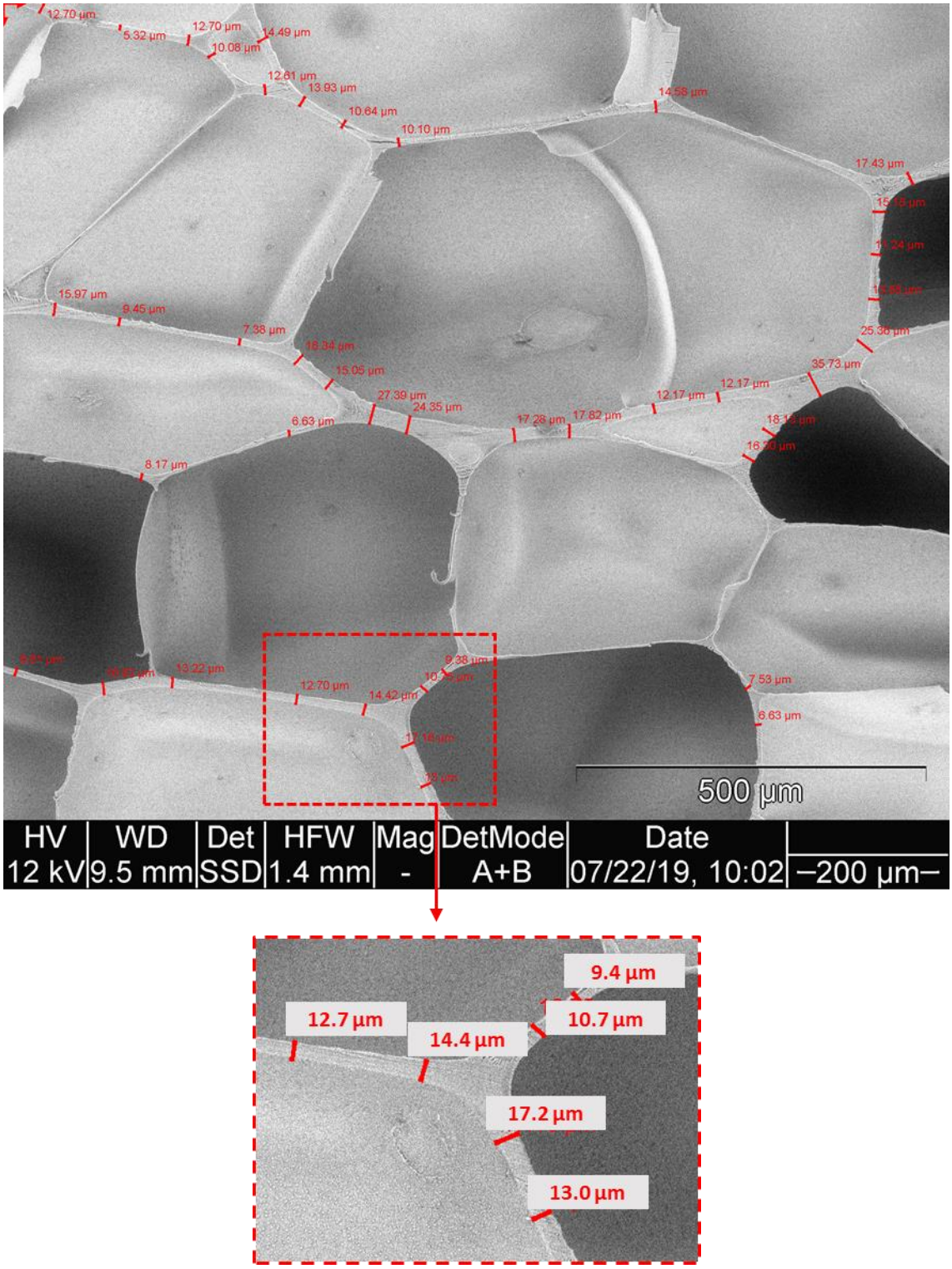

Figure D 4. Cell wall (edge) thickness measurement on plane B of a specimen within the H130 grouping.

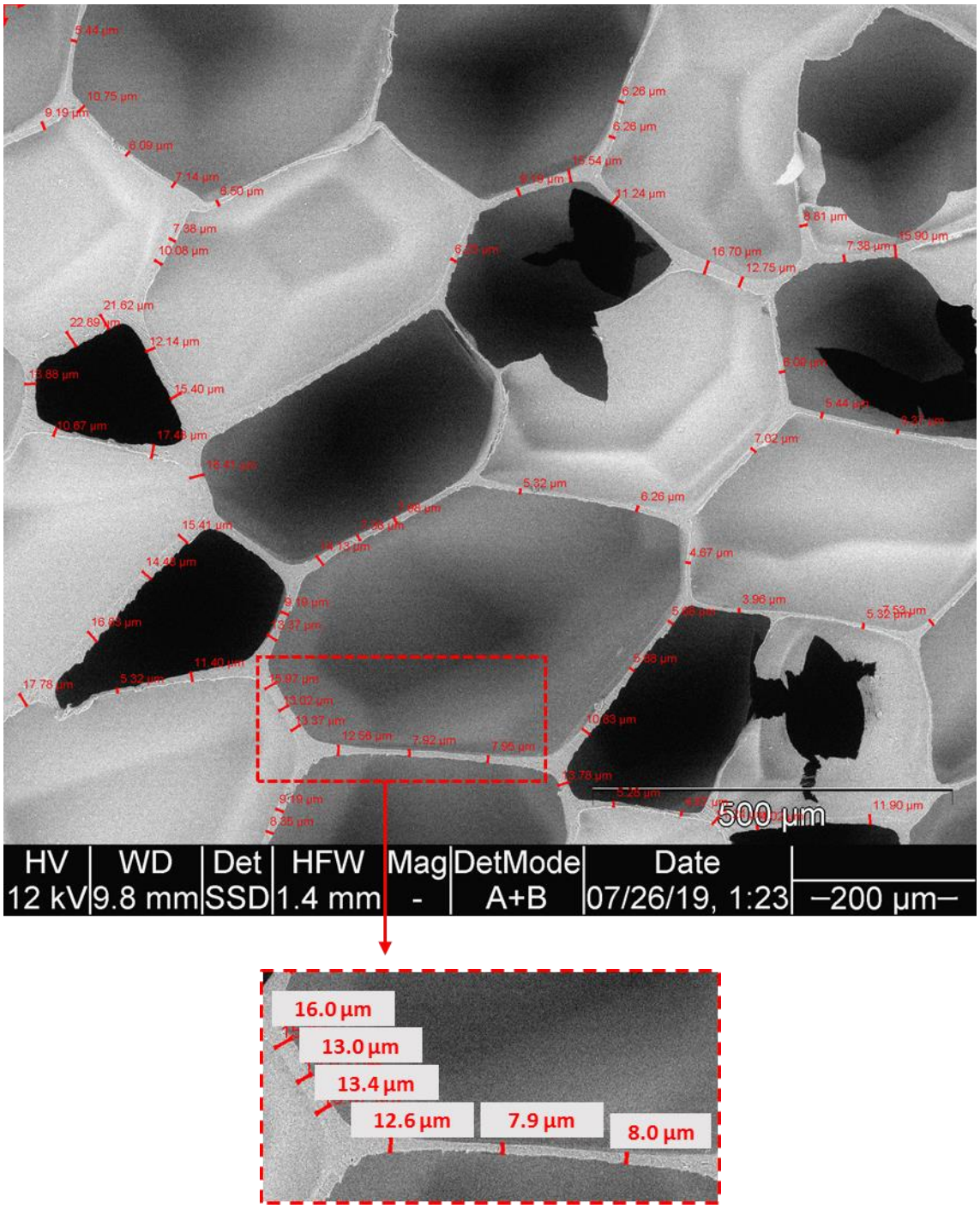

Figure D 5. Cell wall (edge) thickness measurement on plane A of a specimen within the F130 grouping.

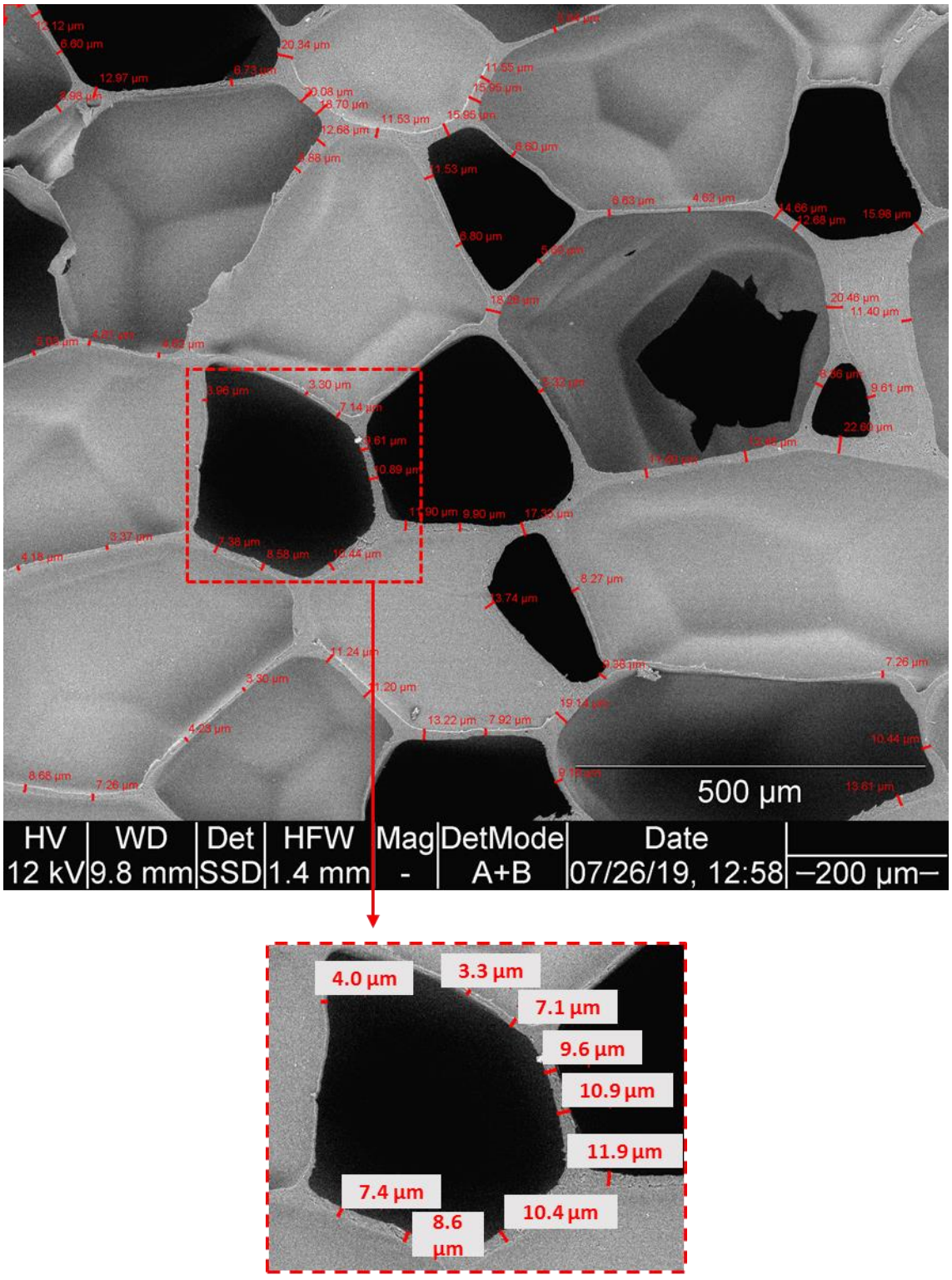

Figure D 6. Cell wall (edge) thickness measurement on plane B of a specimen within the F130 grouping.

Appendix E: Deformation uniformity

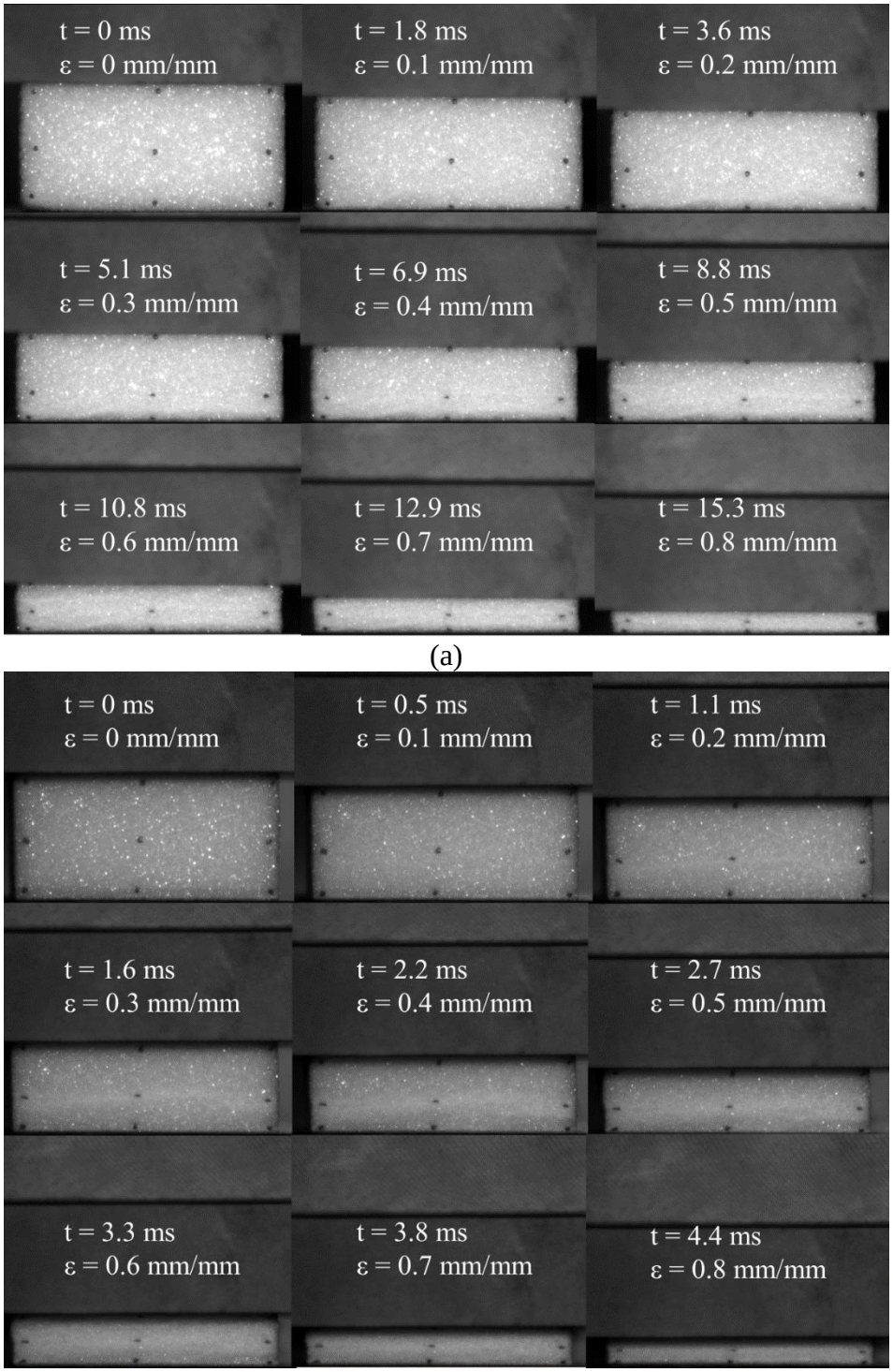

Figure E 1. Successive images of different stages of the deformation of a specimen within the H45 grouping when loading parallel to the foam rise direction with strain rates of (a) 50 s^{-1} and (b) 200 s^{-1}.

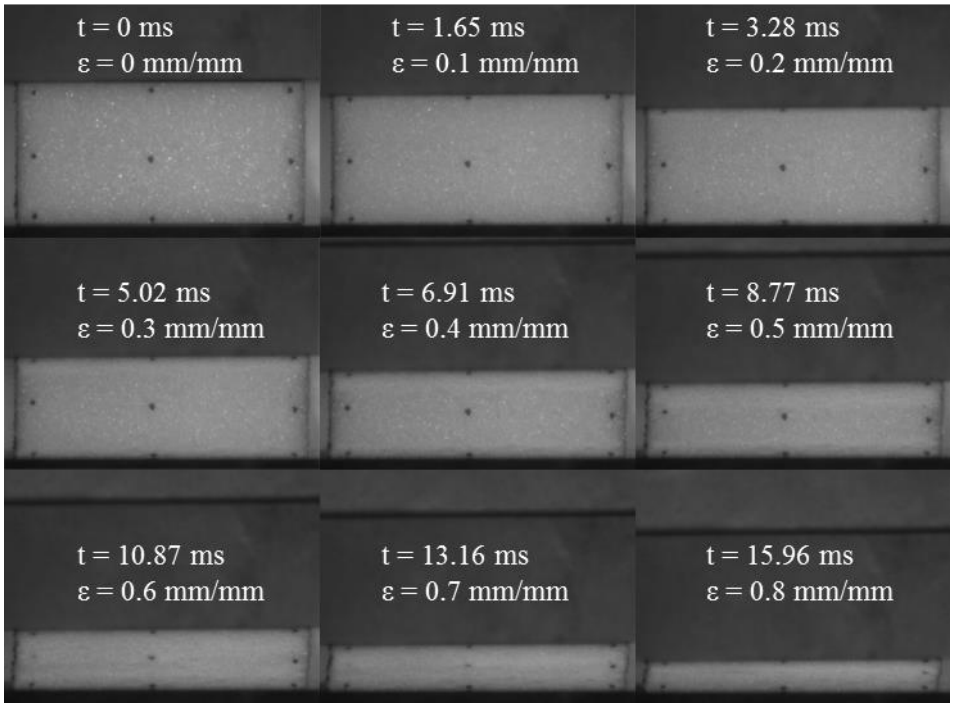

(a)

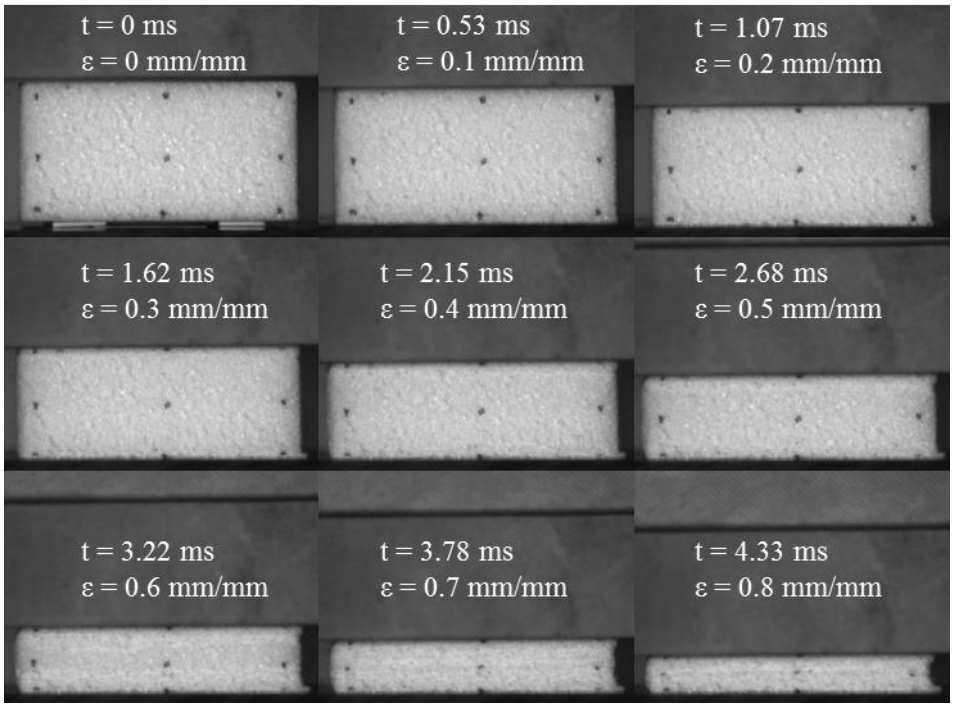

(b)

Figure E 2. Successive images of different stages of the deformation of a specimen within the F50 grouping when loading parallel to the foam rise direction with strain rates of (a) 50 s^{-1} and (b) 200 s^{-1}.

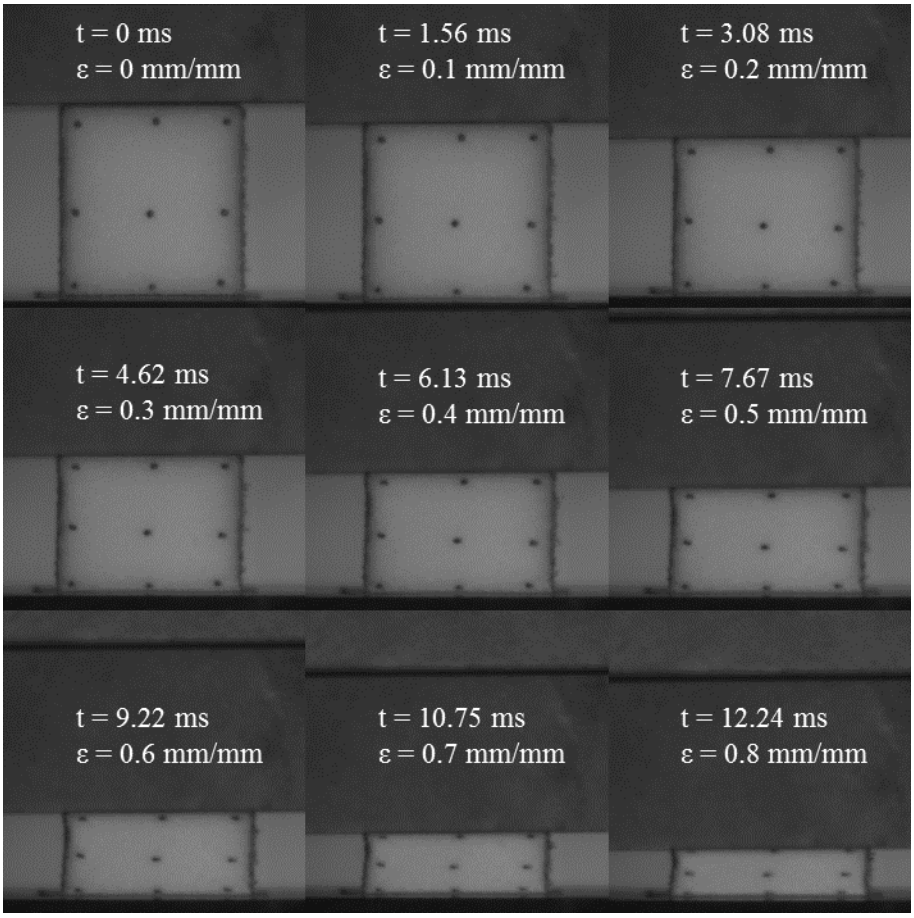
t = 0 ms
ε = 0 mm/mm
t = 1.56 ms
ε = 0.1 mm/mm
t = 3.08 ms
ε = 0.2 mm/mm
t = 4.62 ms
ε = 0.3 mm/mm
t = 6.13 ms
ε = 0.4 mm/mm
t = 7.67 ms
ε = 0.5 mm/mm
t = 9.22 ms
ε = 0.6 mm/mm
t = 10.75 ms
ε = 0.7 mm/mm
t = 12.24 ms
ε = 0.8 mm/mm

(a)

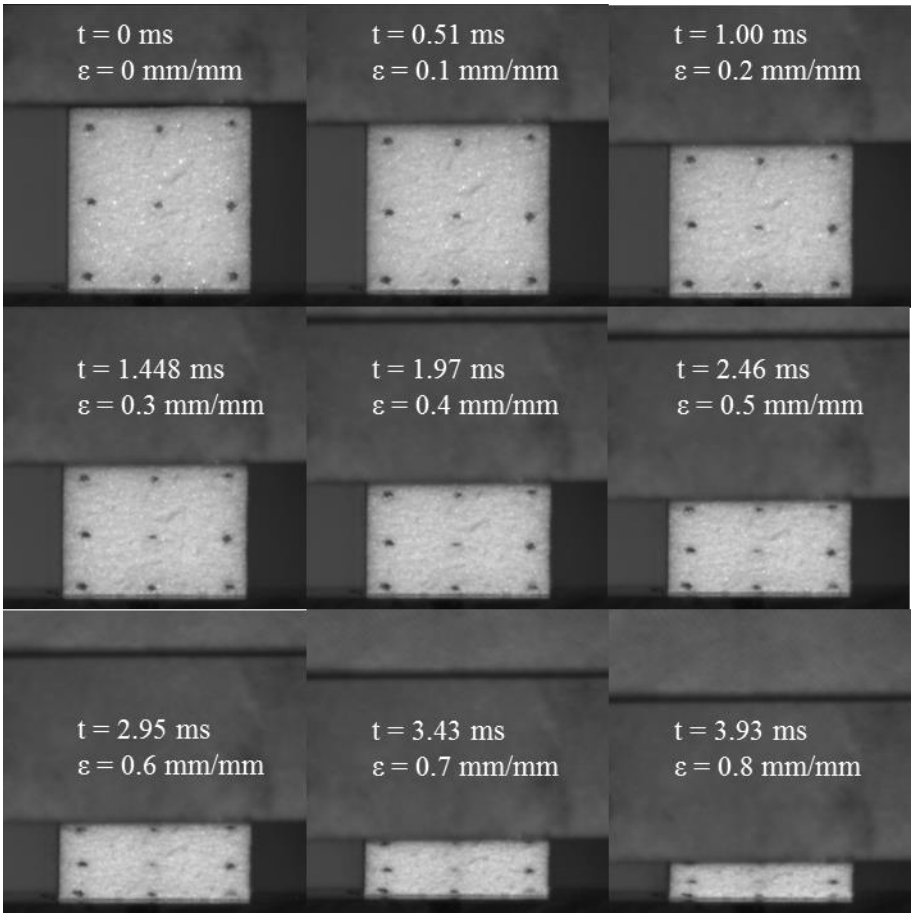

(b)

Figure E 3. Successive images of different stages of the deformation of a specimen within the F50 grouping when loading perpendicular to the foam rise direction (loading on plane B) with strain rates of (a) 50 s^{-1} and (b) 200 s^{-1}.

VITA AUCTORIS

NAME:	Yue (Luke) Liu
PLACE OF BIRTH:	Shandong, China
YEAR OF BIRTH:	1992
EDUCATION:	B.A.Sc., Shandong Jianzhu University, China, 2015
CANDIDATE:	M.A.Sc., University of Windsor, Windsor, ON, 2020